Active Transport Across Biological Membranes: Quantification and Limits

Dissertation

zur Erlangung des Doktorgrades der Naturwissenschaften

(Dr. rer. nat.)

der

Naturwissenschaftlichen Fakultät II
Chemie, Physik und Mathematik

der Martin-Luther-Universität
Halle-Wittenberg

vorgelegt von

Frau Soné Kotze
geb. am 14.05.1996 in Windhoek

Gutachter: Prof. Dr. Kai-Uwe Goss
Prof. Dr. Gert Fricker

Tag der öffentlichen Verteidigung: 29 April 2025

ABSTRACT

Active Transport Across Biological Membranes: Quantification and Limits

Caco-2/MDCK assays are essential in vitro tools for evaluating the membrane permeability and active transport of chemical compounds. Understanding active transport, particularly efflux, is crucial for chemical compounds because it can significantly influence their bioavailability, toxicity, therapeutic efficacy, and potential for drug-drug interactions. The efflux ratio (ER), determined via bidirectional Caco-2/MDCK assays, is a key metric for identifying substrates of efflux transporters such as P-glycoprotein (P-gp). Generally, active transport is measured qualitatively by ER: If the ER of a compound is found to be greater than 2, it is classified as a substrate of an efflux transporter. However, using the ER in this way raises concerns due to the lack of comparability between assay measurements brought about by certain experimental parameters, such as the pH or compound concentration. As a result, a compound may be classified differently if measured under different conditions. Circumventing these issues requires the introduction of an intrinsic quantity that would enable the quantification of active transport. Previous studies have taken the first steps towards such a quantifiable intrinsic value by relating the ER to intrinsic membrane permeability (P_0) and P-gp-mediated permeability (P_{pgp}). However, their simplified models did not consider the possible effect of the aqueous boundary layers (ABLs) and the filter on which the cell monolayer is grown, nor the effect of paracellular transport. These factors can significantly influence apparent permeability (P_{app}) measurements in these assays, and it is thus crucial to consider their potential effect on the ER. Nevertheless, previous models were simply assumed to be not applicable to ABL-limited compounds, and the effect of paracellular transport was mistakenly assumed to be negligible. Chapter 2 of this work probes the viability of using intrinsic values such as P_{pgp} by introducing an extended model that incorporates the additional aqueous resistances, and demonstrates mathematically and experimentally that the quantitative ER relationship remains valid under these more realistic conditions. Additionally, the model also accounts for paracellular transport and shows how it can significantly affect the ER. Experimental results confirm that paracellular dominance reduces the ER to unity, potentially masking efflux. The tentative intrinsic value for P-gp-mediated efflux (P_{pgp}) is then probed further. Since this intrinsic value should be pH-independent, it is necessary to determine whether P-gp transports the neutral or ionic species of a compound. Using MDCK assays, this study investigates a method for determining transporter substrate fraction preference by examining ER pH-dependence for basic, acidic, and non-dissociating compounds. The results are compared to model fits based

on various assumptions of transporter species preference. As an unexpected consequence of these assays, evidence is also provided for an additional influx transporter in the basolateral membrane, and the model was further extended to incorporate this transport. The combined effects of paracellular transport, the additional basolateral influx transporter, and potential pH effects complicate the extraction of intrinsic values for active efflux from the ER. Furthermore, the study finds that the use of inhibitor affects paracellular transport measurements. All of these effects made the analysis of the intrinsic value and the substrate species preference inconclusive.

The final chapter of this study hypothesises that the disposition of compounds above a certain membrane permeability threshold are unlikely to be affected by efflux transporters. This hypothesis is supported by the fact that it would be too energetically expensive for the cell (and thus the organism) to counteract the high rates of passive diffusion for such compounds by maintaining active efflux against it. A tentative membrane permeability threshold for active efflux is proposed ($\log P_{\mathrm{m}}$ = -3) and investigated using three separate datasets that were compiled for the most consequential efflux transporters. The datasets were assembled from available literature MDCK assay ER values, and membrane permeability (P_{m}) was determined for each compound. All compounds with significant reported ER values that were found to have P_{m} values above the proposed permeability threshold were identified as preliminary outliers to the theory, and were consequently systematically investigated. Barring a single compound, all outliers were reclassified on the basis of independently-determined ER values or recalculated P_{m} values and were found not to defy the energy limit. Compounds that lie near the threshold line were reclassified as "borderline" compounds. For these compounds, efflux is especially dependent on concentration, as the energy limit is reached more quickly at high concentrations. This is an effect that simple classification via membrane permeability cannot represent, and necessitates going back to the fundamental idea of the energy limit and working with a maximal flux value instead. Maximal flux in this case refers to the maximum moles of compound that can be actively transported per unit area and time ($\mu\mathrm{mol\,cm^{-2}\,s^{-1}}$) given the limited energy production of the cell. Using concentration-dependence assays for selected borderline compounds and accompanying model fits, a more precise maximal flux value is determined of $1 \times 10^{-5}\,\mu\mathrm{mol\,cm^{-2}\,s^{-1}}$ for our MDCK cells. This flux threshold is then linked to a threshold P_{m} value and a sensitivity analysis shows that paracellular transport, the activity of the basolateral influx transporter and compound charge have little effect on the P_{m} threshold. However, compound concentration, the apical membrane surface area (i.e the effect of the microvilli) and the maximal flux value can significantly shift the threshold P_{m} value. As such, the application of a P_{m} threshold to classify compounds as unlikely to be affected by efflux transporters comes with several considerations. The most important of which is the cell type (since different cells have varying apical membrane surface areas and maximal energy capacities) and the compound concentration. However, a membrane permeability cut-off line for actively transported compounds was clearly identifiable from the data, which proves the hy-

pothesis that compounds with a high membrane permeability are not actively effluxed due to the energy constraints of the cell. Determining what the energy threshold is for active efflux allows for quick and simple determination of compounds that are not actively transported based on their membrane permeability, circumventing the need for time- and resource-intensive in vitro assays.

ZUSAMMENFASSUNG

Aktiver Transport über Biologische Membranen: Quantifizierung und Grenzen

Caco-2/MDCK-Assays sind essenzielle in vitro-Werkzeuge zur Bewertung der Membranpermeabilität und des aktiven Transports chemischer Verbindungen. Das Verständnis des aktiven Transports, insbesondere des Effluxes, ist für chemische Verbindungen entscheidend, da dieser ihre Bioverfügbarkeit, Toxizität, therapeutische Wirksamkeit und das Potenzial für Arzneimittelwechselwirkungen erheblich beeinflussen kann. Das Efflux-Verhältnis (ER), das über bidirektionale Caco-2/MDCK-Assays bestimmt wird, ist eine zentrale Kennzahl zur Identifizierung von Substraten von Efflux-Transportern wie P-Glykoprotein (P-gp). Allgemein wird aktiver Transport qualitativ durch das ER gemessen: Wenn das ER einer Verbindung größer als 2 ist, wird sie als Substrat eines Efflux-Transporters eingestuft. Die Verwendung des ER auf diese Weise wirft jedoch Bedenken hinsichtlich der Vergleichbarkeit von Messungen auf, da bestimmte experimentelle Parameter wie der pH-Wert oder die Konzentration der Verbindung die Ergebnisse beeinflussen können. Infolgedessen kann eine Verbindung unter unterschiedlichen Bedingungen unterschiedlich klassifiziert werden. Um diese Probleme zu umgehen, ist die Einführung einer intrinsischen Größe erforderlich, die eine Quantifizierung des aktiven Transports ermöglicht. Frühere Studien haben erste Schritte in Richtung eines solchen quantifizierbaren intrinsischen Werts unternommen, indem sie das ER mit der intrinsischen Membranpermeabilität (P_0) und der P-gp-vermittelten Permeabilität (P_{pgp}) in Beziehung setzten. Ihre vereinfachten Modelle berücksichtigten jedoch weder die möglichen Effekte der wässrigen Grenzschichten (ABLs) und des Filters, auf dem die Zell-Monoschicht wächst, noch die Effekte des parazellulären Transports. Diese Faktoren können die apparente Permeabilität (P_{app}) in diesen Assays erheblich beeinflussen, weshalb ihre potenziellen Auswirkungen auf das ER berücksichtigt werden müssen. Dennoch wurden frühere Modelle einfach als nicht anwendbar auf ABL-limitierte Verbindungen angenommen, und die Wirkung des parazellulären Transports wurde fälschlicherweise als vernachlässigbar betrachtet. Kapitel 2 dieser Arbeit untersucht die Machbarkeit der Verwendung intrinsischer Werte wie P_{pgp} durch die Einführung eines erweiterten Modells, das die zusätzlichen wässrigen Widerstände einbezieht, und zeigt mathematisch und experimentell, dass die quantitative ER-Beziehung unter diesen realistischeren Bedingungen weiterhin gültig bleibt. Außerdem berücksichtigt das Modell auch den parazellulären Transport und zeigt, wie dieser das ER erheblich beeinflussen kann. Experimentelle Ergebnisse bestätigen, dass eine Dominanz des parazellulären Transports das ER auf eins reduziert und

dadurch Efflux gegebenenfalls maskiert. Der vorläufige intrinsische Wert für den P-gp-vermittelten Efflux (P_{pgp}) wird anschließend weiter untersucht. Da dieser intrinsische Wert pH-unabhängig sein sollte, ist es notwendig zu bestimmen, ob P-gp die neutrale oder ionische Spezies einer Verbindung transportiert. Unter Verwendung von MDCK-Assays untersucht diese Studie eine Methode zur Bestimmung der Substratfraktionspräferenz des Transporters, indem die pH-Abhängigkeit des ER für basische, saure und nicht-dissoziierende Verbindungen betrachtet wird. Die Ergebnisse werden mit Modellanpassungen verglichen, die auf verschiedenen Annahmen über die Präferenz des Transporters für bestimmte Spezies basieren. Als unerwartete Folge dieser Assays liefern die Ergebnisse auch Hinweise auf einen zusätzlichen Influx-Transporter in der basolateralen Membran, und das Modell wurde entsprechend erweitert, um diesen Transport einzubeziehen. Die kombinierten Effekte des parazellulären Transports, des zusätzlichen basolateralen Influx-Transporters und möglicher pH-Effekte erschweren die Ableitung intrinsischer Werte für den aktiven Efflux aus dem ER. Darüber hinaus zeigt die Studie, dass der Einsatz von Inhibitoren die Messung des parazellulären Transports beeinflusst. All diese Effekte machten die Analyse des intrinsischen Werts und der Substratspräferenz letztlich nicht schlüssig.

Das abschließende Kapitel dieser Arbeit stellt die Hypothese auf, dass Verbindungen oberhalb eines bestimmten Membranpermeabilitätsschwellenwertes wahrscheinlich nicht von Efflux-Transportern beeinflusst werden. Diese Hypothese wird durch die Tatsache gestützt, dass es für die Zelle (und damit den Organismus) zu energieaufwendig wäre, den hohen Passivdiffusionsraten solcher Verbindungen durch einen aktiven Efflux entgegenzuwirken. Ein vorläufiger Schwellenwert für die Membranpermeabilität für den aktiven Efflux wird vorgeschlagen ($\log P_{\mathrm{m}}$ = -3) und anhand von drei separaten Datensätzen untersucht, die für die wichtigsten Efflux-Transporter zusammengestellt wurden. Die Datensätze wurden aus verfügbaren Literaturwerten von MDCK-Assay-ER-Werten zusammengestellt, und die Membranpermeabilität (P_{m}) wurde für jede Verbindung bestimmt. Alle Verbindungen mit signifikanten berichteten ER-Werten, die P_{m}-Werte über dem vorgeschlagenen Permeabilitätsschwellenwert aufwiesen, wurden als vorläufige Ausreißer der Theorie identifiziert und folglich systematisch untersucht. Mit Ausnahme einer einzigen Verbindung wurden alle Ausreißer auf Basis unabhängig bestimmter ER-Werte oder neu berechneter P_{m}-Werte neu klassifiziert und stellten sich als konform mit der Energiebeschränkung heraus. Verbindungen, die sich nahe der Schwellenwertlinie befanden, wurden als „Grenzfälle“ neu klassifiziert. Für diese Verbindungen ist der Efflux besonders konzentrationsabhängig, da bei hohen Konzentrationen die Energiegrenze schneller erreicht wird. Dieser Effekt kann durch eine einfache Klassifikation über die Membranpermeabilität nicht dargestellt werden und erfordert eine Rückkehr zur grundlegenden Idee der Energiebeschränkung und die Arbeit mit einem maximalen Flusswert. Der maximale Fluss bezieht sich hierbei auf die maximale Menge an Verbindungsmolekülen, die pro Fläche und Zeiteinheit ($\mu\mathrm{mol\,cm^{-2}\,s^{-1}}$) bei der begrenzten Energieproduktion der Zelle aktiv transportiert werden können. Durch konzentrationsabhängige Assays für ausgewählte Grenzfallver-

bindungen und entsprechende Modellanpassungen wird ein präziserer maximaler Flusswert von 1×10^{-5} µmol cm^{-2} s^{-1} für unsere MDCK-Zellen bestimmt. Dieser Flussschwellenwert wird dann mit einem Schwellenwert P_{m} verknüpft, und eine Sensitivitätsanalyse zeigt, dass parazellulärer Transport, die Aktivität des basolateralen Influx-Transporters und die Ladung der Verbindung nur geringe Auswirkungen auf den P_{m}-Schwellenwert haben. Die Konzentration der Verbindung, die apikale Membranoberfläche (d. h. der Effekt der Mikrovilli) und der maximale Flusswert können den Schwellenwert P_{m} jedoch erheblich verschieben. Daher bringt die Anwendung eines P_{m}-Schwellenwerts zur Klassifizierung von Verbindungen, die wahrscheinlich nicht von Efflux-Transportern beeinflusst werden, mehrere Überlegungen mit sich. Die wichtigsten davon sind der Zelltyp (da verschiedene Zellen unterschiedliche apikale Membranoberflächen und maximale Energiekapazitäten aufweisen) und die Verbindungskonzentration. Dennoch konnte anhand der Daten eine Membranpermeabilitäts-Grenzlinie für aktiv transportierte Verbindungen klar identifiziert werden, was die Hypothese stützt, dass Verbindungen mit hoher Membranpermeabilität aufgrund der Energieeinschränkungen der Zelle nicht aktiv effluxiert werden. Die Bestimmung des Energieschwellenwerts für den aktiven Efflux ermöglicht eine schnelle und einfache Identifikation von Verbindungen, die aufgrund ihrer Membranpermeabilität nicht aktiv transportiert werden, und erübrigt die Notwendigkeit von zeit- und ressourcenintensiven in vitro-Assays.

Preface

The present work was conducted from February 2022 to November 2024 at the Helmholtz Centre for Environmental Research (Leipzig) in the Department Computational Biology and Chemistry. The thesis is written as a monograph and is based in part on original, peer-reviewed research articles.

Chapter two is based on the following publications:

- Kotze, S., Ebert, A., and Goss, K. U. (2024). Effects of Aqueous Boundary Layers and Paracellular Transport on the Efflux Ratio as a Measure of Active Transport Across Cell Layers. Pharmaceutics, 16(1).
  Sone Kotze: Investigation, Visualisation, Formal Analysis, and Writing — Original Draft. **Kai-Uwe Goss**: Conceptualisation, Methodology, Writing — Review and Editing, and Supervision. **Andrea Ebert**: Methodology, Formal Analysis, and Writing — Review and Editing.

- Kotze, S., Goss, K. U. and Ebert, A. (2024). The pH-dependence of efflux ratios determined with bidirectional transport assays across cellular monolayers. International Journal of Pharmaceutics: X, 8.
  Sone Kotze: Investigation, Visualisation, Formal Analysis, and Writing — Original Draft. **Kai-Uwe Goss**: Conceptualisation, Methodology, Writing — Review and Editing, and Supervision. **Andrea Ebert**: Methodology, Formal Analysis, Conceptualisation, and Writing — Review and Editing.

Note that text passages, tables and figures in this monograph are partly taken from the above listed publications without further indication. The abstracts of the original publications are included in Chapter 5.

Contents

1 Introduction

1.1 Cell membrane permeability and active transport

Permeability through biological membranes significantly impacts the absorption, distribution, metabolism and excretion (ADME) of drugs, and thus plays a crucial role in the pharmacokinetics of chemicals [1], [2]. Passive diffusion and active transport are the two primary mechanisms of permeation across cellular monolayers [3]. This study focuses on active transport, a process in which carrier proteins mediate the permeation of chemicals. Active transport is energy-dependent and can occur even against a concentration gradient [4]. There is a remarkable amount of carrier proteins that partake in active transport, all differing in structure, specificity, function and tissue location. The ATP-Binding Cassette (ABC) transporter family makes up the bulk of the membrane-integrated proteins implicated in active transport, and are all coupled to ATP hydrolysis for energy. Apically located efflux proteins from this family are responsible for actively pumping out xenobiotics from cells, thereby reducing the efficacy of drug delivery for several important pharmaceuticals [5]–[7]. Indeed, multidrug resistance (MDR) of cancerous tissue is largely attributed to the over-expression of efflux proteins, due to their role in decreasing the intracellular concentration of cytotoxic compounds, including chemotherapeutic agents [8]. Due to their broad substrate specificity, the three main carrier proteins associated with MDR are Multidrug Resistant Protein 1 (MDR1), otherwise known as P-glycoprotein (P-gp), Breast Cancer Resistance Protein (BCRP), and Multidrug Resistance-Associated Protein 2 (MRP2) [9]. The study of efflux transporters remains a crucial point of interest in pharmaceutical research due to their central role in MDR and their ability to significantly impede the oral bioavailability of drugs.

The epithelial permeability and intestinal absorption of compounds can be determined with bidirectional transport assays using intestinal cell lines such as Madin-Darby canine kidney cells (MDCK) or human colorectal (Caco-2) cells. MDCK/Caco-2 transport assays are considered essential in vitro tools to determine the membrane permeability (P_{m}) of chemical compounds, as well as the involvement of active transport [10]–[12]. MDCK cells transfected with the abcb1 gene leads to the over-expression of the MDR1/P-gp protein. These transfected cells, known as MDCKII-MDR1 cells, can be used to study efflux mediated by this important transporter [13]. However, these assays are not limited to P-gp. The activity of any efflux transporter can be evaluated using such assays, provided that a suitable cell line is used (e.g transfected with the efflux pump of interest, and/or knocking-out the genes of other prominent transporters [14]–[16]). Drug regulatory agencies such as the Food and Drug Administration (FDA) and the European Medicines Agency (EMA) recommend bidirectional MDCK-MDR1 and MDCK-BCRP (MDCK cells over-expressing BCRP) assays for all compounds of interest during drug development in order to evaluate any potential role that these vital efflux transporters may play in the uptake and distribution of pharmaceuticals, as well

as any potential drug-drug interactions [17]–[19]. In such MDCK transport assays, the apparent permeability (P_{app}) of a compound is measured between a donor and acceptor compartment, separated by a confluent cellular monolayer grown on a permeable support (filter). For bidirectional assays, flux (J) is measured in both the apical-to-basolateral ($A \rightarrow B$) direction and the basolateral-to-apical direction ($B \rightarrow A$) and the quotient of these values is known as the efflux ratio (ER):

$$ER \equiv \frac{J_{B \rightarrow A}}{J_{A \rightarrow B}} \tag{1}$$

1.2 Using intrinsic values to quantify active transport

Membrane permeability (P_{m}) is extracted from the P_{app} measured with such in vitro bidirectional essays. However, according to the pH-partition hypothesis, only the neutral fraction (f_{n}) of a chemical can pass through membranes by passive diffusion due to its exceedingly hydrophobic nature [20]. This renders the permeability of the ionic fraction negligible [21]. The P_{m} of ionisable chemicals is therefore dependent on pH, and not comparable if determined under different pH conditions. To remedy this, Avdeef [22] introduced the pH-independent intrinsic membrane permeability of the neutral species (P_0):

$$P_m = P_0 \cdot f_n \tag{2}$$

P_0 is thus a pH-independent measure of passive membrane permeability, i.e an intrinsic value for passive transport. When it comes to active transport, the efflux ratio is the widely-used metric to evaluate active efflux. As a rule, establishing that the ER for a given chemical is greater than some predefined threshold value (most often 2) is sufficient to classify it as a substrate of the investigated transporter [17]. As such, the ER is primarily used as a qualitative metric. However, efforts have also been made recently to derive a relationship that could allow for the quantification of active transport based on the ER. The ER is by its very nature a measure of the interplay of both passive and active transport, and as such it cannot be utilised as a direct measure for active transport. Equation 3 shows the relationship that was derived for the ER by Sugano et al. which was intended to enable the quantification of transporter-facilitated efflux [23]. It expresses the ER as a function of active efflux permeability facilitated by the P-gp transporter (P_{pgp}), and the passive diffusion through the apical membrane ($P_{\text{m,a}}$):

$$ER = \frac{P_{pgp}}{P_{m,a}} + 1 \tag{3}$$

Notably, the simple relationship presented in Equation 3 has the potential to be very meaningful, as it provides direct access to a proposed intrinsic value for active trans-

port (P_{pgp}) if the ER and the P_0 of the compound are known. This intrinsic value for active transport, would be analogous to the intrinsic P_0 value for passive transport [24]. As such, it should also be independent of both pH and other transport processes. Because of this, it would allow quantitative assessment of a compound's efflux which would be far more consequential than the ER. A quantitative understanding of active transport could be very beneficial for optimising drug disposition and action. Furthermore, it is needed for in vitro-in vivo extrapolation (IVIVE) of transport parameters and for physiologically based pharmacokinetic (PBPK) modelling, which would enable the development of predictive methods that could simulate various transport scenarios for pharmaceutical compounds of interest.

1.2.1 The effect of the ABL, filter and paracellular transport on the ER

Because the notion of intrinsic values as a measure of active transport covers new territory, its promise and validity must be probed. As stated before, an intrinsic value should naturally exclude effects from other transport processes. However, Equation 3 was derived for a simple three-compartment model that did not account for the aqueous boundary layer (ABL) or filter found in transport assays. Furthermore, paracellular transport, though included in the derivation of Equation 3 by Sugano et al. [23], was assumed to be negligible - an assumption that this current work proves to be invalid. Because of these conspicuous omissions to the model and the derivation of Equation 3, it cannot be presumed that this simplistic relationship remains valid for a more complete model that better represents the in vitro situation by accounting for ABL and filter permeability, as well as for paracellular transport. Without knowing whether the experimentally obtained ER truly represents only the two intrinsic values for passive and active transport, it cannot be certain that the right values for these processes are extracted using this relationship.

1.2.2 Ionisation and transporter species charge preference

Ionisation and species fractions also become relevant in more representative mathematical equations for the MDCK transport system - especially when it comes to ionisable compounds. For such compounds, it is crucial to know which species the efflux transporter preferentially acts on (if any) so that this can be factored into the model. Several in silico docking studies have attempted to answer the question of whether transporters have a preference for a particular species, but results have been largely inconclusive or contradictory. Some studies assume only transport of unionised compounds by default [25], [26], while others that compared both charged and neutral docking reported improved fits when only neutral docking was assumed [27]–[29]. However, there are also studies that found no difference in binding affinities between charged and neutral forms [30], [31]. The inconclusive nature of these in silico molecular docking studies highlight the fact that substrate species preference remains an open question.

1.3 Proposing an energy limit for active efflux

The second part of this work presented in Chapter 3 was in the pursuit of determining an energy threshold for active transport. The starting point for this work is the hypothesis that highly permeable compounds are less likely to exhibit significant transporter-facilitated efflux, as it would be too energetically expensive for the cell (and thus the organism) to counteract the high rates of passive diffusion for such compounds. Assuming there is a limit to the energy per time that a cell can maximally invest into its transporters, and if there is a 1:1 stoichiometry in the number of molecules transported and the number of ATP hydrolysed, then it should be possible to identify a membrane permeability value at which the passive influx of a chemical is higher than the maximally possible efflux, so that the cell can simply not afford efficient efflux any more. Chemicals which have a P_{m} value that exceeds the threshold P_{m} value are unlikely to exhibit significant efflux, as their high permeability would impose an unsustainable energy demand.

Aside from being used for the qualitative determination of whether compounds are efflux transporter substrates, results from bidirectional transport assays have also been used to accumulate data on the chemical nature of efflux transporter substrates. Comprehensive datasets, which include P-gp substrates and non-substrates alongside various physicochemical properties, have been compiled to identify patterns that correlate chemical properties with P-gp-mediated efflux [32]–[36]. If certain properties are found to be indicative of typical efflux substrates, it could streamline candidate selection for further drug development. Given the role of P-gp overexpression in MDR, which reduces the efficacy of chemotherapeutics, antibiotics, and antivirals, there is a strong demand for cost-effective, rapid methods to identify P-gp substrates. Such methods could not only help predict a compound's toxicity, bioavailability, and drug-drug interaction potential [37], but also enable the early elimination of problematic candidates, mitigating MDR-related challenges during drug discovery [35]. Ultimately, these studies aim to establish predictive tools or guidelines that highlight the shared properties of efflux substrates, aiding in the identification of compounds likely to interact with key efflux transporters. Several complex and quite detailed in silico models based on statistical techniques or machine learning (including Quantitative Structure Activity Relationship (QSAR)) models, have already been employed for the development of such theoretical models [33], [35], [36], [38]–[42]. A review of the methods, descriptors used and performance of these and other models can be found in Chen et al. [43]. However, such models suffer from a series of drawbacks that makes them unwieldy guides for most chemists during lead optimisation. These disadvantages include its poor interpretability due to the advanced nature of the algorithms, or the large amounts of elaborate, often obscure, descriptor types they utilise. Furthermore, these predictive models are usually trained on rather limited datasets that only cover a narrowly-defined chemical space, which means their suitability for the broader chemical space remains unproven. The quality of these models and their output is highly dependent on the quality of the underlying data, and the robustness of most of the datasets used for these tools

is dubious since data from different experimental protocols are often mixed together. Monolayer efflux, ATPase and calcein-AM/Rhodamine 123 fluorescence assays, etc. are used indiscriminately to group compounds into different classes- often with conflicting results between assays or sources.

In addition to these highly complex models, and in order to address their drawbacks, efforts have also been made to develop simple and fast interpretations of the molecular features that contribute to being an efflux substrate [33], [44], [45]. These studies aim to establish simple and widely-applicable "rules of thumb" for hit-to-lead optimisation. It has been posited that such simple rules may have a greater impact than complex, predictive models [37]. At the very least, they can certainly complement statistical models. In this Chapter, we propose another simple and easily applicable rule-of-thumb through the idea of the energy limit. Stated simply, we argue that compounds above a certain passive permeability threshold will not be significantly affected by active efflux. The idea that drugs with a high passive permeability do not exhibit significant efflux is not particularly novel, as the Biopharmaceutics Classification System (BCS) [46] states that Class I drugs (highly permeable and highly soluble drugs) are minimally affected by transporters. As a result, the FDA has granted biowaivers for BCS Class I drugs, making them the only drug class exempt from the typical recommendation to conduct monolayer efflux assays during development, since efflux transporters are not expected to significantly influence their disposition [47]. More recently, the Biopharmaceutics Drug Disposition Classification System (BDDCS) [48], re-affirmed that Class III and Class IV drugs in the low permeability category are predominantly eliminated unchanged (and therefore unmetabolised) into urine and bile. The proposition that the disposition of very permeable drugs are not affected by efflux transporters is also affirmed by several other sources, such as Fischer et al. [49] who found that molecules with low membrane permeability are more prone to be transported by P-gp compared to molecules with similar P-gp interaction potential and higher membrane permeability. Furthermore, studies by Mahar Doan et al. [50] and Wager et al. [51] already reported that highly permeable central nervous system (CNS) drugs are less likely to be P-gp substrates. Indeed, 70 % of CNS drugs on the market are highly permeable and thus not P-gp substrates [52]. Broccatelli et al. [52] took this further by linking the properties that are often implicated in "simple rules" for P-gp substrates with increased chances of being a P-gp substrate and having a low permeability, rendering such drugs blood brain barrier (BBB) negative drugs due to their high efflux rates and consequent inability to penetrate the CNS.

The aim of the work performed in Chapter 3 was to investigate our starting hypothesis and to see whether it could be translated into a rule for quick, membrane permeability-based separation of compounds that can exhibit significant transporter-facilitated efflux from those that cannot. At this juncture, it is vital to differentiate between this proposed method of separation and other classification methods. To be clear, the permeability-based separation proposed here does not differentiate between efflux substrates and non-substrates. Instead, it distinguishes compounds whose disposition can

be significantly influenced by efflux transporters from those that cannot, regardless of whether they are actual substrates. A rule-of-thumb for permeability-based separation could be very useful if applied in drug classification, or could be used for the rational direction of lead optimisation towards desired efflux effects (whether that be efflux or no efflux). In contrast to the aforementioned BCS/BDDCS and FDA biowaiver where categorisation of low vs high permeability drugs is primarily based on bioavailability studies, the energy threshold rule could directly be linked with membrane permeability, for which reliable estimates can be obtained comparatively easy, often without the need for additional experimental assays. Furthermore, since this rule is based on a fundamental physical principle (the energy limit of the cell) it is not restricted to P-gp only, but should be applicable to any efflux transporter. As such, we not only investigate this principle for P-gp as the most important efflux transporter, but also for the two other aforementioned ATP-dependent, apically-localised efflux transporters implicated in MDR: BCRP and MRP2.

1.4 Objectives

1.4.1 Probing the viability of the intrinsic value for efflux

The first part of this work presented in Chapter 2 was an attempt to probe the viability and utility of using intrinsic values to quantify active transport, instead of relying on the ER as a primary measure of drug efflux. As such, the aims were (i) to determine what the possible effects are on the ER when the measured permeability of a compound is dominated by the ABL and/or the filter, (ii) to determine the influence of paracellular transport on the ER and iii) to explore a potential method for determining the efflux pump's substrate species preference to account for the speciation of ionisable chemicals.

1.4.2 Determining an energy threshold for efflux

The second part of this work presented in Chapter 3 was an investigation into the theory of an energy threshold. It is proposed that for compounds past a certain permeability, it would be too energetically expensive for the cell to maintain efflux against their high rates of passive diffusion. As such, the aims were (i) to evaluate existing MDCKII ER data for the three most important efflux transporters (MDR1, BCRP and MRP2) and to identify a crude membrane permeability cut-off line above which compounds no longer seem to be affected by active efflux. Compounds that appear to violate the established threshold can then be identified as outliers and systematically investigated using a variety of measures. Secondly, it was aimed (ii) to identify compounds that lie at or near the threshold so they can be investigated with concentration-dependent monolayer efflux assays. These data can then be used to identify the maximal flux (i.e the maximal amount of compound that can be actively effluxed) and the corresponding energy plateau for such compounds. Finally, we aimed (iii) to link this energy limit with a certain P_{m} value and to perform a sensitivity analysis, highlighting all the caveats and limitations that come with such a rule-of-thumb P_{m} threshold.

2 Quantification of Active Transport

2.1 Theory

2.1.1 Transport model for MDCK cells

Figure 1 shows a comparison between permeation over a cell monolayer grown on a filter, and permeation across the epithelial cells of the intestine. This figure illustrates the difference between the in vivo and in vitro scenarios: the additional resistance introduced by the filter in in vitro assays, as well as the in vitro system's thicker ABL.

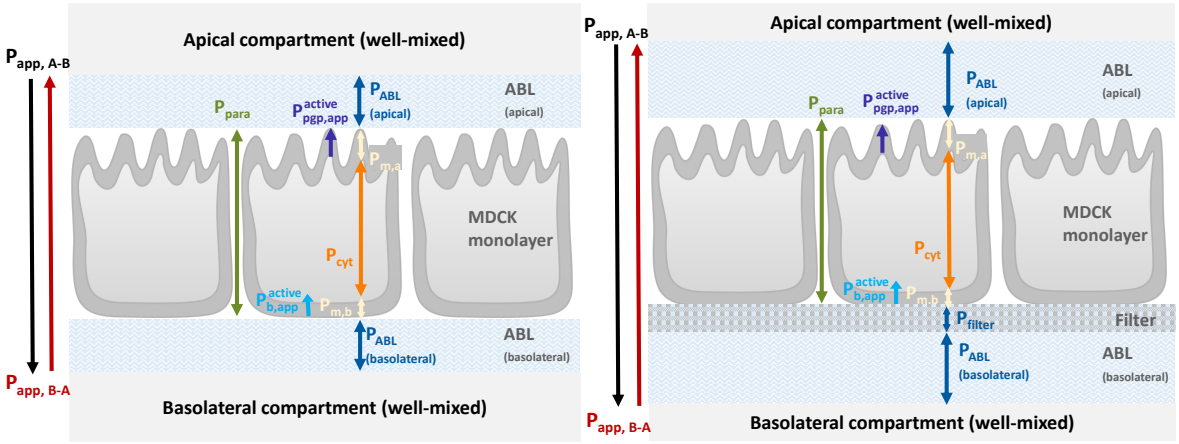

Figure 1: **Permeation barriers and associated permeabilities in vivo and in vitro**. In vivo, well-mixed donor and acceptor compartments are separated by apical ABL, cell monolayer, and basolateral ABL. The in vitro system introduces a filter layer and thicker ABL (not to scale). From Kotze et al. [53]

The mechanistic transport model used in this work was initially set up to describe the passive permeation of compounds over a complete monolayer [24], [54], taking into account the additional or altered resistances brought about by the in vitro transwell set-up. The starting point of this current study on active transport was to adapt the existing passive transport model so that it encompasses the active efflux facilitated by a transporter like P-gp. Thus, in addition to accounting for the filter and ABL resistances, active efflux from the apical membrane was also incorporated into the model to account for the significant P-gp activity expected in MDCKII-MDR1 cells. However, during the course of this work, we also established the presence of an additional uptake transporter located in the basolateral membrane. Though it was not unexpected that other transporters besides P-gp are expressed in these cells, efflux activity determined from assays with transfected cells (such as the MDCKII-MDR1 line) is generally ascribed solely to apically located efflux transporters such as P-gp or BCRP. However, due to evidence gathered in this study that an uptake transporter affects both the $B \rightarrow A$ apparent permeability and the ER in MDCK cells, the permeability facilitated

by this transporter was also eventually included in the model. The addition of both transporters, as well as the implications of the ABL and filter for efflux ER will be discussed in the succeeding Section 2.1.2.

The transport model is composed of the varying resistances found in series and parallel that a compound encounters as it permeates from one compartment to another across the cell layer. The permeability (P) through each barrier is inversely proportional to its resistance. From Figures 1-2 it can be seen that the first serial resistance encountered is that of the apical ABL ($P_{\mathrm{ABL,a}}$). Following this, there are two pathways found in parallel that a compound may use to cross the monolayer. Compounds can either cross through the membranes and cytosol of the cells, thereby taking the transcellular (trans) pathway (P_{trans}). However, compounds can also permeate through water-filled pores in the tight junctions between cells, thereby taking the paracellular (para) pathway (P_{para}). When compounds take the trans route, the first resistance encountered is that of the apical membrane ($P_{\mathrm{m,a}}$), followed in series by the cytosol (P_{cyt}) and the basolateral membrane ($P_{\mathrm{m,b}}$). Within the cell layer, the active transporters P-gp (P_{pgp}) and the basolateral uptake transporter (P_{b}) are found in parallel to the passive diffusion through the membrane in which the respective transporter is embedded. In contrast to passive diffusion, the permeability facilitated by these active transporters is uni-directional. After crossing the monolayer, the compound finally encounters the filter (P_{filter}) and the basolateral ABL ($P_{\mathrm{ABL,b}}$), both found in series. The total permeability through all these barriers which is measured by the transport assays is known as the apparent permeability, P_{app}, which is thus a function of all individual permeabilities found in series and parallel. P_{app} can be sub-divided into the contributions of these constituent parts, which allows for the individual evaluation and quantification of permeability through each layer.

Passive diffusion through the aqueous layers is calculated from the thickness of the respective layer (x) and the diffusion coefficient of the compound in water (D_{w}), which can be estimated from the molecular weight of the compound according to the relationship determined by Avdeef et al. [55], [56]. The permeability through the ABL, for example, is simply the quotient of these two factors, $\frac{D_w}{x}$. However, for other aqueous layers such as the filter, the reduced surface area available for permeation through the filter pores is also factored into P_{filter} [57]. For P_{cyt} it is instead the diffusion coefficient of the chemical in the cytosol D_{cyt} that is used, which is estimated as one quarter of D_{w} [58].

The apical membrane is folded to form microvilli. As a result, it is generally assumed to have a greater surface area than the basolateral membrane. Thus, in the initial stages of this work a factor of 24 was applied to Eq. 2 to calculate apical membrane permeability [59]. However, uncertainties in this factor was acknowledged due to differences between Caco-2 cells and MDCK cells [60]. The factor has been reported to be lower for MDCK cells [61], suggesting that its use could potentially result in an underestimation of apical membrane resistance. Remaining conscious of the uncertainty around this

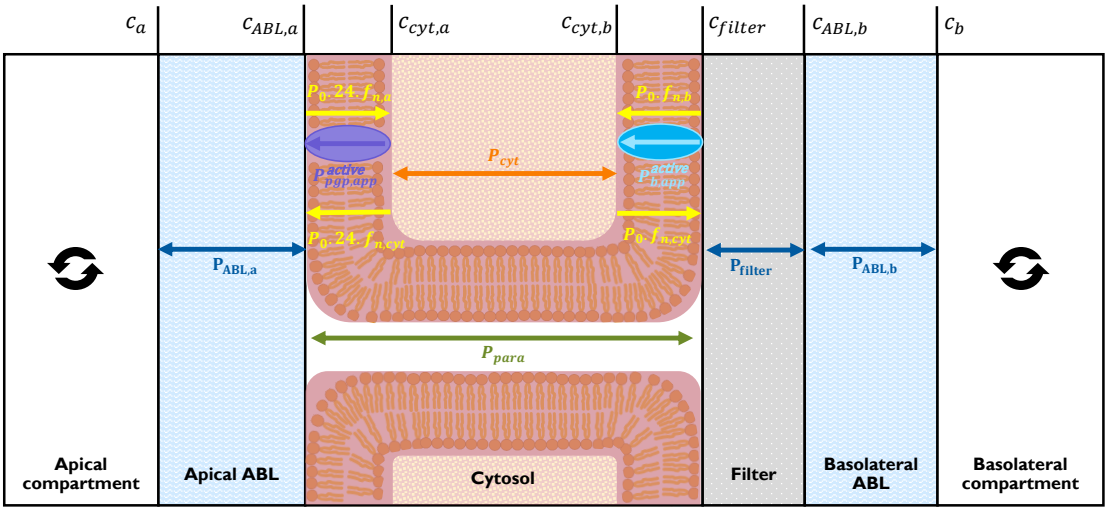

Figure 2: **Permeation barriers, associated permeabilities and concentrations in Caco-2 and MDCK transwell assays.** From Kotze et al. [53]

factor, conclusions drawn from this study were tested with and without this factor of 24. For the work presented in Chapter 2, the magnitude of the factor used had no bearing on the qualitative results.

2.1.2 Model adaptations

Assuming the iso-pH method (where the basolateral and apical pH is the same), the following expression was derived for the steady-state flux in the $A \rightarrow B$ direction under constant donor concentrations (C_a, the concentration in the apical compartment in the $A \rightarrow B$ direction) and infinite sink conditions (concentration in the basolateral compartment $C_b = 0$):

$$J_{A\rightarrow B} = \frac{1}{\frac{1}{P_{ABL,a}} + \frac{1}{P_{trans,A\rightarrow B}} + (1 + \frac{P^{active}_{pgp,app}}{P_0 \cdot 24 \cdot f_{n,cyt}}) \cdot (\frac{1}{P_{filter}} + \frac{1}{P_{ABL,b}})} \cdot C_a \tag{4}$$

where:

$$P_{trans,A\rightarrow B} = \frac{1}{\frac{1}{P_0 \cdot 24 \cdot f_{n,a}} + (1 + \frac{P^{active}_{pgp,app}}{P_0 \cdot 24 \cdot f_{n,cyt}}) \cdot (\frac{1}{P_{cyt} \cdot \frac{f_{n,a}}{f_{n,cyt}}} + \frac{1}{P_0 \cdot f_{n,a}})} \tag{5}$$

Accompanying equations for $J_{B\rightarrow A}$ and $P_{trans,B\rightarrow A}$, as well as all flux and transport equations in both directions (including derivations) that comprise the model can be found in Kotze et al. [53] (without the basolateral transporter) and Kotze et al. [62]

(with the basolateral transporter). Substituting the flux equations into Equation 1 (iso-pH method) results in the following expression for the ER:

$$ER = \frac{P_{trans,A\to B} \cdot (1 + \frac{P_{pgp,app}^{active}}{P_0 \cdot 24 \cdot f_{n,cyt}}) \cdot (1 + \frac{P_{b,app}^{active}}{P_0 \cdot f_{n,b}}) + P_{para}}{P_{trans,A\to B} + P_{para}} \quad (6)$$

The following sections expound on the adaptations to the model applied in this study which can be observed in the above equations.

2.1.2.1 Inclusion of efflux transporter in the apical membrane. As described in the previous section, the model which initially only described passive permeation was adapted to include active transport by accounting for apical efflux by P-gp in the MDCKII-MDR1 cells. Figure 2 (which depicts the compartments and permeation resistances that comprise the model) accentuates two very crucial differences between active transport and passive diffusion that need to be considered when incorporating an active transporter. First, active transport (in this case $P_{\text{pgp}}^{\text{active}}$) is unidirectional, whereas passive diffusion is not. Secondly, active transport is driven by the substrate concentration at the transporter's binding site, and not by a concentration gradient [53].

2.1.2.2 Inclusion of ABL, filter and paracellular transport in derivation of ER. Compared to previous studies, this study was the first to derive an expression for the ER of MDCKII-MDR1 assays that accounts for the filter and ABL. These resistances were not only included in the transport equations, but it was also experimentally investigated how they may affect the ER. To simplify the analysis for this question, compounds with a greater passive permeability were selected. For such compounds, it can be expected that the P_{app} is dominated or affected to various extents by the ABL or filter [53]. It could thus also be assumed that the role of paracellular transport for these compounds is negligible. In this case, a simplified version of Equation 6 was used in which P_{para} is insignificant [53].

Aside from this very particular aforementioned scenario where P_{para} can safely be assumed to be insignificant, the effect of this pathway on the ER has not yet been established prior to this study. Though other studies did take paracellular transport into account in their model, it was presumed to be negligible with seemingly no basis for such an assumption [23]. Because this assumption was not validated and suspected to be unrealistic for most compounds, another change to the model in this study was to explicitly include paracellular transport in the model in order to quantify the effect of this pathway on overall flux and the ER [53]. P_{para} is expected to be the dominant transport route for all chemicals with a lower passive membrane permeability, and it may also become relevant for ionisable compounds at certain pH values [24].

2.1.2.3 Inclusion of a basolateral uptake transporter. As mentioned in Section 2.1.1, after obtaining evidence for an uptake transporter embedded within the basolateral membrane, the model was also adapted to include the permeability facilitated by it ($P_{\mathrm{b}}^{\mathrm{active}}$) with similar considerations as mentioned in Section 2.1.2.1 [62].

2.1.2.4 Inclusion of species preference for transporters. When dealing with ionisable chemicals, it must be considered whether the ionisation state could affect active transport. Similar to membrane permeability, if transporters primarily act on either the neutral or ionic species, this could have quite significant consequences and certainly has to be accounted for in the model. As such, the model was adapted to account for such a possibility [62]. Because it is not known which species the transporters prefer, different scenarios were evaluated and compared by factoring the neutral or ionic fractions (f_{n} or f_{i}) into their permeabilities. For this, we defined the apparent permeability facilitated by P-gp and the basolateral transporter as $P_{\mathrm{pgp,app}}^{\mathrm{active}}$ and $P_{\mathrm{b,app}}^{\mathrm{active}}$, respectively. These variables are defined as follows under the different scenarios:

1. The transporter acts on the neutral species:

$$P_{pgp,app}^{active} = P_{pgp} \cdot f_{n,cyt} \tag{7}$$

2. The transporter acts on the ionic species:

$$P_{pgp,app}^{active} = P_{pgp} \cdot f_{i,cyt} \tag{8}$$

For P-gp, as an efflux transporter which pumps molecules out of the cell, the speciation factors are applied to the cytosolic concentration (Eq. 7-8). These equations are explicitly depicted here for P-gp, but the same principles apply for the treatment of the basolateral transporter, and is thus applied to the concentration in the basolateral compartment instead.

2.2 Materials and Methods

2.2.1 Cells and cell culture

The MDCKII cells transfected with with the human MDR1 gene for over-expression of P-gp were obtained from The Netherlands Cancer Institute (Amsterdam, The Netherlands). The cell medium was Dulbecco's modified Eagle medium (DMEM) (1X) + GlutaMAX™-I from Life Technologies Ltd. (Paisely, UK) supplemented with 10% fetal bovine serum (FBS), 100 U/mL penicillin and 100 µg/mL streptomycin from Life Technologies Corporation (New York, USA). Cells were maintained at 37 °C in an atmosphere of 5% CO_2 and passaged twice a week.

2.2.2 Bidirectional MDCK transport assays

MDCII-MDR1 cells (passages 20 and 40) were seeded onto 12-well transwell inserts from CellQART (Northeim, Germany; pore size: 0.4 µm; filter thickness: 11.5 µm) with a porosity of 100×10^6 pores/cm^2, unless otherwise indicated. Cells were seeded at a density of 1.5×10^5 cells/insert. After seeding, cells were maintained as described in Section 2.2.1 for 4 days to ensure confluent monolayer growth. One day before experimentation, the cell medium was exchanged. Inserts were washed with Hank's balanced salt solution (HBSS) from Biowest SAS (Nuaillé, France) to remove residual DMEM before initiation of the transport assays. The transport rates of test compounds were determined in both the apical-to-basolateral ($A \to B$ direction) as well as the basolateral-to-apical ($B \to A$ direction). Stock solutions of compounds were prepared in the transport buffer, and all solutions were pre-warmed to 37 °C. Experiments for each compound also included a reference compound to confirm consistent P-gp expression and/or activity. The pH of the buffer and stock solutions were controlled with a rapid pH automated pH meter (Hudson Robotics, Inc., Springfield, NJ, USA) prior to the experiment, as well as the pH of all samples after experiment completion. Inserts were used in 12-well plates from TPP Techno Plastic Products AG (Trasadingen, Switzerland). The basolateral compartment volume was 1.6 mL, and the apical compartment volume was 0.5 mL. Transport in the $A \to B$ direction was measured by placing inserts in plates with transport buffer in the basolateral compartment, after which the test compound solution was added to the apical compartment to initiate the transport assay. At each sampling step, inserts were placed into fresh buffer and the buffer from the previous step was sampled. For the $B \to A$ direction, inserts were placed in plates with the test compound solution in the basolateral compartment, after which transport buffer was added to the apical compartment for assay initiation. At each sampling step, 300 μL were sampled from the apical compartment (the maximum volume that could be removed without disturbing the cell layer) and replaced with an equal volume fresh buffer. Sampling occurred at 3-4 time intervals. Time steps of sampling were determined specifically for each compound and direction of measurement to ensure sink conditions. Between sampling steps, plates were kept in a Titramax and Inkubator 1000 orbital shaking incubator from Heidolph Instruments GmbH & Co. (Schwabach, Germany) at 450 rpm and 37 °C. For both directions of measurement, the donor compartment was sampled at the final sampling step to determine the mass balance.

2.2.2.1 Varying ABL and filter resistances To evaluate the effect of the ABL and filter on the ER, these two resistances were experimentally varied. P_{filter} was varied by using filters with different pore densities. P_{ABL} was varied by keeping plates stationary instead of shaking, thereby increasing the thickness of the ABL. To this end, the assays described in Section 2.2.2 were adjusted as follows: To study the effect of varying filter resistance, inserts from the same supplier with the standard high porosity of 100×10^6 pores/cm^2, as well as those with a low porosity of $2 \times$

10^6 pores/cm^2 were used. Bidirectional transport was determined in duplicate under different stirring and filter conditions: high-porosity filters, stirred (HPS); high-porosity filters, unstirred (HPU); and low-porosity filters, stirred (LPS). The transport buffer was HBSS with 25 mM HEPES from Sigma-Aldrich (St. Louis, USA) at pH 7.4. HPU experiment plates were not placed in the orbital shaker, but were instead kept stationary at 37 °C in a Heraeus HERAcell 150 CO_2 Incubator from Thermo Electron LED GmbH (Langenselbold, Germany). Candidate compounds for which paracellular transport is not expected to affect P_{app} were chosen based on reported efflux ratios > 2, and according to their $\log K_{hex/w}$ as predicted by the UFZ LSER database [63] to ensure ABL-limitation. The compounds dipyridamole from Alfa Aesar (Haverhill, USA)($\log K_{hex/w}$:−4.89), quinidine (Sigma-Aldrich) ($\log K_{hex/w}$:0.14), and loperamide (Sigma-Aldrich) ($\log K_{hex/w}$:−0.45) were used.

2.2.2.2 Measurement of P_0 Where possible, parallel assays were performed for each compound to determine P_0. Inserts for such assays were pre-incubated for 30 min in HBSS with 2 µM of the P-gp inhibitor elacridar (Sigma-Aldrich) in DMSO from Th. Geyer (Renningen, Germany). Stock solutions of the test compound with 2 µM elacridar were used for these assays. The final DMSO concentration of the stock solution was never more than 0.05 %, thereby avoiding any potential effects of DMSO on the transporter [64]. Consequently, an equal concentration of DMSO was added to the transport buffer to prevent potential DMSO gradient effects. The pH values of transport buffers and stocks were selected to avoid paracellular or ABL dominance.

2.2.2.3 Measurement of P_{para} In order to determine paracellular transport for a given compound, assays were performed as described in Section 2.2.2 with the following changes: When the measured compound was known to be actively transported, inhibitor was used. Thus, inserts for such assays were also pre-incubated with elacridar, and stock solutions of test compounds with 2 µM elacridar were used. The buffer and stock pH values were selected to ensure paracellular dominance depending on the pKa of the compound. Where paracellular marker compounds were used and known not to be transported, no inhibitor was used.

2.2.2.4 pH dependence From Equations 7-8 and the ER expression it was postulated that the ER measured as a function of pH can give an indication as to whether increasing or decreasing the available fraction of a specific species has likely affected P_{pgp}, provided that P_{para} is not dominant. It has been established that cytosolic pH changes with external pH [24], [65], [66] rather than being buffered to remain at pH 7.4 as is often suggested. As such, cytosolic pH was estimated as a function of external pH according to the linear relationship determined by Dahley et al. [24]. Consequently, MDCKII-MDR1 experiments were performed where the ER was determined for the same compound at different external pH values (using the iso-pH method). These experiments were performed across a range of pH values which were determined to not

be detrimental to the integrity of the monolayer [67]. The assays described in Section 2.2.2 were performed in duplicate or triplicate for 4-5 different pH values between pH 5 and pH 9. The transport buffer was HBSS buffered with 10 mM MES (Sigma-Aldrich) for pH 5 and 6, 25 mM HEPES for pH 7, 7.4 and 8, and 10 mM TAPS (Sigma-Aldrich) for pH 9. Stock solutions were prepared in the transport buffer and pre-warmed to 37 °C. Candidate compounds for pH dependence assays were selected based on reported P-gp substrates with efflux ratios > 2 [68]–[70]. Three bases were used: 15 μM acebutolol (pKa: 9.18 [71]), 100 μM doxorubicin (pKa: 9.56 [72]) and 14 μM talinolol (pKa: 9.4). One acid was used: 10 μM etoposide (pKa: 8.53 [71]). And finally, two non-dissociating compounds were used: 10 μM digoxin and 50 μM colchicine. Concentrations were chosen to avoid saturation effects and still be within the limits of LC-MS quantification.

2.2.2.5 Evaluation of cell monolayer integrity Prior to and after the transport assays, the trans-epithelial electrical resistance (TEER) across the cell monolayer was measured for each insert at 37 °C at three positions using an EVOM epithelial tissue volt/ohmmeter (World Precision Instruments Inc., Sarasota, FL, USA) to confirm that the integrity of the cell monolayers was maintained throughout the experiment, and to ensure consistent and even monolayer formation between experiments. In addition, Lucifer yellow (LY) from Sigma-Aldrich was used as a paracellular marker to confirm the integrity of the cell monolayer. After the transport assays, the LY permeability of each insert was evaluated by measuring the fluorescence intensity (Ex: 485 nm, Em: 538 nm) of samples from the basolateral compartment using a SpectraMAX Gemini EM spectrophotometer (Molecular Devices LLC., San Jose, CA, USA). Inserts with a LY permeability above the pre-defined threshold of 1.5×10^{-6} cm/s were excluded [73], except if the derived P_{app} results of those inserts were qualitatively similar to those determined for replicate inserts within the LY threshold (based upon responsible scientific judgment).

2.2.2.6 Sample analysis Samples were analysed with an Infinity II 1260 LC system coupled with a 6420 triple quadrupole 145 with ESI source (Agilent Technologies Inc., Santa Clara, CA, USA). Either a Kinetex® F5 (2.6 µm; 100 Å; 50 ∗ 3.0 mm) or a Kinetex® C18 (2.6 µm; 100 Å; 50 ∗ 3.0 mm) LC column was used (Phenomenex Inc., Torrance, CA, USA). Gradient elution was performed with double-distilled water (1% MeOH and 0.1% HCOOH; pH 2.7) as well as MeOH (0.1% HCOOH), which were used as the aqueous and organic eluents, respectively. P_{app} was calculated from acceptor compartment concentrations, C_A, measured for at least two consecutive timepoints as follows:

$$P_{app} = \frac{C_{A,tx} - C_{A,tx-1}}{t_x - t_{x-1}} \times \frac{V_A}{A \times \Delta C} \tag{9}$$

where $\frac{C_{A,tx}-C_{A,tx-1}}{t_x-t_{x-1}}$ is the change in the cumulative concentration in the acceptor compartment per each elapsed time interval, V_A (cm^3) is the volume of the acceptor com-

partment, A (cm^2) is the filter area, and ΔC ($\mu g/mL$) is the concentration difference between the compartments calculated for each individual time step. A correction for the incomplete volume exchange in the $B \rightarrow A$ was factored into the calculation of P_{app} in this direction. P_{app} values at each timestep were corrected with the calculated recovery as done by Neuhoff [74]. Data are presented as the mean of the recovery-corrected $P_{app} \pm$ standard deviation of at least two timestep samples of both replicates. The first timestep in the $A \rightarrow B$ direction was excluded in order to account for lag time [75]. The ER was calculated as the ratio of the mean P_{app} values in the $B \rightarrow A$ direction and $A \rightarrow B$ direction according to Eq. 10:

$$ER = \frac{P_{app,B\rightarrow A}}{P_{app,A\rightarrow B}} \tag{10}$$

2.2.3 Modeling

Global fits of both $A \rightarrow B$ and $B \rightarrow A$ transport were performed by employing varying assumptions using Igor Pro 7 software (WaveMetrics Inc., Lake Oswego, USA) and were weighted by standard deviation. The following three scenarios were evaluated: a) Both transporters act on the neutral fraction, b) both transporters act on the ionic fraction and c) the apical transporter acts on the neutral species, and the basolateral transporter acts on the ionic species. The latter configuration was included in our analysis due to an evaluation of the literature which suggests that the basolateral transporter in epithelial cells could be an ATP-independent organic cation or anion transporter (of the OAT or OCT families) [76]–[81]. P_{cyt}, P_{filter}, pK_a, the diffusion coefficient in water D_w, the surface area of the apical membrane, as well as the individual thickness of the apical (x_a) and basolateral ABL (x_b) (determined experimentally for our set-up [62]) were set as fixed parameters. As described in Section 2.1.1, a factor of 24 was used to account for the increased surface area of the apical membrane, however, due to the uncertainties regarding this value the fits were also performed under the assumption of equal membrane surface areas.

2.3 Results and Discussion

2.3.1 Effect of ABL and filter on bidirectional flux and the ER

Full flux equations considering all the transport processes and resistances outlined in Section 2.1 were formulated for both transport directions, and analysis was done with simplified versions of these equations. Under the assumption of negligible paracellular transport (justified for neutral compounds that are ABL-limited) and using the iso-pH method, it was found that each single resistance, including P_{pgp}, can completely dominate $A \rightarrow B$ flux if it is large enough. In contrast, the influence of active efflux by P-gp can never dominate $B \rightarrow A$ flux, but can at best level out the resistance in the apical membrane and ABL so that the total flux is governed only by the basolateral

resistance.

When the formulated bidirectional transport equations are substituted into Equation 10, the following expression for the ER as a function of the permeability of the apical membrane ($P_{m,a} = P_0 \cdot 24 \cdot f_{n,cyt}$) and the intrinsic permeability of the P-gp transporter (P_{pgp}) is obtained:

$$ER = \frac{P_{pgp}}{P_{m,a}} + 1 \tag{11}$$

Notably, this simplistic expression for the ER mirrors the one obtained by Sugano et al. [23] for the less realistic three-compartment model (Equation 3). Thus, results for the more detailed model indicate that the resistances of the cytosol, basolateral membrane, filter, and both ABLs cancel out in their effect on the ER. The fact that this simple equation holds true (under the iso-pH method) for our more representative model approach is by no means intuitive, since including the additional resistances with their respective physical considerations results in a considerably more complex mathematical scenario. In this unique case, the ER thus solely depends on the relative influence of active transport and the passive resistance in the apical membrane (or, more precisely, the passive resistance that is found in parallel with the active transporter). Therefore, affirming this relationship renders the ER a very meaningful parameter for the quantification of intrinsic information of active efflux provided that P_{para} is negligible and there is no pH gradient. Evidently, experimental ER values provide easy access to the proposed intrinsic value of P_{pgp} if $P_{\text{m,a}}$ is known. These mathematical results suggest that the ER is actually independent of ABL/filter limitation, and that the dominance of these aqueous layers has no bearing on efflux data.

This mathematically-derived hypothesis that the ER should be independent of ABL and/or filter effects was then investigated experimentally in order to determine what the influence of ABL/filter variance is on the ER in reality. The P_{app} values were measured in both directions for each respective condition described in Section 2.2.2.1. These values, as well as the resultant ER values are depicted in Table 1. Table 1 shows that P_{app} values determined under these varying experimental conditions differ substantially. This is to be expected for the relatively hydrophobic chemicals examined, as the flux in one or both directions would be dominated by the ABL or filter resistance under one or more of the three experimental conditions. In other words, the P_{app} determined in either direction is a measure of P_{ABL} or P_{filter} as it is varied. These data corroborate our mathematical findings that aqueous permeation barriers do indeed affect absorptive and secretory flux, as P_{app} values for the tested compounds differ by up to a factor of 10 when these barriers are experimentally manipulated. Notably, the ER remains almost constant, fluctuating only within the experimental error, unlike the substantial differences observed in P_{app} between directions measured and experimental conditions.

Table 1: P_{app} values in the $A \rightarrow B$ and $B \rightarrow A$ directions ± standard deviation. P_{app} represents the mean of at least three timepoints and two replicates (n = 2). ER represents the quotient of $P_{app,B\rightarrow A}$ over $P_{app,A\rightarrow B}$. HPS: High-porosity filter, stirred. LPS: Low-porosity filter, stirred. HPU: High-porosity filter, unstirred.

		$\boldsymbol{P_{app,A\rightarrow B}}$ [$\times$ $\mathbf{10^{-6}}$$\boldsymbol{cm/s}$]	$\boldsymbol{P_{app,B\rightarrow A}}$ [$\times$ $\mathbf{10^{-6}}$$\boldsymbol{cm/s}$]	**ER**	**Recovery** [%]
Dipyridamole (12 μM)	HPS	4.03 ± 0.28	97.2 ± 13.9	24.2 ± 4.1	91.0–108
	LPS	0.38 ± 0.06	7.20 ± 1.30	19.8 ± 5.7	90.3–114
	HPU	2.71 ± 0.42	52.5 ± 8.77	19.3 ± 1.5	78.9–90.9
Quinidine (12 μM)	HPS	65.2 ± 6.32	145 ± 8.26	2.2 ± 0.13	73.7–98.5
	LPS	12.4 ± 0.07	24.9 ± 0.87	2.0 ± 0.11	78.9–100
	HPU	27.0 ± 5.65	52.3 ± 9.75	2.0 ± 0.26	76.8–121
Loperamide (10 μM)	HPS	46.7 ± 5.03	126 ± 27.8	2.7 ± 0.73	75.0–88.1
	LPS	5.65 ± 0.42	15.9 ± 4.24	3.2 ± 0.91	69.2–86.1
	HPU	9.80 ± 2.84	29.2 ± 3.31	2.8 ± 0.87	62.3–81.3

The experimental results depicted in Table 1 validate our mathematical findings that the effects of the ABL and filter are cancelled out and have no bearing on the ER. This finding is quite consequential, as it indicates that when performing monolayer transport assays to determine the ER, one does not need to be concerned with measures (whether stirring, pH manipulation, etc.) to ensure that compounds are measured above the ABL or filter limitation for the investigation of hydrophobic chemicals. In contrast, such measures are crucial in the determination of passive membrane permeability.

2.3.2 Effect of paracellular transport on bidirectional flux and the ER

For hydrophilic chemicals, or depending on the pKa and pH of the assay, paracellular transport does indeed become significant and can no longer be assumed negligible. In this case, P_{para} must be explicitly considered in the flux and ER equations. These derivations show that in this case, Equation 11 is no longer valid, and the ER equation becomes substantially more complex (Equation 6). Of particular note is the special case when P_{para} dominates in both transport directions. In this case, it is found that the ER = 1. This means that when a compound is primarily transported via the para route, carrier-mediated transport may be masked. As a result, when assays are performed with chemicals for which P_{para} dominates, it may be incorrectly assumed that no efflux occurs because a non-significant ER of one is measured. In reality, there may be transport that can simply not be quantified as a consequence of P_{para} dominance and its effect on the ER. Evidently, in contrast to ABL limitation, paracellular transport does have a notable effect on the ER, and the effect can be significant enough to reduce the ER to unity. As a result, it appears that while it is not necessary to

take measures to avoid ABL or filter limitation, it is imperative to avoid complete paracellular transport dominance, or to account for the paracellular contribution when calculating the ER. Otherwise, any meaningful determination of intrinsic values would be impossible. Experimental evidence that substantiates these findings and illustrates the effect of paracellular transport on flux and the ER will be presented in the next section.

2.3.3 Transporter species preference

2.3.3.1 The pH dependence of the ER Figure 3 shows the ER and P_{app} values determined across a range of pH values for each of the six compounds investigated in the pH dependence assays. If one assumes that the function of the transporters is not affected by pH, it can be postulated that non-dissociating compounds will not show much discrepancy in P_{app} values, and that the ER will remain relatively stable across the pH range. Figure 3: E and F depict the results obtained for the two non-dissociating compounds, colchicine and digoxin. For these compounds, the f_{n} is the same at every pH, however, one can see that the $P_{app,B\rightarrow A}$ does fluctuate somewhat, and that the ER drops at the extreme ends of the pH range. This suggests that one or both of the transporters may be susceptible to pH effects, a finding that complicates this approach towards the transporter species preference. For the basic compounds acebutolol, doxorubicin and talinolol (Figure 3: A, B and C), the ER tends to increase with increasing pH (i.e increasing f_{n}) in the low pH range. As such, one would expect the opposite trend for acidic compounds, where f_{n} increases with decreasing pH, and this is indeed observed for the anionic compound etoposide (Figure 3: D).

The decrease in ER with decreasing f_{n} is to be expected due to the influence of paracellular transport described in Section 2.3.2. As discussed, we determined that the ER reduces to unity when paracellular transport dominates the flux in both directions. Furthermore, even when not dominant, paracellular transport can affect the ER. The closer it is to dominance, the greater the effect. As such, for the bases (A, B and C) the clear trend of increasing ER with increasing pH (in the low pH range) shows that at lower f_{n} values, paracellular transport competes with transcellular transport, or dominates the flux entirely, which results in lower ER values or an ER of 1. Likewise, the acidic etoposide shows the opposite trend, with the same rationale that paracellular transport is more likely to be favoured the smaller the f_{n} available for transcellular transport.

The unexpected drop in ER observed for the bases acebutolol and talinolol at pH 9 and 8, respectively, might indicate at least partially transported ions (see Kotze et al. [53] for theoretical graphs curves depicting the pH dependence of P_{app} and ER for a generic efflux substrate under different transport assumptions). However, due to the observed decline in active transport even for non-dissociating compounds (Figure 3 E and F) at high pH values, these trends could also be ascribed to potential effects of these extreme pH values on the transporter. Even though the range of buffer

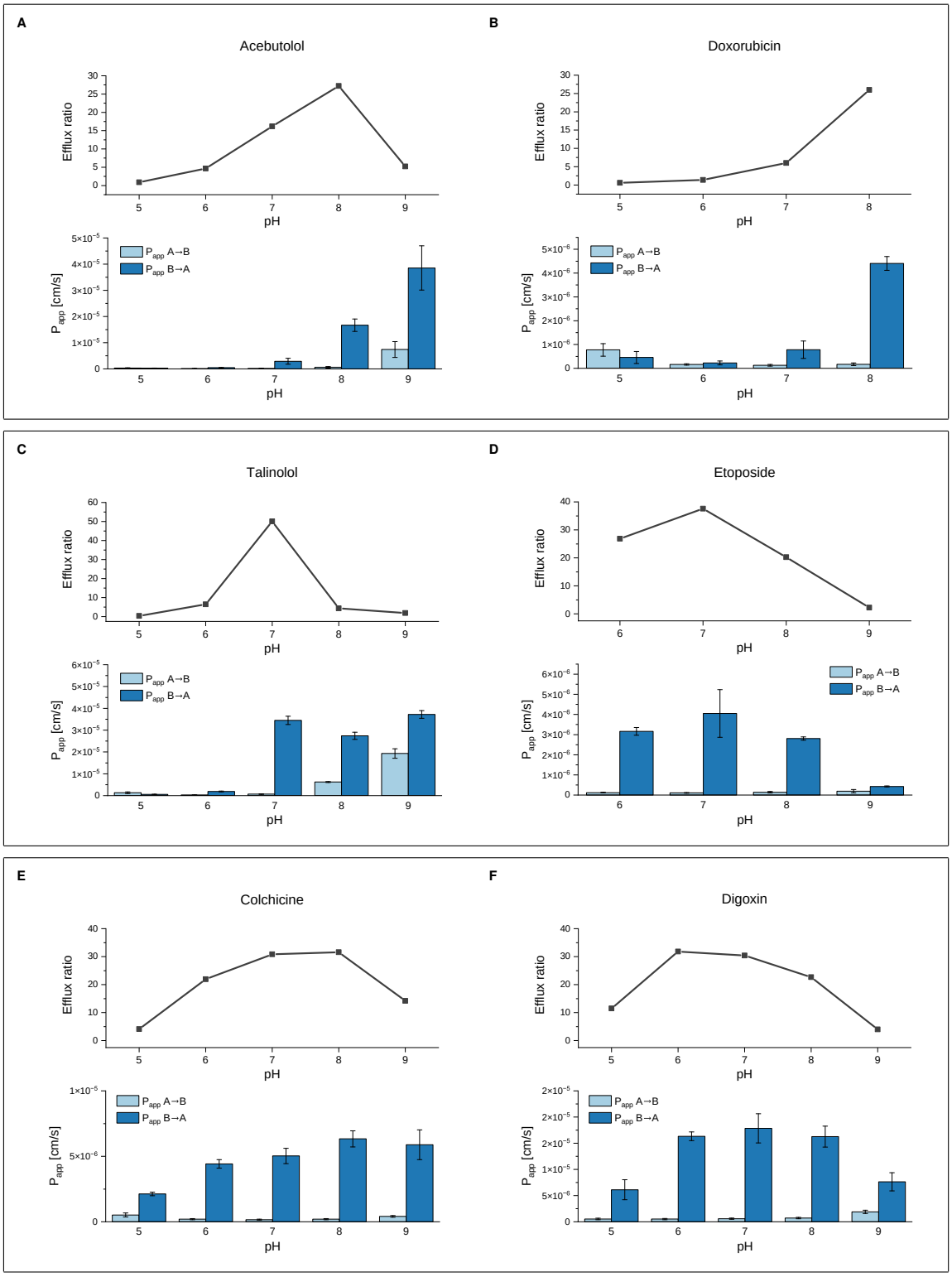

Figure 3: **Apparent permeability and efflux ratios as a function of pH for basic (A-C), acidic (D) and non-dissociating compounds (E-F).** Error bars represent standard deviation. The ER (line graph, top panels) is the quotient of mean $P_{app,B\to A}$ over mean $P_{app,A\to B}$ values. Taken from Kotze et al. [62].

pH values under investigation was determined not to be cytotoxic to the MDCKII cells within the time range of these assays [67], any pH effects on the transporters cannot be ruled out definitively. Furthermore, the error in measured P_{app} is higher at pH 9 for acebutolol, making the interpretation even more dubious. Evidently, these uncertainties render the evaluation of P_{app} and ER data across a pH range for different compounds an inadequate method of determining the favoured species of P-gp. This is because it is unavoidable that paracellular transport would affect these data at some pH for any given compound. These effects, combined with the newly-included basolateral influx transporter, confounds any conclusions that might otherwise be drawn from such experiments. As a consequence, in the next section, a more holistic view is considered by comparing the experimental P_{app} values with model fits that account for paracellular transport.

2.3.3.2 Model fits As discussed previously, the objectives of this study had been to adapt the transport model to incorporate certain a priori knowledge of the MDCK system- for example the obvious influences of aqueous resistances and the paracellular pathway. However, during the course of this work, unanticipated empirical observations necessitated adapting the model to a greater extent than originally intended. Before discussing the resultant fits from the complete model, these unforeseen changes and the observations that precipitated them will be briefly discussed.

Evidence for the inclusion of a basolateral uptake transporter. As described in Section 2.2.2, assays using a P-gp inhibitor were performed in parallel with the pH experiments where possible in order to determine intrinsic passive permeability (P_0) values. These assays revealed that contrary to expectations, the $P_{app,B\to A}$ was significantly lower with inhibitor than without. For transport in the $B \to A$ direction, the compound must cross the basolateral membrane first before it becomes available in the cytosol to be transported across the apical membrane by P-gp. Therefore, this passive diffusion across the basolateral membrane would be the rate-limiting step for $P_{app,B\to A}$ even if P-gp accelerates active transport across the across the apical membrane. However, when P-gp facilitated efflux from the apical membrane is inhibited, compounds must cross both membranes via passive diffusion. Thus, in theory, the process should be twice as fast at most if it only needs to cross the basolateral membrane, after which P-gp takes over transport across the second (apical) membrane. This factor of 2 is determined under the unlikely assumption of equal membrane surface areas, and would be even smaller when the apical membrane resistance is less than that of the basolateral, which is expected to be the case due to the likely increased surface area of the apical membrane. Yet, empirical data reveal a more substantial increase in $P_{app,B\to A}$ without the inhibitor, routinely exceeding this maximally twofold expectation. An extensive analysis of such data for compounds from our own experiments as well as other literature sources can be found in Kotze et al. [62]. The significant increase in $P_{app,B\to A}$ without inhibitor implies that transport across the basolateral membrane is

also enhanced in some way, thereby increasing the cytosolic concentration available for apical efflux. These findings, along with suggestions from Troutman and Thakker [68], Li et al. [82] and others [77], [83], [84] that a transporter on the basolateral membrane may be responsible for the uptake of compounds into the cytosol of the MDCK cells led to the adaptation of our model for this cell system to include such transport.

The use of inhibitor likely affects the experimental determination of paracellular transport. In initial model fits, experimentally obtained values for P_{para} determined by the assays described in Section 2.2.2.3 were used. Briefly, P_{para} was determined by measuring the P_{app} of the relevant compound at a pH value where paracellular transport was expected to dominate. Since the compounds in this study are P-gp substrates, elacridar was used to inhibit P-gp. Under these conditions, the measured P_{app} is expected to be a measure of P_{para}. However, these assays resulted in P_{para} values in the range of 1x10^{-5} to 1x10^{-6} cm/s, and it was found that the fits could not be performed by fixing the parameter P_{para} to these experimentally determined values. However, when P_{para} was set as free parameter the data could be fitted, and paracellular transport was invariably estimated to be 0.5 log units lower than the measured value. Because of this, it was suspected that the use of inhibitor may affect paracellular measurement. Experiments were conducted using various other paracellular markers and inhibitors to probe this suspicion, the full details and results of which can be found in Kotze et al. [62]. Table 2 compares the results obtained for the attempted measurement of P_{para} for the non-P-gp substrate chlorothiazide without inhibitor, along with three different P-gp inhibitors: elacridar (2 µM), verapamil (100 µM) and cyclosporin A (10 µM).

Table 2: **Comparison of P_{app} values and calculated logP_{para} for chlorothiazide with various P-gp inhibitors.** P_{app} values are the mean of three timepoints per replicate, for one replicate ± standard deviation.

Compound	P_{app} $[\times 10^{-6} cm/s]$	logP_{para}	ER
Chlorothiazide A→ B	0.2 ± 0.0	-6.6	1
Chlorothiazide B→ A	0.2 ± 0.0	-6.7	
Chlorothiazide A→ B + elacridar	0.9 ± 0.0	-6.0	-
Chlorothiazide A→ B + verapamil	1.4 ± 0.1	-5.9	-
Chlorothiazide A→ B + cyclosporin-A	0.7 ± 0.0	-6.1	-

From Table 2 it can be seen that for all three of these common P-gp inhibitors, the measured logP_{para} was higher than without any inhibitor. The reason for this is unclear, and it was beyond the scope of this study to systemically investigate this matter further. From these assays and others presented in the Supplementary Materials of Kotze et al. [62], we concluded that the method of reducing f_{n} and using inhibitor does not yield

reliable measurements for P_{para}. These experiments suggest that using an inhibitor might influence either P_{para} itself or its measurement. Because of this, P_{para} was left free to be fitted by the model, and it was rather consistently estimated to be within the range of 1x10^{-7} to 5x10^{-7} cm/s (see Kotze et al. [62] Supplementary Materials), which translates to a logP_{para} of between -7 and -6.3. These values correspond more favourably with the logP_{para} obtained for typical paracellular marker compounds (i.e non-P-gp substrates measured without inhibitor, the transport of which is expected to be dominated by the paracellular route).

Model fits As described in Section 2.3.3.1, pH-dependent evaluations of the ER were not sufficient to make any reliable conclusions as to the efflux transporter's fraction preference due to the influence of paracellular transporter and potential effects of pH on the transporters. However, following the refinement of the model to incorporate the basolateral transporter, the model fits generated as described in Section 2.2.3 from our mathematical equations were compared with the experimental data. This represented another approach that was made to determine transporter species preference, taking into account both the model and the empirical data. Figure 4 depicts the Igor fits (dashed lines) along with the experimental P_{app} data (markers) in both directions generated for the compound acebutolol.

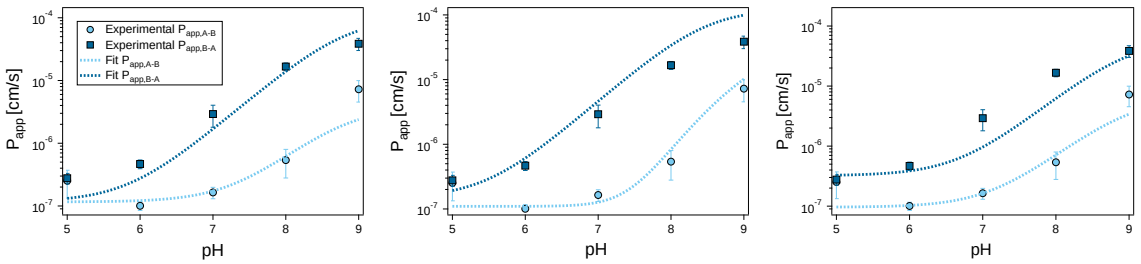

(a) neutral-neutral (b) ionic-ionic (c) neutral-ionic

Figure 4: **Experimental apparent permeability as a function of pH for acebutolol plotted along with model fits under varying assumptions.** A) Both transporters act on the neutral fraction, B) Both transporters act on the ionic fraction and C) The apical transporter acts on the neutral species, and the basolateral transporter acts on the ionic species.

As is evident, all fits generated from the three scenarios describe the data rather well, which lends confidence to the model as a whole. However, none of the assumptions result in a fit that is substantially superior, which does not enable a confident identification of the most likely case. Furthermore, none of the assumptions result in a fit that is unsatisfactory enough to allow for the reasonable exclusion of it as a probable scenario either. Although only the fits for acebutolol are depicted in Figure 4, the results were equally inconclusive for all other compounds evaluated in this study, and

this conclusion is based on the critical evaluation of all fits, for all compounds. The corresponding graphs comparing these fits as well as details about the parameters can be found in the Supplementary Material of Kotze et al. [62]. Even though this result is unsatisfying, it is not surprising: the unforeseen inclusion of the basolateral transporter means that there are three free parameters (P_{para}, P_{pgp}^{active} and P_{b}^{active}) that must be fitted with the limited data-points that can be generated in the restrictive viable pH range.

3 Energy Limit for Active Transport

3.1 Theory

The central hypothesis for this Chapter is that the disposition of highly permeable compounds should not be significantly affected by efflux transporters, as it would be energetically unfeasible for the cell to maintain effective efflux against high rates of passive diffusion. The approach to ascertaining and refining such a value for our MDCKII system set-up was multi-faceted.

3.1.1 Membrane permeability as a rudimentary threshold value

Firstly, while a theoretical calculation and value for maximum flux (the maximum moles of compound that can be actively transported per unit area and time given the limited energy production of the cell) is interesting, it is not so useful when evaluating a database of compounds and determining which adheres to or which defies the energy limit. As such, we aimed to ultimately link the theoretical flux limit with a metric that is almost always at hand (or easily determinable if not): membrane permeability, P_{m}. If a cell has a maximum limit to the energy it can invest into its transporters per unit of time, and if there is a 1:1 ratio between the number of molecules transported and ATP hydrolysed, then it should be possible to identify a specific P_{m} value where the passive influx of a chemical exceeds the cell's maximal efflux capacity. At this point, the cell can no longer maintain efficient efflux. Chemicals which have a P_{m} that exceeds this threshold are likely not affected by active transport, since their efflux would induce an unsustainable expense of energy. Using P_{m} as the filtering metric is very useful here in the investigation stage, as it allows for the easy identification of outlier compounds (explained in detail in Section 3.2). However, it will also eventually be more useful for any "simple rule" classifications, since the P_{m} of any compound can be determined rather quickly and easily through reliable P_0 or $K_{\mathrm{hex/w}}$ values, as described in Section 3.2.1.1. This circumvents the need for any resource- and time-intensive in vitro assays in the initial stages. However, simply using the P_{m} value as metric for the proposed energy limit cut-off does not suffice without at least providing several conditions. Some generalisations have to be made and it is important to bear in mind the limitations and/or conditions under which such a simple rule could be applied. Chief among these caveats is the fact that any P_{m} cut-off value would be tied to a specific concentration. Here concentration refers to the exposure concentration of the compound (e.g as applied in the donor compartment of the MDCK assays). Since this work deals with apically-located efflux transporters, the cytosolic concentration on the apical side is the most consequential value for the active transporter. However, the cytosolic concentration is dictated by the external concentration. The exposure concentration is easy to manipulate and report exactly, whereas the cytosolic concentration needs to be calculated and is not so easily at hand. As such, within Chapter 3 unless stated otherwise, concentration always refers to the external concentration.

3.1.2 Determination of an empirical energy limit

While using a rough cut-off P_{m} was practical and useful in the methodical part of this work to identify and investigate outliers, a different approach was used to finally identify an energy threshold that could be expressed in the moles of compound that is transported by P-gp per unit area and time ($\mu\mathrm{mol\,cm^{-2}\,s^{-1}}$), assuming 1:1 stoichiometry of drug transport and ATP hydrolysis. In the course of this work, several compounds were identified that were suspected to lie at or around the threshold P_{m} used. These compounds often exhibited similar properties, for example (in the cases of loperamide and quinidine) either being reported as having very high ER values by some sources, or having low/no ER values by others, while always being confirmed P-gp substrates by multiple types of assays aside from monolayer efflux studies. Since an energy threshold depends on many factors, it was never envisioned or proposed that it would be a hard, definite cut-off line, but rather that there would be some intermediary window of permeability values. In this window of transitionary permeability values that separate compounds that can be effectively effluxed from those that cannot, the concentration of the compound plays a particularly pivotal role. For some compounds identified or suspected to fall within this window (classed as "borderline" compounds), monolayer efflux assays were performed across a range of concentrations. The rationale behind such assays being that at lower concentrations, there is little enough of the compound available that it can be effluxed efficiently without overexerting the energy budget of the cell. However, the higher the concentration gets, the greater the amount of compound entering the cell, and the nearer it would get to approaching the energy limit. Finally, at some higher concentration and above, the amount of compound passively permeating into the cell far exceeds what can be effluxed, since the energy budget has been depleted. As a result, efflux would no longer be evident at this point. In Section 3.2 these concentration-dependent assays are explained in further detail.

Using the apparent permeabilities at each concentration obtained in the aforementioned experiments, the experimental apparent permeabilities were then fitted in order to determine the contribution of P-gp and to calculate the resultant flux ($J_{\mathrm{pgp,\ active}}$ in $\mu\mathrm{mol\,cm^{-2}\,s^{-1}}$. The rationale being that even if the ER of the borderline compounds varies across the concentration range, the flux would plateau at higher concentrations once the energy limit has been reached. For this, the transport model equations and principles for permeability through individual layers (presented in detail in Chapter 2 and the associated publications) were used. The idea is that if an energy limit exists, the $J_{\mathrm{pgp,\ active}}$ value would be the same in both directions for every borderline compound, regardless of concentration. Compounds with lower permeabilities are not expected to be close to this limit, and thus would not be in the range of the energy limit, which is why it is was necessary to perform these experiment with compounds for which the P_{m} value is at, or close to, the energy limit. Ideally, there would be a comparison between several compounds in order to see whether these $J_{\mathrm{pgp,\ active}}$ values are the same. This would confirm a final, approximate energy limit value based on multiple compounds at multiple concentrations to show that it is not compound-dependent, but rather due to

a physical energetic limit. After probing the outliers and several so-called "borderline" compounds, we attempt to link the definite energy limit a more specific P_{m} threshold. Since this P_{m} threshold depends on factors such as the concentration of the substrate, the surface area of the cell membranes and the relative activity of the basolateral influx transporter, a sensitivity analysis is performed to evaluate how these respective factors may influence the P_{m} threshold.

3.1.3 Theoretical estimation of energy limit

Finally, a theoretical calculation was performed to compare with the empirical value as a plausibility check. Starting out with a rather simplified calculation enables, at the very least, the ascertainment of the general range or starting estimate for the energy limit. As such, the rather crude calculation was performed by obtaining a value for the energy production of the cell- expressed through ATP turnover. Figure 5 shows how this can be approached through measurements of oxygen or glucose consumption on a physiological or cellular level.

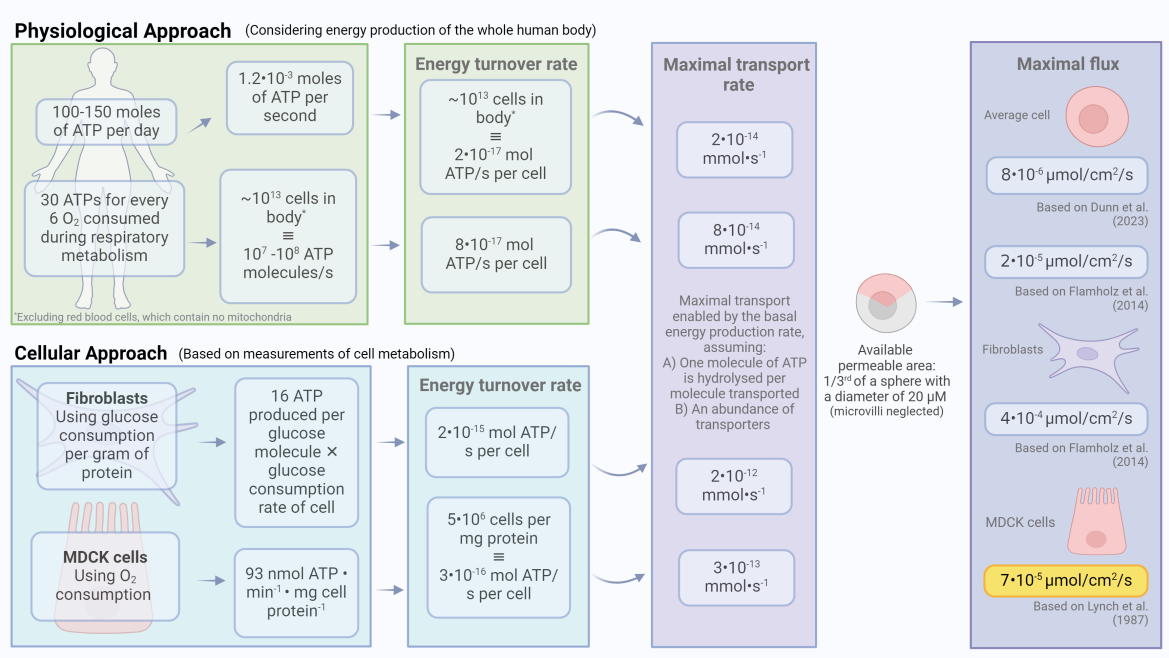

Figure 5: **Physiological and cellular approaches towards calculating theoretical maximal flux values.** The maximal efflux that can be facilitated by cells is estimated from the rate of ATP production per cell and the surface area of a cell available for permeation. Since different cells have different energy demands depending on their location and function, the maximal flux value will differ between cells.

Three different sources of ATP turnover were used [85]–[87]. On a physiological level, this production was pegged by one study at a value of 5×10^{-7} ATP molecules produced per cell, which translates to about $8.3 \times 10^{-17}\,\mathrm{mol\,s^{-1}}$ (moles of ATP per second)

[87]. Using the same principles, values from another study generated a similar rate of $3.9 \times 10^{-17}\,\mathrm{mol\,s^{-1}}$ [85]. Both of these estimates were originally enumerated for the entire human body, and then calculated per cell by assuming that there are about $\approx 10^{13}$ cells in the body (this figure excludes red blood cells, which contain no mitochondria and make up $\approx$ 70% of all cells) [87], [88]. As such, these estimated ATP production rates are an average value for all cells. However, it is worth remembering that different cells may have varying energy consumption based on their location and function. For example, muscle and brain cells have much higher energy needs (and thus more mitochondria) than adipocytes or skin cells. ATP production values were found for fibroblasts, which have a very high energy demand when they are in the activated state. Indeed, they were estimated to have a higher maximal transport rate than the general cell averages above, calculated at $1.7 \times 10^{-15}\,\mathrm{mol\,s^{-1}}$. Since this study deals with MDCKII cells, an ATP production rate determined specifically for these cells was determined, and it was also about factor 10 higher than the averages reported above at $3.1 \times 10^{-16}\,\mathrm{mol\,s^{-1}}$ [86]. This is not surprising, since it could be expected that MDCK cells require more energy than the average cell due to their increased metabolic and active transport rates, and the fact that they also need to maintain their polarised state. If it is assumed that one molecule of ATP is hydrolysed for every one molecule transported [89] (and assuming sufficient amounts of transporter proteins in the cell), then an ATP production rate of $3.1 \times 10^{-16}\,\mathrm{mol\,s^{-1}}$ would enable a maximal transport rate of $3.1 \times 10^{-13}\,\mathrm{mmol\,s^{-1}}$. We then estimated the surface area of the cell as one third of the surface area of a sphere with a diameter of 20 μM (neglecting the microvilli). This results in an estimate for the maximal flux in MDCK cells of $7.4 \times 10^{-5}\,\mathrm{\mu mol\,cm^{-2}\,s^{-1}}$. The preceding calculation is highly simplified, and the simplifications will result in errors at each step which might skew the values. However, we are merely attempting to get an order-of-magnitude estimate as a comparison for more exacting calculations.

3.2 Materials and Methods

3.2.1 Dataset curation

Three separate datasets were curated for P-gp, BCRP and MRP2 substrates as the three most clinically relevant apically-located efflux transporters. To populate the lists for each transporter, a literature search was performed to obtain compounds for which the ER was $\geq$ 2.5 [51], as determined with bidirectional MDCKII transport assays. Therefore, at the stage of data collection, a decision was made not to mix the results from various types of assays, and only to include data from monolayer efflux studies. For compounds where ER values from more than one source was available, values from all sources were included in the analyses, even if some sources had a conflicting ER below the cut-off value. For each compound, the ER value and source was noted. A total of 296 datapoints were gathered, representing 153 unique compounds, with those from MDCKII-MDR1 assays making up the bulk of the data, since MDCK-BCRP and MRP2 monolayer efflux assays are far less common.

3.2.1.1 Determination of $P_{\mathbf{m}}$ from $P_{\mathbf{0}}$ values For all compounds, a pKa value was sourced preferentially from experimental values [71]. When not available, pKa values were instead determined using the ACD Percepta Software [72]. Using these pKa values, the f_{n} at pH 7.4 was determined [90]. The P_{m} of each compound was then determined according to Equation 2. For this, P_0 values were preferentially sourced from Ebert et al. [91], who extracted P_0 values from experimental data from several sources (including from the companion publications of Kotze et al. [53], [62]) taking into account the many pitfalls of P_0 determination. As such they are considered the most reliable P_0 values available. When no reliably extracted experimental P_0 value was available, P_0 was predicted according to the solubility-diffusion model (SDM) using hexadecane as a model for the hydrocarbon core of the membrane [54], [67], [92]:

$$P_0, SDM = \frac{D_{hex} \cdot K_{hex/w}}{x_m} \tag{12}$$

Where D_{hex} is the diffusion coefficient of the compound in hexadecane, $K_{\mathrm{hex/w}}$ is the hexadecane-water partition coefficient of the compound, and x_m is thickness of the hexadecane-like hydrocarbon core of the cell membrane. The compound's D_{hex} is assumed to be one tenth of the D_{w} [54], and was thus calculated as a function of molecular weight of the compound, corrected to account for the temperature of 37 °C [55], [56], [93]. The $K_{\mathrm{hex/w}}$ was determined using the LSER database [63]. $K_{\mathrm{hex/w}}$ values determined from experimental descriptors were preferred and sub-categorised into the "Experimental Descriptors" group. For compounds where experimental descriptors were not available, $K_{\mathrm{hex/w}}$ values determined from calculated descriptors were used instead, and such compounds were likewise designated to the "Calculated Descriptors" sub-category. For the sake of comparison, $K_{\mathrm{hex/w}}$ values were also generated for all compounds using the quantum chemically-based software COSMOthermX18 (COSMOlogic GmbH & Co KG, Leverkusen, Germany) [94]. COSMOthermX18 values were used for compounds with a permanent charge or a molecular weight $> 1000 g/mol$, or referred to when further analysis was necessary for a given compound. The P_0 of the MDCKII cell membrane ($P_{0,MDCK}$) was then calculated from $P_{0,\mathrm{SDM}}$ using the correlation determined by Dahley et al. [67]:

$$\log P_{0,MDCK} = 0.84 \ \log P_{0,SDM} \ - \ 1.85 \tag{13}$$

3.2.1.2 P-gp dataset MDCKII-MDR1 assay data from 23 different sources were used [16], [50], [51], [68]–[70], [95]–[111]. The dataset was comprised of 227 data points (i.e ER values) from 111 unique compounds. The dataset of MDCKII-MDR1 ER values and the concomitant $\log P_{\mathrm{m}}$ values for the respective compounds are depicted in Figure 6.

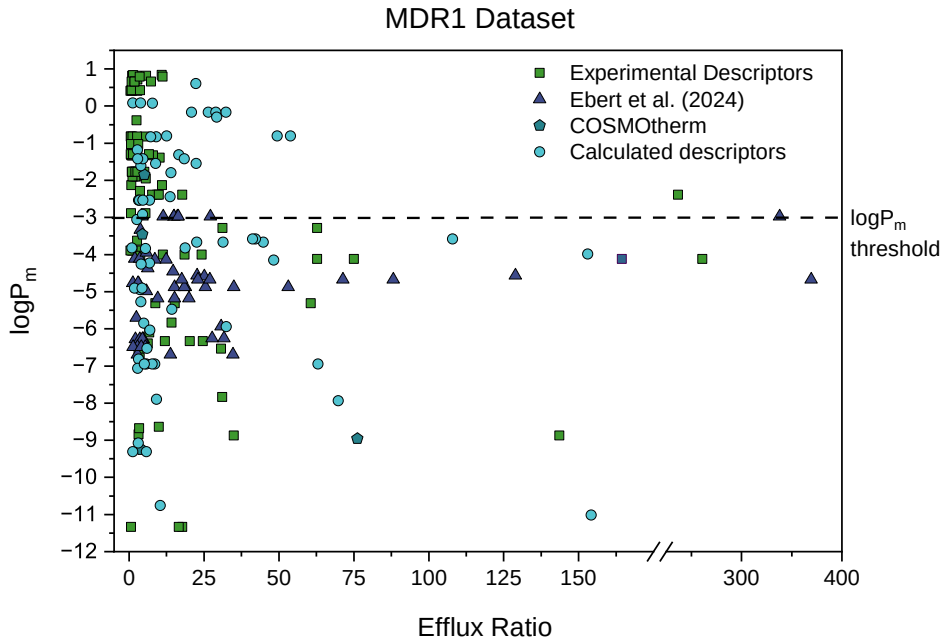

Figure 6: **Efflux ratios and logP_{m} values for the MDCKII-MDR1 dataset.** Data were sub-categorised based on whether the P_0 was from Ebert et al. or determined with the SDM model and LSER $K_{\mathrm{hex/w}}$ values from either experimental or calculated descriptors. P_0 values for permanently charged compounds or those with a molecular weight > 1000 were generated from $K_{\mathrm{hex/w}}$ values calculated with COSMOthermX18. The indicated P_{m} threshold is discussed in Section 3.2.2.

3.2.1.3 BCRP dataset MDCK-BCRP assay data from 15 different sources were used [16], [112]–[125]. The dataset was comprised of 55 data points from 33 different compounds. The dataset of MDCK-BCRP ER values and the concomitant logP_{m} values for the respective compounds are depicted in Figure 7.

3.2.1.4 MRP2 dataset MDCK-MRP2 assay data from 8 different sources were used [126]–[133]. The dataset was comprised of 14 data points from 9 different compounds. The dataset of MDCK-MRP2 ER values and the concomitant logP_{m} values for the respective compounds are depicted in Figure 8.

3.2.2 Identification of outliers

For all datasets, compounds with a permanent charge were excluded from further analyses since they have no neutral fraction that can passively permeate through the hydrophobic core of the membrane. Furthermore, zwitterionic compounds were also excluded, since it is challenging to determine their neutral fractions [93]. For the remaining compounds, a rough approximation of the cut-off value for compound permeability was delineated to enable rational direction of the initial investigations. This

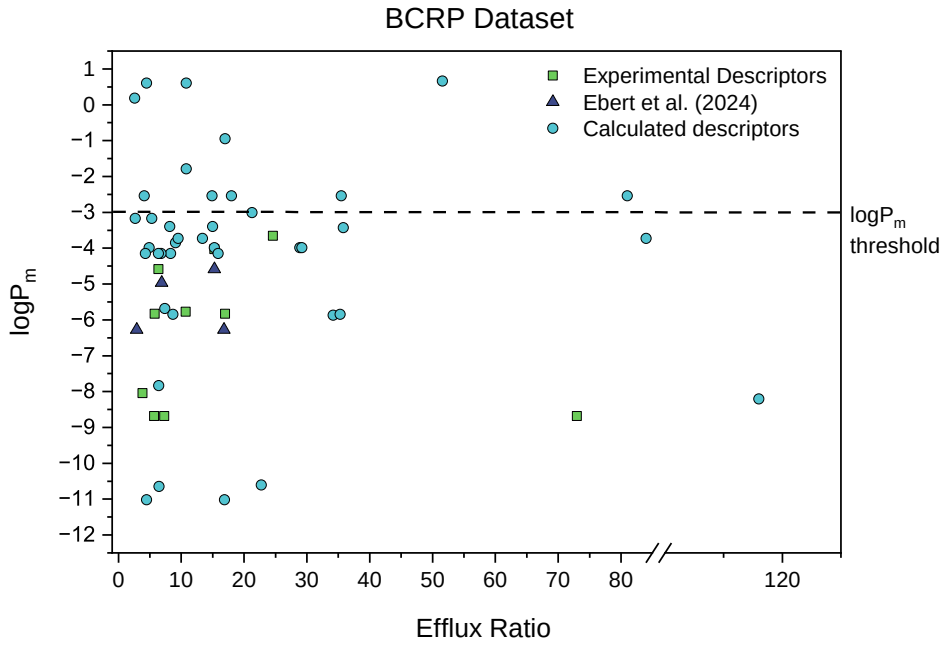

Figure 7: **Efflux ratios and logP_{m} values for the MDCK-BCRP dataset.** Data were sub-categorised based on whether the P_0 was from Ebert et al. or determined with the SDM model and LSER $K_{\mathrm{hex/w}}$ values from either experimental or calculated descriptors. The indicated P_{m} threshold is discussed in Section 3.2.2.

cut-off P_{m} value was determined by assessing the distribution of all the data (Figures 6, 7 and 8). As a first step, particular weight was given to those data points which had P_{m} values based on the very reliable P_0 values extracted by Ebert et. al [91] for which significant efflux was also documented. It was noted (and as can be observed in Figures 6, 7 and 8) that the highest of these reliable logP_{m} values was approximately -3, and that all other data points from the Ebert et al. sub-category had a logP_{m} lower than this maximal value across all three datasets. Thus, as a first approximation as to where the energy threshold (and thus concomitant membrane permeability threshold) could lie, a preliminary threshold line was drawn at log$P_{\mathrm{m}} = -3$ and outlier data points were identified as those lying above this line, with an ER ≥ 2.5 and with a log$P_{\mathrm{m}} > -3$. As stated before, this was a convenient delineation to make, since the P_{m} of any compound can be determined rather quickly and easily through reliable P_0 or $K_{\mathrm{hex/w}}$ values as described in Section 3.2.1.1, circumventing the need for any resource-intensive in vitro assays in the initial stages.

3.2.3 Investigation of outliers

As mentioned before, outliers were sub-categorised into three groups based on whether the P_0 was from Ebert et al. [91] (deemed very reliable) or whether it was determined from the LSER $K_{\mathrm{hex/w}}$ values, either in the Experimental Descriptors category

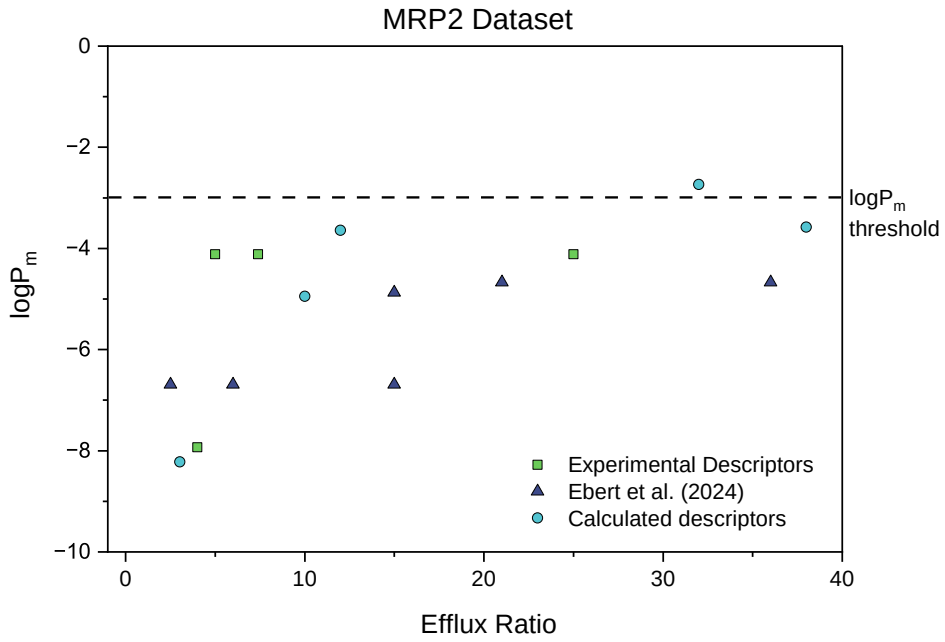

Figure 8: **Efflux ratios and logP_{m} values for the MDCK-MRP2 dataset.** Data were sub-categorised based on whether the P_0 was from Ebert et al. or determined with the SDM model and LSER $K_{\mathrm{hex/w}}$ values from either experimental or calculated descriptors. The horizontal line indicates the tentative threshold line, and all compounds above this line were deemed outliers. The indicated P_{m} threshold is discussed in Section 3.2.2.

or Calculated Descriptors category. $K_{\mathrm{hex/w}}$ values from experimental descriptors are generally regarded as quite reliable, as such, for outliers in this category it was deemed more likely that the determined ER values were false. In contrast, $K_{\mathrm{hex/w}}$ values from calculated descriptors are not deemed as reliable, and thus for outliers in this category it was generally assumed that the calculated P_{m} was false. The aforementioned assumptions were merely used as a general guideline to determine which experimental method would be preferentially implemented to investigate a given outlier. Thus, for the outliers in the "Experimental Descriptors" category where a false ER was assumed, MDCKII assays were first performed to determine the ER independently in an attempt to reproduce the results of the original source study. Since only the MDR1 dataset had outliers in this category, only MDCKII-MDR1 assays were performed. For those outliers in the "Calculated Descriptors" category, parallel artificial membrane permeability assays (PAMPA) were preferentially performed. Though PAMPA is more commonly used to measure the passive permeability of compounds across a synthetic membrane that is meant to mimic biological membranes, the measured permeability in such assays can also be used to determine the equilibrium partition constant. Using hexadecane as the membrane in PAMPA has been shown to effectively simulate the passive diffusion across cell membranes, rendering it a simple but well-suited model

for more complex biological membranes. It follows that the permeability derived from such PAMPA measurements could be used to back-calculate the hexadecane partition coefficient ($K_{\mathrm{hex/w}}$) of the compound. These reliable, experimentally-derived $K_{\mathrm{hex/w}}$ values could then be used (via Equations 12 and 13 [67]) to provide a much more reliable P_{m} for MDCK cells as well. However, as mentioned before, this was only a generalised procedure, and for many compounds both MDCKII as well as PAMPA were eventually performed. Where necessary, outliers were investigated in ways other than performing these assays, and thus re-classified or excluded based on other reasons. As a prime example, some compounds suspected to be at or near the threshold P_{m} were investigated with MDCKII concentration-dependent assays and accompanying model fits. Compounds with a logP_{m} value between -2 and -3 were classified as borderline compounds. That is, compounds found in the transitionary window that separates compounds with a lower membrane permeability that can have significant efflux, from those with a higher membrane permeability which are unlikely to be affected by efflux transporters.

3.2.3.1 MDCKII-MDR1 assays to determine ER Bidirectional assays were performed for selected compounds: Emetine dihydrochloride, amprenavir, terfenadine, clemastine fumarate, chlorpromazine hydrochloride, desipramine hydrochloride, doxylamine succinate, pyrilamine maleate, loperamide hydrochloride, quinidine, reserpine, sertraline hydrochloride, ritonavir, loratadine, diphenhydramine chloride, acebutolol hydrochloride and verapamil hydrochloride was sourced from from Sigma-Aldrich (Sigma-Aldrich, Co., St. Louis, MO, USA). Phenelzine sulfate was sourced from BPCL (British Pharmacopoeia Commission Laboratory, Teddington, London, UK). Prazosin hydrochloride was sourced from ThermoFisher GmbH (Thermo Fisher Scientific, Waltham, MA, USA). Brompheniramine maleate and chlorpheniramine maleate was sourced from HPC Standards (HPC Standards GmBH, Bordsdorf, Germany). Clomipramine hydrochloride was sourced from Merck (Merck KGaA, Darmstadt, Germany). Fluoxetine hydrochloride was sourced from Dr. Ehrenstorfer GmbH (LGC Standards, LGC Limited, Teddington, United Kingdom). Lopinavir was sourced from Cayman Chemicals (Cayman Chemical, Ann Arbor, MI, USA). MDCKII-MDR1 cells were used for these assays, and cultured as described in Section 2.2.1. Bidirectional transport assays were performed as described in Section 2.2.2. Assays were performed at pH 7.4 using the iso-pH method. Where possible, P_0 assays with inhibitor and possibly alternative pH values were performed in parallel as described in Section 2.2.2.2. To confirm their integrity, all cell monolayers were subjected to LY permeability and TEER measurements as described in Section 2.2.2.5. The average TEER was 135 $\pm$ 8 Ω cm^2 before and 130 $\pm$ 14 Ω cm^2 after the transport experiments, thereby confirming the integrity of the cell monolayers throughout the experiment. Samples were analysed as described in Section 2.2.2.6. MDCKII assays for this section were performed in duplicate, and sampling occurred at 4 consistent time intervals. Data are presented as the mean of the recovery-corrected P_{app} $\pm$ standard deviation of at least

three timestep samples for both replicates.

3.2.3.2 PAMPA to determine $K_{\mathbf{hex/w}}$ values PAMPA was performed for selected compounds: Emetine dihydrochloride, eletriptan hydrobromide, darifenacin hydrobromide, desloratadine, mequitazine, terfenadine, amprenavir and gefitinib was sourced from Sigma-Aldrich. Prazosin hydrochloride was sourced from ThermoFisher GmbH. Phenelzine sulfate was sourced from BPCL. Erlotinib hydrochloride and lapatinib was sourced from ChemPUR (CHEMPUR Feinchemikalien und Forschungsbedarf GmbH, Karlsruhe, Germany). Nilotinib hydrochloride was sourced from TargetMol (TargetMol, Wellesley Hills, MA, USA). Nelfinavir was sourced from AdipoGen Life Sciences, Inc. (San Diego, CA, USA). PAMPA assays were performed at a suitable pH value determined for each compound. The pH values used for each compound were selected based on a predicted P_{app} value to avoid ABL limitation. P_{app} predictions for the PAMPA set-up were determined with pKa values and predicted LSER or COSMOthermX18 $K_{\mathrm{hex/w}}$ values, or from preliminary experiments values where available. Experiments were repeated at different pH values if the initial pH proved to not avoid ABL-limitation, or resulted in acceptor concentrations that were too low. The acceptor compartment fraction relative to the donor was kept below 80 % to ensure that equilibrium has not yet been reached. Buffers were prepared from distilled H_2O with 10 mM β-Alanine for buffers with a pH of 4-4.5, 5 mM each of β-Alanine and MES for buffers with a pH of 5, 10 mM MES for buffers with a pH of 5.5-6.5, 10 mM MOPS for buffers with a pH of 7-7.5, 10 mM TAPS for buffers with a pH of 8-9 and 10 mM CAPSO for buffers with a pH of 9.5-10. Stock solutions were prepared in buffer solutions to their maximum aqueous solubility where possible, or as high as possible otherwise to avoid sorption effects. Where DMSO was required for solubility, it was kept below 0.1 % and the accompanying acceptor compartment buffer was supplemented with an equal concentration of DMSO. After dissolving the compound in buffer, it was placed in the ultrasonic bath at 37 °C for 10 min to aid with dissolution. To ensure that no undissolved compound remains, stock solutions were then passed through 13 mm glass fibre filters with a pore size of 0.7 μm (Carl Roth GmbH + Co. KG, Karlsruhe, Germany). After filtration, the pH of the stock solutions was tested again and adjusted if necessary to the desired pH. Millipore 96-well Collection Plates (MATRNPS50) were used in combination with Millipore Multiscreen 96-well plates (MAIPN4450) with hydrophobic PVDF membranes and a pore size of 0.45 μm (both Merck KGaA, Darmstadt, Germany). Prior to initiation of the experiment, 3.5 μL hexadecane (Acros Organics, Thermo Fisher Scientific, Waltham, MA, USA) was added to each of the plate membranes. The bottom plate was used as the receiver compartment, and 280 μL of the buffer was added to a bottom well for each replicate. The top plate was used as the donor compartment, and 200 μL stock solution was added per well after placing the top plate onto the bottom plate. The PAMPA plate sandwich was placed into the incubator at 37 °C (without shaking) and the time started. The total assay time for the compounds tested was either 2, 4 or 24 hours,

depending on how fast the compound was predicted to permeate. After the assay time had elapsed, the plate was removed from the incubator and the donor and receiver compartments for each well sampled. After this, an extraction was performed with ethanol (EtOH) to ensure that any compound that may have sorbed to the plate material is removed and measured, so that it can be accounted for in the mass balance calculations. For this, pure LiChrosolv EtOH (Merck KGaA, Darmstadt, Germany) was supplemented with 1 % of either pH 4 (for acidic compounds) or pH 10 (for basic compounds) buffer to ensure the maximal neutral fraction of the compounds possible to aid with the extraction. Any residual buffer/stock was removed from both the receiver and donor wells, then 200 μL and 280 μL of the EtOH solution was added to the donor and receiver wells, respectively. The top plate was placed into a new bottom plate, as the EtOH solution passes through the well membrane and is then collected in a new well. Lids were placed on both plates, sealed with parafilm and the extraction was allowed to occur over the course of one hour. Afterwards, the EtOH solution was sampled from both the donor and receiver compartments for analysis. Two calibration curves were prepared from the stock solution of each compound; one with the assay buffer for the primary PAMPA samples and one with EtOH for the extraction samples. The donor and receiver samples of both the primary experiment and EtOH extraction were diluted for analysis where necessary. Three replicates were performed for each compound. Samples were analysed with the LC-system as described in Section 2.2.2.6. P_{app} was calculated and corrected for missing sink conditions [91], [134], [135]. The final $K_{\text{hex/w}}$ values were calculated from the mean of the $K_{\text{hex/w}}$ values for all replicates.

3.2.4 Investigation of Borderline compounds

3.2.4.1 MDCKII-MDR1 assays with concentration variation Bidirectional transport assays were performed as described above, with slight differences. Instead of using stock solution at just one concentration, five concentrations were chosen to span the range of viable concentrations within the limits of the experimental procedure and LC-MS quantification. Where DMSO was required for solubility, the total concentration was kept constant at a limit of 0.1 %, and the transport buffer was supplemented with the same concentration to prevent a DMSO gradient between compartments. Assays were performed for loperamide (0.1, 0.4, 4, 10 and 21 μM), acebutolol (6, 12, 20, 60 and 150 μM), amprenavir (0.2, 2, 10, 15 and 20 μM), quinidine (0.05, 0.5, 5, 20 and 50 μM), prazosin (0.01, 0.1, 1, 8 and 15 μM) and eletriptan (0.1, 1, 10, 20 and 40 μM). MDCKII assays for this section were performed in triplicate, and sampling occurred at 4 consistent time intervals. Data from these assays (found in Section 3.3.4) are presented as the mean of the recovery-corrected $P_{app}\pm$ standard deviation of at least three timestep samples for all replicates.

3.2.4.2 SOLVER Model Fits The recovery-corrected $A \rightarrow B$ and $B \rightarrow A$ permeabilities determined for each concentration (Section 3.2.4.1) were used in a Excel SOLVER function to fit the experimental apparent permeabilities at each concentration

and to estimate the relative contributions by P-gp and the basolateral transporter. The thickness of the apical and basolateral ABL, the thickness of the filter and its effective surface area, as well as the P_0, D_w, D_{cyt} and pKa of each respective compound (from the concentration variation MDCKII assays described above) were used to calculate the permeability through the individual resistances (ABLs, membranes, cytosol and filter). Paracellular permeability was calculated according to Bitterman et al. [54] and a factor of 0.1 applied so that its final value matches the paracellular permeabilities typically observed for our MDCKII-MDR1 cell set-up [62]. The external neutral fraction was once again calculated according to Escher et al. [90] based on the compound's pKa values and the external pH. The neutral fraction in the cytosol was similarly calculated after determining the cytosolic pH as a function of the external pH according to Dahley et al. [67]. In contrast to Chapter 2, the difference (if any) in surface area between the apical and basolateral membrane is suspected to be very consequential here and will have a significant effect on the results. It has been speculated that the factor of 24 (to account for the increase in apical membrane surface area due to microvilli) was likely too high, and this uncertainty was touched on in Chapter 2. As such, for this chapter a comparison of a more moderate apical membrane surface area factor of 7.5, as well the other two proposed factors on the more extreme ends of 24 and of 1 was used. The factor of 1 naturally indicates that there is no difference in surface area between apical and basolateral membranes. The factor of 7.5 was sourced from Butor and Davoust [61], determined specifically for MDCKII cells as the mean value of MDCKII cells grown on different filters.

The experimental P_{app} and known P_0 values were then used to fit the apparent permeabilities facilitated by P-gp and the basolateral uptake transporter ($PS_{Pgp,app}$ and $PS_{b,app}$). $PS_{Pgp,app\ A\to B}$ was fitted at each concentration with the Excel SOLVER function which minimises the difference between the calculated and experimental apparent permeability by varying $P_{pgp,app}$. Using the extracted $P_{pgp,app}$ as well as the starting concentrations ($\mu mol\,L^{-1}$), the calculation of compound concentrations adjacent to the apical membrane in the cytosol was possible ($c_{cyt,a}$). The flux of actively transported compound could then be calculated from $P_{pgp,app} * c_{cyt,a}$ in $\mu mol\,cm^{-2}\,s^{-1}$. This resulted in the $J_{pgp,\ active}$ value that is ultimately compared with the calculated theoretical energy limit (see Section 3.1). Ideally, a consecutive calculation would be performed: First, for the basolateral transporter PS_b, by fitting the $B \to A$ permeability under the assumption that the basolateral membrane is not a significant resistance in this direction of transport. Then PS_{Pgp} would be determined by fitting $A \to B$ permeability. However, due to unforeseen experimental effects only $A \to B$ permeability was fitted to determine $PS_{Pgp,app}$. This is elaborated upon and justified in Section 3.3.5.

3.3 Results

3.3.1 MDR1 dataset outliers

In this dataset, nine compounds are zwitterionic and another three have a permanent charge and were thus all excluded from further analysis. In total, 64 data points from this dataset were identified as outliers, representing 39 compounds. Of the outlier data points, 38 were from compounds with a $K_{\mathrm{hex/w}}$ value based on experimental descriptors, and 26 based on calculated descriptors.

3.3.1.1 MDR1- Experimental Descriptors The compounds in this category had a LSER $K_{\mathrm{hex/w}}$ value based on experimental descriptors, and therefore it was presumed that the P_{m} value would be more reliable than the ER. Therefore, for almost all outliers in this category, performing MDCK bidirectional assays to independently determine the ER was the preferred investigatory method. It is worth noting that two thirds of the outlier compounds for the MDR1 dataset were contributed by only 3 of the 22 sources. Data sourced from Wager et al. [51] represented more than 30 % of the outliers, a comparatively large share. Moreover, barring one compound, all Wager et al. outliers fell in the "Experimental Descriptors" category, meaning that the ER value (not the P_{m}) is more likely dubious for these outliers. ER values ≥ 2.5 reported by Wager et al. and two other sources prevalent in the outlier data, Obradovic et al. [99] and Wang et al. [97], were also often contradicted by one or more other sources, which would report no significant ER. Based on these doubts, MDCK assays were performed for many of the outlier compounds contributed by these three sources, and in the majority of cases this resulted in non-significant ER values for compounds that were previously classified as substrates by these sources. As such, values from these sources and the outliers they contributed were treated with caution. In most cases, outliers from these sources were reclassified based on contradictory non-significant ER values produced by our own MDCK assays and/or by 1+ other sources. This is the case for about 90 % of the Experimental Descriptors outlier values.

For the 23 compounds identified as outliers in the MDR1-Experimental Descriptors category, three were reclassified as borderline compounds (compounds with a $\log P_{\mathrm{m}}$ between -2 and -3), and therefore not in opposition to the energy argument. All remaining outlier compounds were reclassified as non-outliers due to unreproducible and thus likely erroneous ER values. Table 3.3.1.1 depicts all outlier compounds in this subset of the MDR1 data, the source and the source ER, as well as the calculated $\log P_{\mathrm{m}}$ value. Table 3.3.1.1 also depicts our independently-determined MDCK ER values (where available), the reclassification status of each respective outlier, as well as the justification for its reclassification.

Table 3: MDCK results and reclassification status of outliers from the dataset MDR1 - Experimental Descriptors

Outlier	ER	Source	$\log K_{\mathrm{hex/w}}$ †	$\log P_{\mathrm{m}}$ *	MDCK ER	Reclassification	Reclassification basis
Amitriptyline	2.8	[97]	4.58	0.72	-	Not outlier	Unreliable ER source ER $\leq$ 2.5 based on data from [50]
Atomoxetine	2.5	[51]	2.7	-1.27	-	Not outlier	Unreliable ER source
Brompheniramine	10.2	[99]	2.09	-1.39	0.9	Not outlier	Unreliable ER source; ER $\leq$ 2.5 based on own data
Chlorpheniramine	8.1	[99]	2.12	-1.33	0.8	Not outlier	Unreliable ER source; ER $\leq$ 2.5 based on own data
Chlorpromazine	2.6 5.7	[97] [51]	4.76	0.81	0.6	Not outlier	Unreliable ER sources; ER $\geq$ 2.5 based on own data and [50], [69], [96]
Clomipramine	10.9	[51]	4.78	0.83	0.9	Not outlier	Unreliable ER source; ER $\leq$ 2.5 based on own data and [70]
Clozapine	2.8	[51]	0.94	-1.21	-	Not outlier	Unreliable ER source
Cyclobenzaprine	2.8	[51]	3.78	0.41	-	Not outlier	Unreliable ER source; ER $\leq$ 2.5 based on data from [50], [96]
Desipramine	6.7	[97]	3.49	-1.3	1.9	Not outlier	Unreliable ER source; ER $\leq$ 2.5 based own data and [50], [70], [98]
Diphenhydramine	3.7	[99]	3.86	0.43	1.7	Not outlier	Unreliable ER source; ER $\leq$ 2.5 based own data and [50], [100]
Doxylamine	11	[97]	0.64	-2.13	1.1	Not outlier	Unreliable ER source; ER $\leq$ 2.5 based own data and [50]
Fluoxetine	2.7 5.2	[97] [51]	3.7	-0.82	1.3	Not outlier	Unreliable ER source; ER $\leq$ 2.5 based own data and [50], [96], [98]

Table 3 (continued)

Outlier	ER	Source	$\log K_{\mathrm{hex/w}}{}^{\dagger}$	$\log {P_m}^{*}$	MDCK ER	Reclassification	Reclassification basis
Fluvoxamine	3.1	[51]	1.88	-1.02	-	Not outlier	Unreliable ER source; ER $\leq$ 2.5 based on data from [96]
Loperamide	7.8	[69]	0.45	-2.39	-	Borderline compound	Concentration dependence experiments and simulations, see Section 3.3.4 and 3.3.5
	9.4	[96]					
	9.9	[50]					
	17.8	[70]					
	236.9	[97]					
Loratadine	7.4	[99]	2.46	0.66	0.7	Not outlier	Unreliable ER source; ER $\leq$ 2.5 based on data from [69], [96], [100]
Paroxetine	5.5	[51]	0.95	-2.89	-	Not outlier	Unreliable ER source; ER $\leq$ 2.5 based on data from [96]
Pyrilamine	5.6	[99]	1.04	-1.95	1.0	Not outlier	Unreliable ER source; ER $\leq$ 2.5 based on own data
Quinidine	4.4	[102]	0.14	-2.22	-	Borderline compound	Concentration dependence experiments and simulations, see Section 3.3.4 and 3.3.5
	11.4	[98]					
	15.0	[68]					
	15.0	[100]					
	16.1	[96]					
	16.4	[70]					
	27.2	[69]					
	338	[97]					

Table 3 (continued)

Outlier	ER	Source	log$K_{\mathrm{hex/w}}$ †	logP_m *	MDCK ER	Reclassification	Reclassification basis
Reserpine	3.7	[69]	-0.9	-2.29	2.6	Borderline compound	logP_{m} between -2 and -3
Rimonabant	2.5	[51]	1.25	-0.39	-	Not outlier	Unreliable ER source
Risperidone	2.6	[51]	0.09	-1.90	-	Not outlier	Unreliable ER source; ER $\leq$ 2.5 based on [50], [70], [96]
Sertraline	3.6 11.2	[96] [51]	4.57	0.79	0.8	Not outlier	ER $\leq$ 2.5 based on own data
Verapamil	2.8 5.2	[70] [68]	2.76‡	-0.42	1.9	Not outlier	ER $\leq$ 2.5 based on own data and [50], [51], [69], [96], [98], [102], [103]

† LSER [63] log$K_{\mathrm{hex/w}}$ based on experimental descriptors
* Calculated from LSER $K_{\mathrm{hex/w}}$ using SDM model, see Section 2.2.2.2.
‡ Calculated from PAMPA $K_{\mathrm{hex/w}}$

3.3.1.2 MDR1- Calculated descriptors The compounds in this category had LSER $K_{\mathrm{hex/w}}$ value based on calculated descriptors, and therefore it was presumed that the P_{m} value would be the more dubious value, and not the ER. Therefore, for outliers in this category, performing PAMPA assays to independently determine the $K_{\mathrm{hex/w}}$ value was the preferred investigatory method. The P_{m} was then recalculated based on these more reliable $K_{\mathrm{hex/w}}$ values. However, MDCK efflux assays were also performed in some cases. Table 3.3.1.2 depicts all outlier compounds in this subset of the MDR1 data, the source and the source ER, as well as the calculated $\log P_{\mathrm{m}}$ value. Table 3.3.1.2 also depicts our independently-determined MDCK ER values and/or PAMPA $K_{\mathrm{hex/w}}$ (where available), the reclassification status of each respective outlier, as well as the basis for its reclassification.

Of the 16 outlier compounds in this subset, 4 were reclassified as non-outliers due to unreliable ER values or independently determined non-significant ER values. Another 8 compounds in this subset were reclassified as borderline compounds. For two of these borderline compounds, amprenavir and prazosin, the reclassification as likely borderline compounds were due to their initial $\log P_{\mathrm{m}}$ values. As such, they were subjected to concentration-dependent MDCK assays and model fits (see Section 3.3.4 and 3.3.5). Three compounds in this subset had to be excluded since it was found that its poor aqueous solubility (nilotinib) or instability (lopinavir and ritonavir) impeded the extraction of reliable experimental values. Lopinavir and ritonavir exhibited high ER values but had very variable recovery values in both the MDCK and PAMPA assays, so much so that they could not produce reliable results. It has been shown that ritonavir is unstable and degrades at the more basic pH values [136] that are needed for this compound in PAMPA and MDCK assays, which could explain the observed experimental effects. Finally, one compound, terfenadine, could not be reclassified and remains a true outlier. Our own MDCK assays did find a significant ER value of 2.8, albeit a very low one. Furthermore, a newly-determined PAMPA $K_{\mathrm{hex/w}}$ value confirmed a $\log P_{\mathrm{m}}$ value of 0.08, therefore above the threshold. However, this compound exhibits very poor recovery in the MDCK assays- which would have likely been the case in the assays from the other sources as well. These poor recoveries may very well result in a false ER. Using a three-compartment model (discussed more thoroughly in Section 3.3.5), recoveries in MDCK assays can be simulated based on the properties of the chemical, yet the model failed to reproduce the experimental recoveries. As such, further experiments are needed to establish exactly how recovery affects the presentation of an ER for this compound. Thus, at this point it can neither be excluded nor confirmed as an outlier, since doubts regarding the influence of recovery remain.

Table 4: PAMPA and MDCK results and reclassification status of outliers from the dataset MDR1 - Calculated Descriptors

Outlier	ER	Source	$\log K_{\mathrm{hex/w}}$ †	$\log P_{\mathrm{m}}$ *	MDCK ER	PAMPA $\log K_{\mathrm{hex/w}}$	PAMPA $\log P_{\mathrm{m}}$	Reclassification	Reclassification basis
Amprenavir	20.9 26.5 29.0 32.4	[98] [69] [50] [69]	1.53 COSMO: -1.44	-0.17 COSMO: -2.66	28	-1.7	-2.86	Borderline compound	Concentration dependence experiments and simulations, see Section 3.3.4 and 3.3.5
Clemastine	3.9	[99]	3.95	0.08	1.0	-	-	Not outlier	Unreliable ER source. ER $\leq$ 2.5 based on own data and [50]
Darifenacin	4.0	[95]	1.35	-1.61	-	1.47	-2.00	Borderline compound	PAMPA $\log P_{\mathrm{m}}$ between -2 and -3
Desloratadine	9.1	[100]	3.62	-0.83	-	1.86	-2.4	Borderline compound	PAMPA $\log P_{\mathrm{m}}$ between -2 and -3
Emetine	3.5	[69]	3.46	-0.30	11.7	1.3	-2.11	Borderline compound	PAMPA $\log P_{\mathrm{m}}$ between -2 and -3
Gefitinib	22.3	[16]	2.60	0.61	-	-0.45	-1.96	Borderline compound	PAMPA $\log P_{\mathrm{m}}$ between -2 and -3
Guanfacine	3.0	[97]	0.48 COSMO: -2.83	-0.98 COSMO: -3.76	-	-	-	Not outlier	Unreliable ER source ER $\leq$ 2.5 based on [50] COSMO $\log P_{\mathrm{m}} < -3$
Lopinavir	7.2	[108]	0.78	-0.83	15.2	-	-	Excluded	Unstable
Mequitazine	2.8	[50]	3.45	-1.88	-	2.3	-2.14	Borderline compound	PAMPA $\log P_{\mathrm{m}}$ between -2 and -3

Table 4 (continued)

Outlier	ER	Source	log$K_{hex/w}$ †	logP_m	MDCK ER	PAMPA logK	PAMPA logP_m	Reclassification	Reclassification basis
Nelfinavir	8.9	[69]	2.19	-1.55				Borderline	PAMPA logP_m between -2 and -3
	22.4	[50]	COSMO: 0.2	COSMO: -3.22	-	0.80	-2.72	compound	COSMO logP_m < 3
Nilotinib	14.0	[16]	-0.38	-1.79	-	-	-	Excluded	Poor aqueous solubility
Perospirone	7.8	[51]	2.52	0.07	-	-	-	Not outlier	Unreliable ER source
Phenelzine	16.6	[103]	0.48 COSMO: -1.64	-1.32 COSMO: -3.10	25	-0.83	-2.42	Borderline compound	PAMPA logP_m between -2 and -3
Prazosin	3.2	[96]	-1.13	-2.54	3.2	-3.57	-4.59	Not outlier	PAMPA logP_m less than -3
	3.5	[111]							
	4.6	[69]							
Ritonavir	12.6	[68]	0.84	-0.81	115	-	-	Excluded	Unstable
	49.5	[96]							
	53.9	[69]							
Terfenadine	2.9	[50]	3.01	-1.42	2.8	4.8	0.08		
	4.7	[69]							
	18.4	[99]							

† LSER [63] $K_{hex/w}$ based on calculated descriptors

* Calculated from LSER $K_{hex/w}$ using SDM model, see Section 2.2.2.2.

3.3.2 BCRP dataset outliers

In this dataset, 4 compounds are zwitterionic and thus datapoints from these compounds were excluded from further analysis. In total, 10 datapoints from this dataset were identified as outliers, representing 5 compounds. All outlier datapoints were from compounds with a $K_{\mathrm{hex/w}}$ value based on calculated descriptors. On the basis of newly calculated P_{m} values based on our experimental PAMPA $K_{\mathrm{hex/w}}$ values for these compounds, 2 were reclassified as likely borderline compounds and 1 as not an outlier. Nilotinib was also found in this subset of outliers, and once again had to be excluded due to its poor aqueous solubility, along with the compound lapatininb, which suffered from the same drawback. Therefore, no outliers remained in this category.

3.3.3 MRP2 dataset outliers

In this dataset, one compound is zwitterionic and one has a permanent charge, and these compounds were excluded from further analysis. In total, only one compound from this dataset was identified as an outlier. This compound, docetaxel, also fell into the Calculated Descriptors category. The calculated $\log P_{\mathrm{m}}$ for this compound based on the LSER $K_{\mathrm{hex/w}}$ value was -2.74, thus it was reclassified as a likely borderline compound and not an outlier.

3.3.4 Concentration-dependent investigation of borderline compounds

The results of the concentration-dependent bidirectional MDCKII assays are depicted in Figures 9 and 10. Tabulated P_{app}, recovery and ER values at each concentration can be found in the Appendix. Figure 9 shows that for two compounds, acebutol and amprenavir, the ER does not change or decline over the entire concentration range tested. Only at the last two concentrations does amprenavir start to show a slight decline in $B \rightarrow A$ permeability, however not significant enough to reduce the ER to insignificance as can be observed for the compounds in Figure 10. This means that both of these compounds have not reached P-gp saturation yet. In contrast, for quinidine, loperamide and eletriptan (Figure 10 A, B and D) it can be seen that the decline in ER values is caused by a drop in $B \rightarrow A$ permeability and a concomitant increase in $A \rightarrow B$ permeability. The decline in $P_{app,B\rightarrow A}$ can be attributed to classic saturation effects of the P-gp transporter, which is the predominant resistance in this direction. At low compound concentrations the P-gp transporter is not yet saturated and this results in high transport rates, resulting in high ER values. At higher concentrations, the transporter has likely reached saturation, and active transport no longer increases with concentration. Thus, passive permeability becomes more dominant as it increases proportionally with concentration. The resultant increase in $P_{app,A\rightarrow B}$ contributes to the decline in ER values, leading to substantially lower and even insignificant ER values.

Table 5: PAMPA results and reclassification status of outliers based on calculated descriptors from the BCRP and MRP2 dataset

Outlier	ER	Source	$\log K_{\mathrm{hex/w}}$ †	$\log P_{\mathrm{m}}$ *	PAMPA $\log K_{\mathrm{hex/w}}$	PAMPA $\log P_{\mathrm{m}}$	Reclassification	Reclassification basis
BCRP Dataset								
Erlotinib	17	[119]	0.55	-0.95	-0.7	-2.0	Borderline compound	PAMPA $\log P_{\mathrm{m}}$ between -2 and -3
Gefitinib	4.5	[118]	0.75	0.61	-0.45	-1.96	Borderline compound	PAMPA $\log P_{\mathrm{m}}$ between -2 and -3
	10.8	[16]						
Lapatinib	2.6	[120]	1.98 COSMO: -1.01	0.18 COSMO: -2.33	-	-	Excluded	Poor aqueous solubility
Nilotinib	10.8	[16]	-0.38	-1.79	-	-	Excluded	Poor aqueous solubility
Prazosin	4.1	[117]	-1.13	-2.54	-3.57	-4.59	Not outlier	Concentration dependence experiments and simulations. (See Section 3.3.4 and 3.3.5) PAMPA $\log P_{\mathrm{m}}$ less than -3
	14.9	[16]						
	18	[115]						
	35.5	[113]						
	81	[125]						
MRP2 Dataset								
Docetaxel	7	[127]	-1.43	-2.74	-	-	Borderline compound	$\log P_{\mathrm{m}}$ between -3 and -2

† LSER [63] $K_{\mathrm{hex/w}}$ based on calculated descriptors

* Calculated from LSER $K_{\mathrm{hex/w}}$ using SDM model, see Section 2.2.2.2.

The observed saturation effects coinciding with the energy plateau is no coincidence. Indeed, these two phenomena lead to the same result: no further increase in the activity of the transporter with increasing concentration past some maximal flux value. As such, the energy limit which is dictated by physical principles is enforced by the cell through the mechanism of saturation. While the concept of transporter saturation and its impact on transporter-facilitated efflux is not new [137]–[139], this study is the first to link it to an energy threshold. As such, it is worth emphasising once again that experimental conditions are critical for obtaining meaningful results in MDCK efflux assays. In Chapter 2 it was shown that pH can play a role in the false classification of compounds, as ER values can change based on the pH. Here once again it can be observed that using concentrations that are too high can easily lead to the erroneous conclusion that compounds are not P-gp substrates.

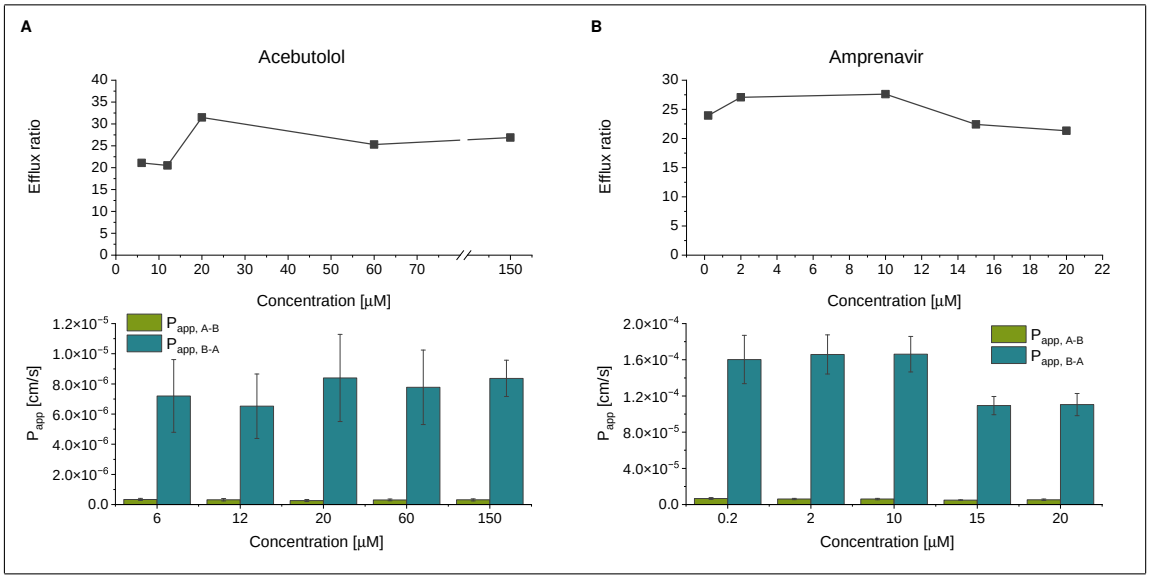

Figure 9: **Apparent permeability and efflux ratios as a function of concentration for less permeable compounds: A) Acebutolol and B) Amprenavir.** Error bars represent standard deviation. The ER (line graph, top panels) is the quotient of mean $P_{app,B\to A}$ over mean $P_{app,A\to B}$ values.

Prazosin (Figure 10 C) veers from the trend observed for the other compounds. Here, it seems as if the $P_{app,A\to B}$ does not increase at higher concentrations. The drop in ER in this case is solely attributed to a decrease in $B \to A$ permeability. This compound is also unique in that the ER values are generally much lower than those recorded for the other compounds, reaching a maximum of 3.5 instead of ≥ 15. The median value of the four ER values for prazosin from the sources in our dataset [16], [69], [96], [111] is 4, and it is not usually reported as a very strong substrate. Due to these low ER values, the data remains inconclusive and no energy limit could be extracted.

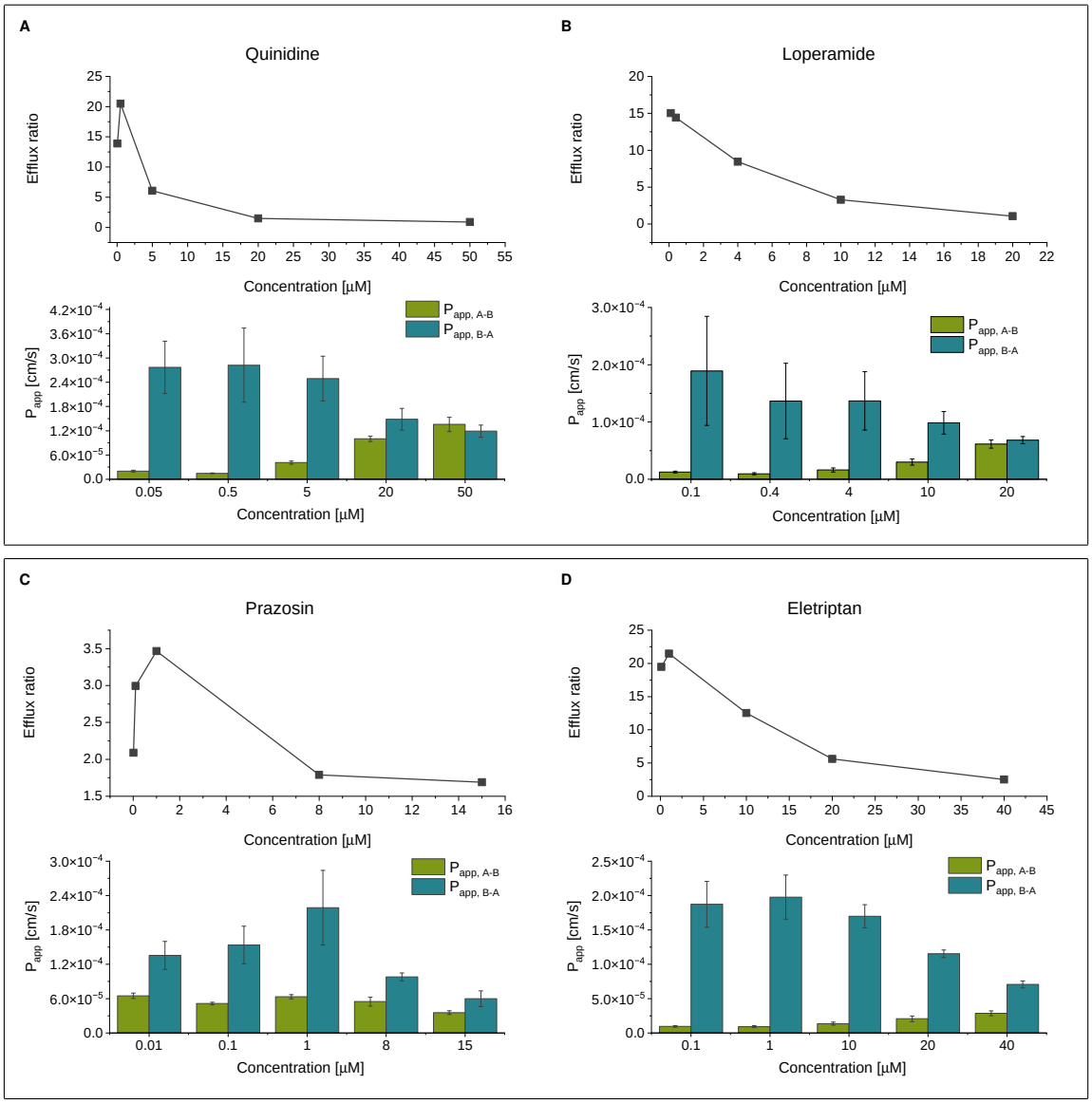

Figure 10: **Apparent permeability and efflux ratios as a function of concentration for more permeable compounds: A) Quinidine, B) Loperamide, C) Prazosin and D) Eletriptan.** Error bars represent standard deviation. The ER (line graph, top panels) is the quotient of mean $P_{app,B\to A}$ over mean $P_{app,A\to B}$ values.

3.3.5 Fitting of P-gp facilitated efflux

While attempting to perform the SOLVER fits for the experimental P_{app} values, it was observed that the fits do not work as they should for the $B \to A$ direction if the apparent permeability for this direction is particularly fast. The $P_{app,B\to A}$ values that were experimentally obtained for these compounds were often faster than what the inevitable limitation by the basolateral ABL would allow for. In these cases, the

fits failed. To locate the root of this issue, the P_0 and lipid-water partition coefficient ($K_{\text{lip/w}}$) values for one of the compounds exhibiting this problem were used in a detailed three-compartment model, where the concentrations over time could be observed in each compartment. Figure 11b shows the concentration in the cytosol as a function of time in the $B \rightarrow A$ direction. From Figure 11 it can be seen that the cytosolic concentration rises and then drops again at each sampling timestep (every 480 seconds in this case).

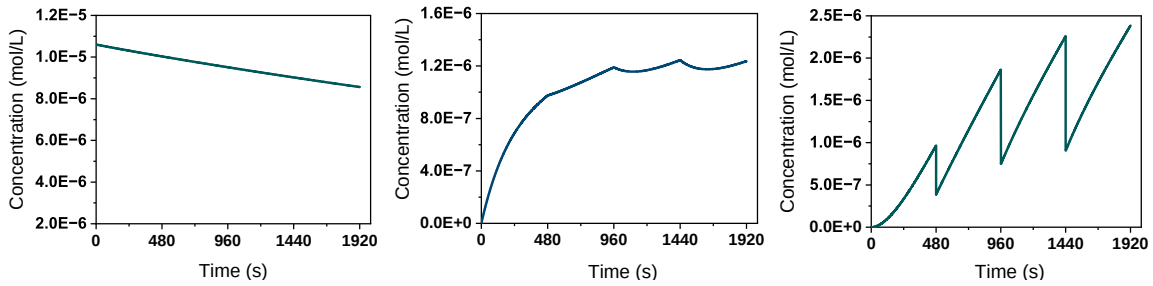

(a) Donor (b) Cytosol (c) Receiver

Figure 11: **Three-compartment model simulations of the concentration over time in the different compartments in the $B \rightarrow A$ direction**. A) Donor compartment, B) Cytosol C) Receiver compartment.

It was deduced that each time volume is sampled from the receiver compartment and replaced with fresh buffer, then the cytosol starts feeding the receiver compartment, which is why the cytosolic concentration drops at this very point. This is also evident when comparing the calculated P_{app} values with the experimentally-obtained ones. Initially the experimental P_{app} is slower than what we would expect mathematically, since the net rate into the cytosol is much higher than out of it, due to its sorption capacity. Then at some point the experimental P_{app} is faster than expected since the cytosol is no longer in steady-state with the other compartments, and the rate from the cytosol to the receiver compartment is higher than the rate from the donor to the cytosol. Ultimately, the observed trend in experimental data is actually predicted by the simulation. However, even though the problem is qualitatively obvious, a solution to avoid this issue experimentally could not be found. Increasing the time between sampling steps would be one way of attempting to address it, but this would compromise the sink conditions. Furthermore, it is also not possible to merely take the first timesteps, as steady-state has not yet been reached in the initial stages.

These conclusions were drawn with the aid of the three-compartment model for the compound quinidine, however for the more permeable compounds used in this section, any point where the $P_{app,B\rightarrow A}$ is faster than the basolateral ABL would technically allow for, it can be presumed that this is an artefact that is caused by this same issue. Ultimately what this means is that the $B \rightarrow A$ direction is simply as fast as

it can possibly be, considering ABL-limitation. However, since these concentration-dependent experiments were also performed for one less permeable compound not near the threshold (acebutolol) it was possible to evaluate how the resultant flux values change when the fit works as expected. Acebutolol did not have the same issue that the other compounds have, with its measured $P_{app,B\to A}$ never being faster than the calculated value. As such, the fit works in both directions, without any adjustments. The $J_{\text{pgp, active}}$ values for P-gp were then fitted both with and without fitting the $B \to A$ direction and compared, and it was observed that fitting the $B \to A$ direction does not make a significant difference to the end-result. As such, the final solution to circumventing the cytosol feeding issue was to only fit the $A \to B$ direction (assuming zero transport in the basolateral membrane) and evaluate P-gp flux only. In the absence of experimental workarounds, this was ultimately found to be the best solution.

Figure 12 shows the P-gp flux determined for the $A \to B$ direction in $\mu\text{mol}\,\text{cm}^{-2}\,\text{s}^{-1}$ for the six compounds investigated with concentration-dependent assays. These compounds were preliminary designated as borderline compounds due to their $\log P_{\text{m}}$ lying at or near the cut-off value used in this study. As such, they were designated for concentration-dependent MDCKII assays since they promised to reveal where the maximal flux limit lies more precisely. However, as can be observed in Figure 12, for most compounds we still see an increasing $J_{\text{pgp, active}}$ value and not an energy plateau. This was expected for acebutolol (B), but not for amprenavir (A) and eletriptan (C). However, consequent recalculations of $\log P_{\text{m}}$ for eletriptan based on the $K_{\text{hex/w}}$ determined through PAMPA assays described in this study shows that this compound does indeed lie well below the permeability threshold. For amprenavir (which was confirmed through PAMPA to lie in borderline area) it is likely that the concentrations used in the MDCK assays were not high enough to reach the maximal $J_{\text{pgp, active}}$ value, due to its poor solubility. For prazosin (D), the ER values were too low to be evaluated or to make reasonable assumptions. As such, it is not surprising that the aforementioned compounds did not reach the plateau.

Only for two compounds, quinidine (E) and loperamide (F) do we see the expected plateau when the transport of these compounds starts reaching the maximal flux value. For quinidine, the $P_{app,A\to B}$ and $P_{app,B\to A}$ at the last two concentrations are practically the same (within the standard deviation). At this concentration, there is complete saturation of the transporter. Despite active efflux operating at its energy-limited maximum, passive diffusion in the opposite direction dominates, resulting in no net efflux. Initially, the $P_{app,A\to B}$ for quinidine at the last two concentrations were too fast to result in a rational fit, so they were adjusted by hand to be lower by a factor of 2, which is within the expected standard deviation for these experiments. As such, the flux value at which quinidine is shown to plateau is actually a maximum value, and the limit could even be below this value.

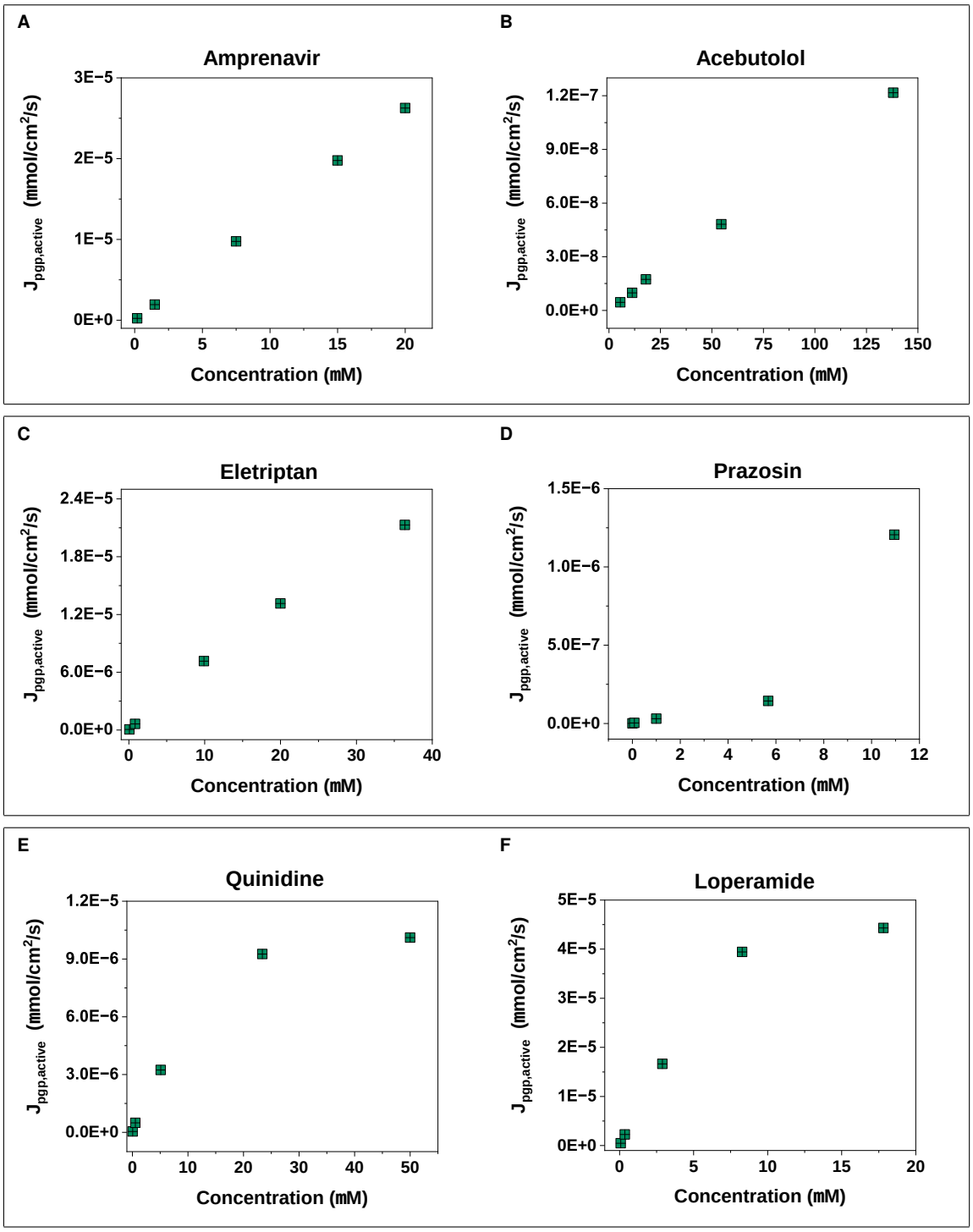

Figure 12: **P-gp facilitated flux fit values versus concentration for six compounds.** Fits were performed for $J_{\text{pgp, active}}$ in the $A \rightarrow B$ direction with an apical surface membrane factor of 1, indicating no difference in surface area between the basolateral and apical membrane.

3.3.6 Determination of energy limit

Because quinidine and loperamide exhibited saturation effects and evidently reached the maximal flux plateau, a classic non-linear Michaelis-Menten fit was performed for these two compounds using IGOR Pro. The results are depicted in Figure 13. The last two data points of quinidine were not used in the fit since they represent a maximal value (as described in the preceding section).

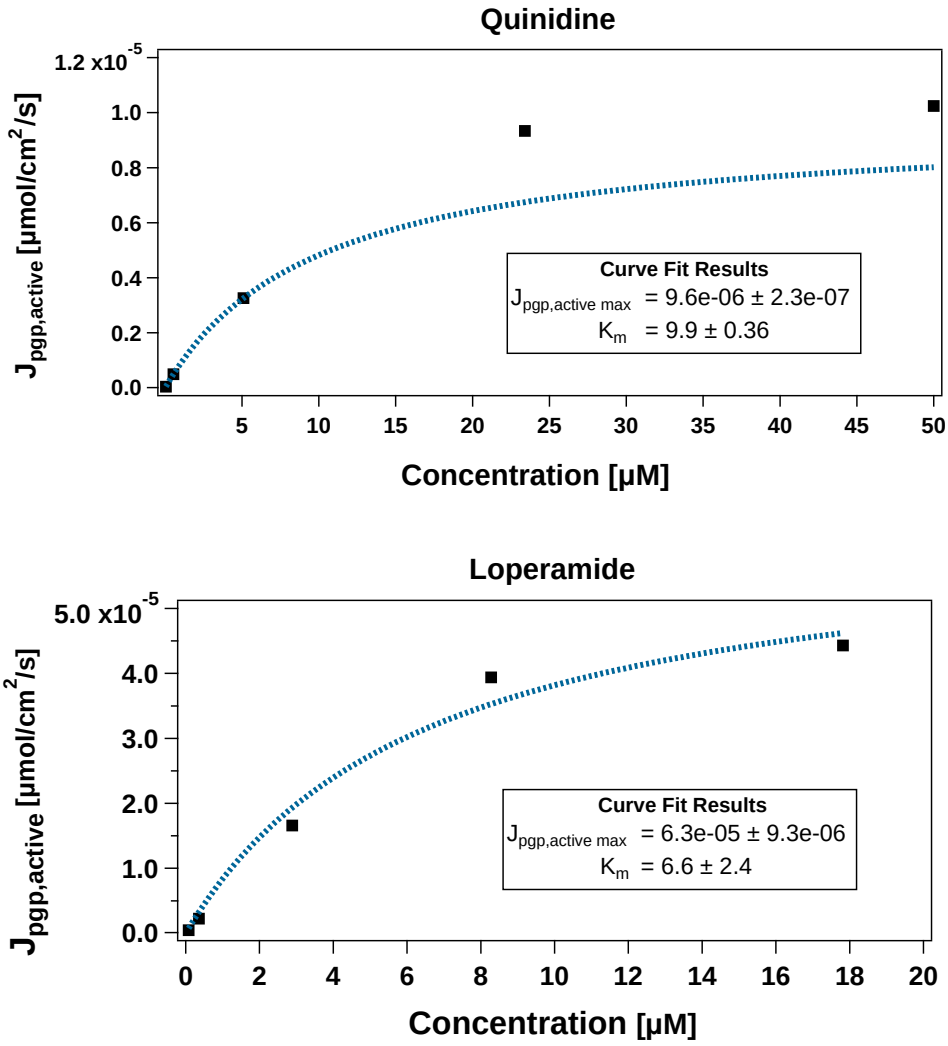

Figure 13: **Non-linear Michaelis-Menten fits for quinidine and loperamide exhibiting the maximal flux value, $J_{\text{pgp, active}}$. Markers indicate concentration-dependent calculated $J_{\text{pgp, active}}$ values, determined from fitted P-gp activity values based on MDCK assays.**

The results for loperamide are less precise because of uncertainty in the P_0 value used to generate the $J_{\text{pgp, active}}$ values. For loperamide, P_0 cannot be determined via MDCK or

PAMPA assays and is thus based only on an SDM prediction. While SDM predictions derived from experimental descriptors can be quite accurate, an experimental P_0 would be more reliable. The uncertainty in the P_0 prediction for loperamide consequently results in uncertainty in the fitted $J_{\text{pgp, active}}$ values. Therefore, the final $J_{\text{pgp, active}}$ value presented in this study is the maximum flux value from the Michaelis-Menten fit for quinidine, as it has a highly reliable experimental P_0 value, unlike loperamide.

The maximal $J_{\text{pgp, active}}$ generated by the Michaelis-Menten fit for quinidine of $1 \times 10^{-5}\,\mu\text{mol}\,\text{cm}^{-2}\,\text{s}^{-1}$ is the energy threshold for efflux transport determined for the MDCII-MDR1 cells used in this study. Essentially: it is unlikely that highly membrane-permeable compounds that demand higher flux than this for its effective efflux would be affected by any efflux transporter. As stated before, compounds that lie in the borderline window of membrane permeability (such as quinidine) could exhibit efflux, depending on their concentration. As the amount of compound increases, the energy required for effective efflux increases until it reaches the energy threshold. Though experimental P_0 values are generally reliable, they are still subject to error. The experimental P_0 for quinidine on which the calculation of the maximal flux value of $1 \times 10^{-5}\,\mu\text{mol}\,\text{cm}^{-2}\,\text{s}^{-1}$ was based may still lead to an estimation that is off by one order of magnitude. Which means that the true maximal flux value can probably be anywhere in the range of $5 \times 10^{-6}\,\mu\text{mol}\,\text{cm}^{-2}\,\text{s}^{-1}$ to $5 \times 10^{-5}\,\mu\text{mol}\,\text{cm}^{-2}\,\text{s}^{-1}$. The expected factor 10 error in experimental P_0 also explains why amprenavir and eletriptan have $J_{\text{pgp, active}}$ values slightly above this range. When the experimental error in these values are considered, they do not defy the maximal flux range. In comparison, for loperamide which does not have an experimental but rather a calculated P_0, the error is substantially higher, at two orders of magnitude. Thus the maximal flux value for loperamide predicted by the Michaelis-Menten fit in Figure 13 of $6 \times 10^{-5}\,\mu\text{mol}\,\text{cm}^{-2}\,\text{s}^{-1}$ does not contradict the value extracted from quinidine.

3.3.7 Linking the energy limit to membrane permeability and sensitivity analyses

While the $J_{\text{pgp, active}}$ value is interesting, it must be linked with a metric such as membrane permeability to be useful in practice. However, even though the energy threshold should be static across compounds and concentrations, translating $J_{\text{pgp, active}}$ into a P_{m} value is dependent on various factors. Because of this, the P_{m} threshold is more dynamic, and a one-size-fits-all P_{m} threshold cannot be provided. The maximal $J_{\text{pgp, active}}$ of $1 \times 10^{-5}\,\mu\text{mol}\,\text{cm}^{-2}\,\text{s}^{-1}$ was used to calculate the corresponding threshold P_{m} value. In other words, what is the maximum membrane permeability a compound can have in order to potentially be affected by active efflux? In the most general case: it was calculated for a neutral compound with a certain molecular weight and at a given concentration what combination of passive membrane permeability and active efflux it can afford for the activity of P-gp to meet the maximal flux value of $1 \times 10^{-5}\,\mu\text{mol}\,\text{cm}^{-2}\,\text{s}^{-1}$. In essence, P_0 was back-calculated from P-gp activity, and it was determined what P_0

value is possible for P-gp activity to equal the maximal flux value.

Figures 14-16 depict the results of the sensitivity analyses that was performed for the P_{m} threshold calculated from our energy limit using the model compound. Figure 14 depicts threshold P_{m} as a function of the energy limit. The solid blue line shows where the P_{m} threshold lies with the maximum $J_{\mathrm{pgp,\ active}}$ (energy limit) that was determined in Section 3.3.6. It is evident that the $\log P_{\mathrm{m}}$ cut-off value of -3 that was used to determine outliers in Section 3.2.2 corresponds quite favourably with the threshold P_{m} value determined independently here. This graph also shows where the threshold P_{m} would lie given different energy limits. For this, the maximum $J_{\mathrm{pgp,\ active}}$ was increased 5-15 times, as well as decreased 5-10 times. As is evident, the energy limit of the cells and thus their maximal $J_{\mathrm{pgp,\ active}}$ is directly proportional to the corresponding P_{m} threshold. Thus, an increase in maximal flux shifts the $\log P_{\mathrm{m}}$ threshold higher by the same factor. Naturally, a lower energy limit thus also results in a proportional decrease in the threshold $\log P_{\mathrm{m}}$ value.

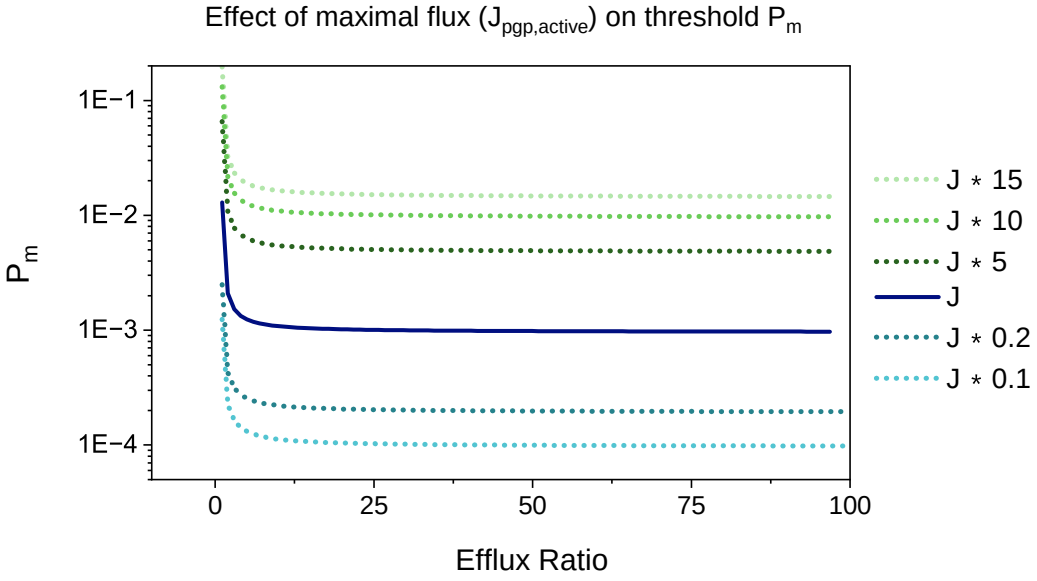

Figure 14: **Sensitivity analysis of threshold P_{m} value based on the maximal flux ($J_{\mathrm{pgp,\ active}}$) value determined for MDCKII cells.** $J_{\mathrm{pgp,\ active}}$ was varied as depicted. Basolateral transport was assumed to be negligible, the apical membrane surface area factor was fixed at 1, the compound concentration at 10 μM, and P_{para} factor at 0.1.

Figure 15 depicts threshold P_{m} as a function of concentration. Once again the importance of concentration for the P_{m} threshold becomes apparent, as increasing the concentration from the 10 μM standard concurrently lowers the P_{m} threshold, and vice versa for decreasing concentrations.

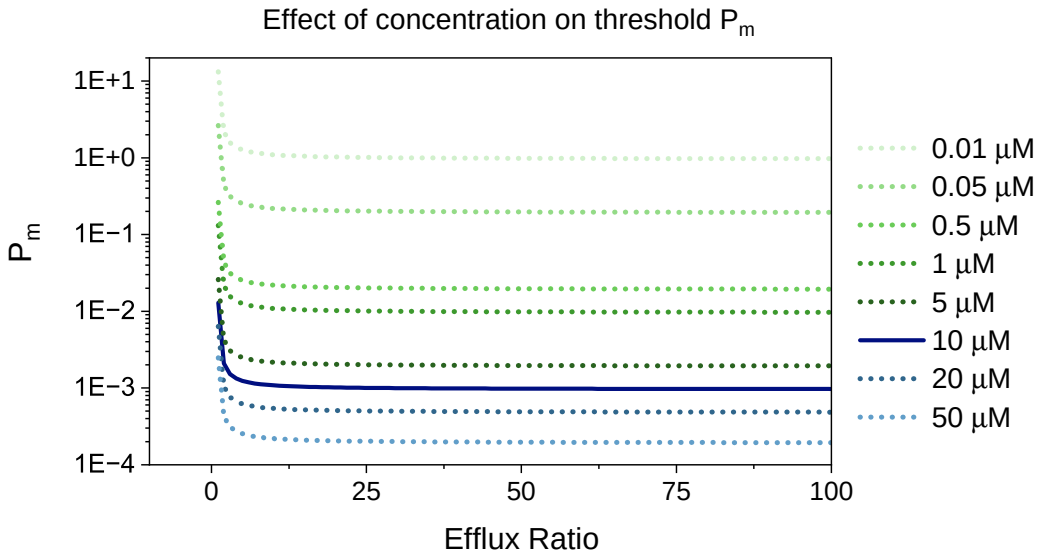

Figure 15: **Sensitivity analysis of threshold P_{m} value based on compound concentration.** Compound concentration was varied as depicted. The basolateral transport was assumed to be negligible, the apical membrane surface area factor was fixed at 1, the $J_{\mathrm{pgp,\ active}}$ at 1×10^{-5} µmol cm^{-2} s^{-1} and the P_{para} factor at 0.1.

The vast majority (> 80 %) of the ER values accumulated from the literature performed were obtained at a concentration between 5-20 μM, which is why the standard concentration was taken to be 10 μM to calculate the threshold. In this case, the P_{m} threshold shift is indirectly proportional to the concentration: the lower the compound concentration, the higher the P_{m} threshold, and vice versa for an increasing concentrations. This once again highlights the importance of considering concentration when determining a P_{m} threshold, and also considering the compound concentration that was used in the transport assays when evaluating a compound against the threshold.

Figure 16 depicts threshold P_{m} as a function of the apical surface membrane factor (S). It has already been discussed that the factor of 24 used in Chapter 2 was likely too high for these MDCK cells. Unlike in Chapter 2, this was expected to be consequential for the results of this chapter. Indeed, Figure 16 shows once the P_{m} threshold is indirectly proportional to the apical surface membrane factor. When S increases, we can expect the P_{m} threshold to decrease by the same factor. As a result, there is significant difference between the two extreme scenarios of having no difference in surface area between the apical and basolateral membranes, versus having a rather substantial factor of 24 difference. The factor of 7.5 was determined by Butor and Davoust [61] specifically for MDCKII cells. However, most of our analyses was performed using a factor of 1. Further sensitivity analyses that evaluate the less-significant effects of species charge, paracellular transport and the basolateral transporter activity on the threshold P_{m} can be found in the Appendix.

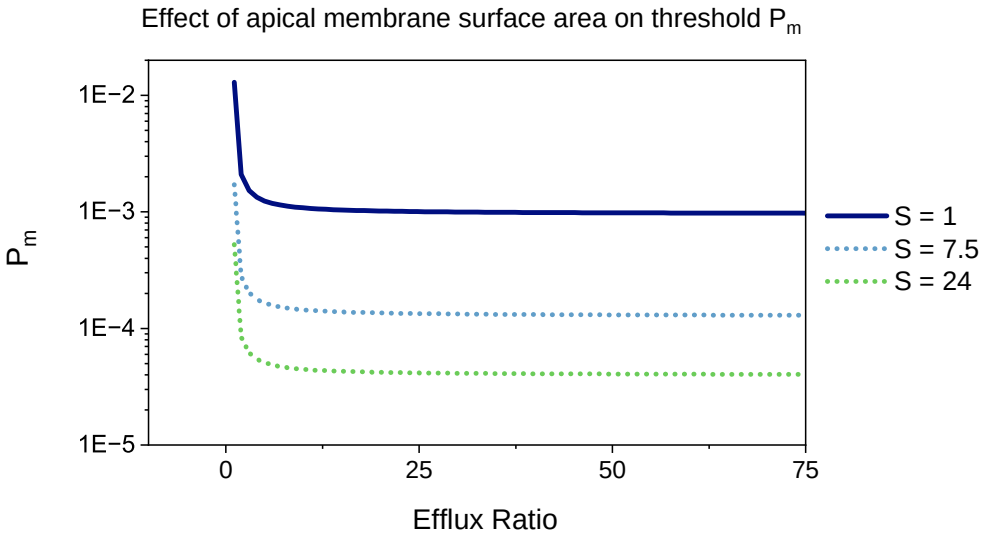

Figure 16: **Sensitivity analysis of threshold $P_{\mathbf{m}}$ value based on apical membrane surface area.** Apical membrane surface area factor (S) varied as follows: Assuming no difference in apical and basolateral surface membrane (S =1), a factor 24 increase in apical surface area (S=24) [59], and a factor 7.5 increase in apical surface area (s=7.5) [61]. The basolateral transport was assumed to be negligible, compound concentration was fixed at 10 μM, $J_{\text{pgp, active}}$ at 1×10^{-5} µmol cm^{-2} s^{-1} and the P_{para} factor at 0.1.

As is also evident from Figures 14 - 16, the P_{m} threshold stays constant across all ER values except in the lower ranges. This trend is constant across all scenarios that were analysed, regardless of which factor is varied. To understand why this is, one needs only to consider that at low ER values when P-gp is less active, passive back-flow of the compound from the cytosol is highly relevant, which is not the case for compounds with high ER values where P-gp is more active. In the low ER value range, in order to double the ER, active efflux has to increase substantially to compete with the passive backflow. However, even with a substantial increase in P-gp activity, there is only a modest drop in cytosol concentration. Thus, in the low ER ranges, P_0 has to decrease in order for the system to continue adhering to the maximal energy consumption value when the ER increases. In contrast, at higher ER values, active efflux dominates, making the passive backflow negligible. Doubling ER in this range involves proportionally smaller increases in P_{pgp} since it already vastly exceeds P_0, and active transport largely dictates the efflux. As a result, the cytosolic concentration decreases proportionally with the increase in P_{pgp} activity. Energy consumption remains the same despite the higher ER and reaches a plateau- leading to a concurrent P_{m} plateau. This is of course a simplified scenario, since the activity of the basolateral transporter and other factors also play a role- but it allows for a fundamental understanding of the phenomenon that can be observed in the lower ER ranges. However, this affects only a small percentage of the significant efflux ratios in our database (those that barely surpass the significance

threshold), therefore, the plateau remains the most interesting value.

3.4 Discussion

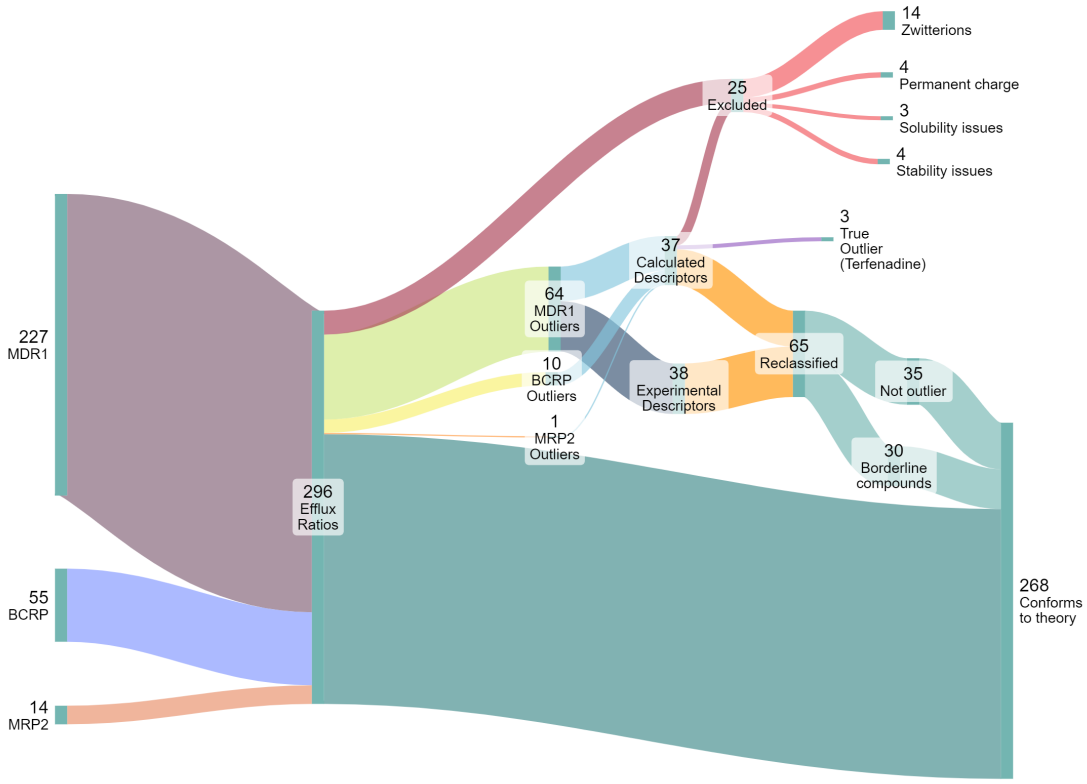

Figure 17: **Diagram illustrating the classification and processing of 296 efflux ratio compounds across MDR1, BCRP, and MRP2 transporter datasets**. Some compounds were excluded based on properties such as zwitterionic nature, permanent charge, solubility, or stability issues. Outliers were identified and investigated with MDCK or PAMPA assays, or by other means. Most outliers were reclassified and found to conform to the energy limit theory. The vast majority of the data (90%) is in agreement that there is a membrane permeability cut-of value for compounds exhibiting significant efflux.

Figure 17 is a scheme that represents the collection, analysis and reclassification of the data. Nearly 300 significant ER values from MDCK assays were collected from 46 different literature sources. More than 70 % of the ER values were for P-gp, however the two other prominent efflux transporters, BCRP and MRP2, were also represented in the data. The membrane permeability (P_{m}) was then determined for each compound. Considering the spread of the experimental data, it was hypothesised that for MDCK cells, compounds with a P_{m} value greater than $1 \times 10^{-3}\,\mathrm{cm\,s^{-1}}$ would be too membrane

permeable for the cell to maintain efficient efflux against their high rates of passive diffusion. From the outset, two thirds of the data did not contradict the hypothesis that compounds that have P_{m} greater than $1 \times 10^{-3}\,\mathrm{cm\,s^{-1}}$ are actively effluxed since their efflux would surpass the maximal possible flux of the cell. That is, they were confirmed efflux substrates with a P_{m} lower than $1 \times 10^{-3}\,\mathrm{cm\,s^{-1}}$. Eighteen values were excluded early in the process because the compounds were zwitterions or permanent charged. Seven more were excluded at the experimental stage due to poor aqueous solubility and stability issues which impeded their analysis. Of all collected data points, 75 were identified as outliers. These outlier values represented 39 unique compounds which had an ER greater than 2.5 reported by at least one source, and membrane permeability greater than $1 \times 10^{-3}\,\mathrm{cm\,s^{-1}}$.

The outliers from the BCRP and MRP2 datasets all had a P_{m} value that was determined based on LSER $K_{\mathrm{hex/w}}$ values from calculated descriptors. For the MDR1 dataset, there were also outliers with P_{m} values based on LSER $K_{\mathrm{hex/w}}$ values from experimental descriptors. The majority of the outliers were reclassified through the independent re-determination of MDCK ER values, and/or new PAMPA $K_{\mathrm{hex/w}}$ values that were used to re-calculate the compound's P_{m}. Of the revised values, 35 were reclassified as not outliers. The compound terfenadine, from the MDR1 - Calculated Descriptors dataset remained as the sole outlier with three reported ER values. For this compound, we determined an independent ER value of 2.8 and a P_{m} of $1.2\,\mathrm{cm\,s^{-1}}$ calculated from a newly- determined PAMPA $K_{\mathrm{hex/w}}$ value. However, this compound suffers from poor recovery in the MDCK assays, and since its ER value barely surpasses the significance threshold of 2.5, it is most likely an artefact of its aberrant recovery.

The remaining 30 outlier values that were reclassified were identified as probable borderline compounds. That is, compounds near the P_{m} cut-off with a P_{m} value between $1 \times 10^{-3}\,\mathrm{cm\,s^{-1}}$ and $1 \times 10^{-2}\,\mathrm{cm\,s^{-1}}$. Concentration-dependence experiments were performed for some of these suspected borderline compounds, since concentration would play a particularly pivotal role for these compounds close to the P_{m} threshold. Two out of the five borderline compounds evaluated did seem to reach the energy limit in their upper concentration ranges, since their $J_{\mathrm{pgp,\ active}}$ values reached a plateau. Using a non-linear Michaelis-Menten fit for these two compounds, it was possible to calculate the maximal P-gp facilitated flux possible, considering the limited energy available for efflux. Since quinidine has a much more reliable experimental P_0 value unlike the other compound, loperamide, its $J_{\mathrm{pgp,\ active}}$ was used as the final maximal flux value. However, there are still several compounds classified as borderline that will be subject to the same concentration dependence experiments in order to further confirm this maximal flux value with additional compounds for an upcoming publication. It is worth noting that the final determined maximal flux value of $1 \times 10^{-5}\,\mathrm{\mu mol\,cm^{-2}\,s^{-1}}$ that was obtained via these experiments correspond favourably with the theoretical value of $7 \times 10^{-5}\,\mathrm{\mu mol\,cm^{-2}\,s^{-1}}$ obtained in Section 3.1, considering the order of magnitude error associated with experimental P_0 values.

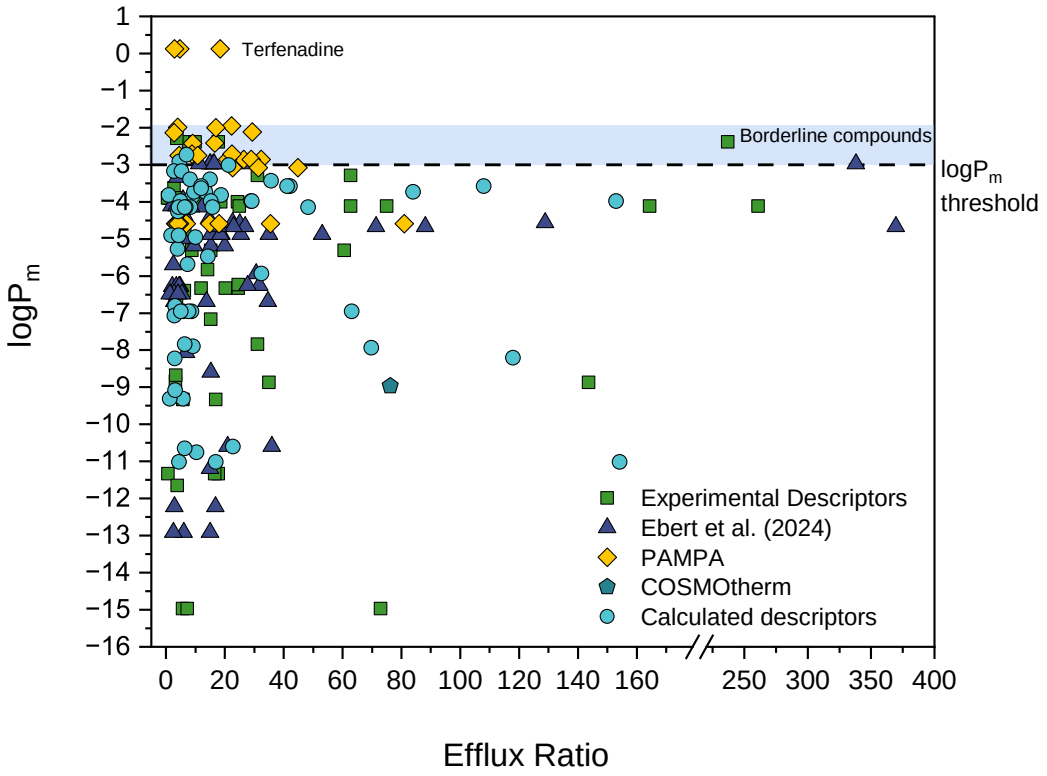

Figure 18: **logP_m vs ER with re-evaluated data, including the logP_m threshold and borderline compounds.** Combined data from the P-gp, BCRP and MRP2 datasets. The logP_m threshold for these MDCKII cells was found to lie at -3. Aside from the single outlier (terfenadine) no compounds with a permeability above $1 \times 10^{-2}\,\mathrm{cm\,s^{-1}}$ were found to be significantly effluxed. The efflux of borderline compounds (P_m between $1 \times 10^{-2}\,\mathrm{cm\,s^{-1}}$ and $1 \times 10^{-3}\,\mathrm{cm\,s^{-1}}$) is highly dependent on concentration.

Figure 18 shows a graph of the ER values vs logP_m of all data (all three transporter datasets), along with the P_m threshold line determined in this study. The depicted P_m threshold includes three essential qualifiers. First, it is based on the energy limit of $1 \times 10^{-5}\,\mu\mathrm{mol\,cm^{-2}\,s^{-1}}$ determined for our MDCK-MDR1 cells in Section 3.3.6. Second, it assumes that there is no difference between apical and basolateral membrane surface areas. Finally, it assumes a compound concentration of 10 μM. As shown in Section 3.3.7, scenarios which veer significantly from these parameters can increase or decrease the P_m threshold. Factors such as the relative activity of the basolateral uptake transporter, the compound charge and the magnitude of paracellular transport seem to have little effect on the P_m threshold (see Appendix). In contrast, the sensitivity analysis showed that the maximal flux of the cells, the concentration of the compound and the apical membrane surface area can all significantly shift the P_m threshold.

It has already been discussed how the maximal flux value can be different for different cell types. In Section 3.1 it was shown that MDCK cells likely have a higher energy

limit than the average cell, since their energy needs are higher than that of other, less active cells. As such, it is critical to stress once more that there will be differences between different cell types, and cells with higher energy demands/production will concomitantly have a higher maximal flux value. Which, as is evident from Figure 14, can significantly increase the P_{m} threshold. Thus we emphasise once again: The P_{m} threshold presented here is not a universal value. It is dependent on the conditions delineated above, and it was determined for the MDCK-MDR1 cells at our disposal. Therefore, the exact same P_{m} cut-off cannot be used across all cell types. For example, cells of the BBB barrier are likely even more active than MDCK-MDR1 cells, since they have extremely tight junctions and express very high amounts of various efflux transporters to maintain stringent control of brain access. As such, it can once again be surmised that if BBB cells have a higher maximal flux value, this will allow for the efficient efflux of compounds with a higher membrane permeability.

However, it is remarkable that such a clear trend was observed. Of all compounds that have been reported in the literature as being substrates of one of the three major efflux transporter implicated in MDR, only one had a P_{m} value above the threshold and its accompanying borderline window. There is no shortage of pharmaceutical compounds with $\log P_{\mathrm{m}}$ of $1 \times 10^{-2}\,\mathrm{cm\,s^{-1}}$ and above. Considering this, it can be concluded that membrane permeability can be a very accurate filtering metric for active efflux. If the energy limit of certain cells expressing an efflux transporter of interest is known or determined, then it can also be determined what the maximal membrane permeability of a compound can be that would still allow the maintenance of efficient efflux. Consequently, for compounds that have a higher P_{m} value it can with some certainty be concluded that their disposition will likely not be affected by any efflux transporters relevant for those cells.

4 Conclusions and Outlook

In Chapter 2 of this work, the feasibility of using intrinsic values for efflux was explored as a method to quantify active transport from efflux ratios obtained with bidirectional MDCK/Caco-2 transport assays. The transport model for the permeation of chemical compounds across in vitro monolayers was extended to include the filter, aqueous boundary layers (ABLs), and paracellular transport. We found that while the additional aqueous resistances introduced by the ABLs and filter can affect the measured apparent permeabilties in either direction, they have no effect on the ER. As a consequence, when performing bidirectional transport assays to determine the ER of a compound, one does not need not be concerned with the often painstaking and time-consuming measures taken to avoid ABL/filter limitations as with assays performed to determine P_0. Furthermore, the existing ER data from literature does not need to be re-evaluated to correct for ABL interference. In contrast, we showed that paracellular transport can have a substantial effect on the ER even when it is not the dominant transport route. As a result, its role must always be considered when interpreting

experimental results. Furthermore, when paracellular transport dominates in both measured directions, then the ER reduces to unity. Thus, determining the ER when paracellular transport is dominant may lead to the false classification of compounds as non-substrates even when efflux is occurring. Our data also revealed the presence of an uptake transporter in the basolateral membrane, and the model was further extended to include this transport. The pH-dependence of the ER was then investigated in an attempt to determine whether P-gp preferentially transports the neutral or ionic species. However, comparisons of the experimental data with model fits were inconclusive due to potential pH effects on the transporter, as well as the increased complexity introduced by the combined effects of paracellular transport and the basolateral uptake transporter. In conclusion, this study found that using intrinsic values to quantify active efflux is preferable when paracellular transport plays a significant role, as ER values in this case can lead to false conclusions. However, the combined influences of paracellular transport, the previously unaccounted for basolateral influx transporter, as well as the inability to identify the species preference of P-gp does substantially increase the complexity of the transport and ER equations. As a result, straightforward extraction of intrinsic P_{pgp} values remains elusive. However, pursuing this question has resulted in the most detailed and comprehensive model for transport across cellular monolayers in MDCK/Caco-2 assays to date. Furthermore, even though we have described the model for P-gp in this study, the model is generalisable to any efflux transporter in the apical membrane, and it can also be extended to include any other significant processes that lead to deviations of experimental measurements from the model (such as additional transporters).

Chapter 3 of this work proposed an energy limit for active efflux, which can be translated into a membrane permeability threshold value for compounds that can exhibit significant efflux. For the MDCKII-MDR1 cells used in this study, it was hypothesised that compounds with a $\log P_{\mathrm{m}}$ value greater than -3 would not be affected by any efflux transporter, as maintaining active efflux against high rates of passive diffusion would incur prohibitive energy costs. Nearly 300 ER values from MDCK assays of three transporters (P-gp, BCRP and MRP2) were sourced from literature to investigate this hypothesis. A systemic analysis of the outlier compounds, which had ER values greater than 2.5 and $\log P_{\mathrm{m}}$ values greater than -3, resulted in the reclassification of most outliers as conforming to the theory. Concentration-dependence assays for borderline compounds enabled the identification of the exact maximal flux value, which was translated into a threshold P_{m} value. Sensitivity analyses of the threshold P_{m} value revealed that the specific energy limit of the cells, compound concentration, and the relative surface area of the apical to basolateral membrane can significantly shift the threshold P_{m}. In contrast, paracellular transport, speciation and the activity of the basolateral transporter has little to no effect on the threshold P_{m}. This study was the first to propose an energy limit for active efflux and to link this energy limit with membrane permeability, thereby providing a method to exclude compounds with P_{m} values above a certain threshold from consideration as candidates for transporter-

facilitated efflux. This approach could reduce the need for time- and resource-intensive transport assays for compounds above the P_{m} threshold. It can also aid rational lead optimisation by enabling drugs of interest to be engineered for desired transporter interactions through adjustments in membrane permeability. Future research will focus on further investigating and validating the energy limit with concentration-dependence assays on additional borderline compounds. The potential of extending the theory to accommodate influx transport is also promising idea that can be explored. Furthermore, the cell's use of saturation as a mechanism to adhere to its energy limit when it comes to efflux can also be studied. For example, to distinguish whether saturation occurs because the energy limit has been reached or due to another cause. Compounds that are not affected by efflux transport will also be investigated by expanding the dataset to include compounds that have ER values below 2.5 in order to evaluate and compare the distribution of P_{m} values between these two categories of compounds. Furthermore, the potential for linking the threshold P_{m} with $K_{\mathrm{hex/w}}$ values will be explored. Finally, future studies could determine the energy limit and corresponding P_{m} threshold for other cell lines.

5 Abstracts of original publications

5.1 Effects of Aqueous Boundary Layers and Paracellular Transport on the Efflux Ratio as a Measure of Active Transport Across Cell Layers

pharmaceutics

MDPI

Article

Effects of Aqueous Boundary Layers and Paracellular Transport on the Efflux Ratio as a Measure of Active Transport Across Cell Layers

Soné Kotze [1], Andrea Ebert [1] and Kai-Uwe Goss [1,2]*

[1] Department of Analytical Environmental Chemistry, Helmholtz Centre for Environmental Research (UFZ), Permoserstraße 15, 04318 Leipzig, Germany
[2] Institute of Chemistry, University of Halle-Wittenberg, Kurt-Mothes-Straße 2, 06120 Halle, Germany
* Correspondence: kai-uwe.goss@ufz.de

Abstract: The efflux ratio (ER), determined by Caco-2/MDCK assays, is the standard in vitro metric to establish qualitatively whether a compound is a substrate of an efflux transporter. However, others have also enabled the utilisation of this metric quantitatively by deriving a relationship that expresses the ER as a function of the intrinsic membrane permeability of the membrane (P_0) as well as the permeability of carrier-mediated efflux (P_{pgp}). As of yet, P_{pgp} cannot be measured directly from transport experiments or otherwise, but the ER relationship provides easy access to this value if P_0 is known. However, previous derivations of this relationship failed to consider the influence of additional transport resistances such as the aqueous boundary layers (ABLs) and the filter on which the monolayer is grown. Since single fluxes in either direction can be heavily affected by these experimental artefacts, it is crucial to consider the potential impact on the ER. We present a model that includes these factors and show both mathematically and experimentally that this simple ER relationship also holds for the more realistic scenario that does not neglect the ABLs/filter. Furthermore, we also show mathematically how paracellular transport affects the ER, and we experimentally confirm that paracellular dominance reduces the ER to unity and can mask potential efflux.

Keywords: efflux transporters; MDCK; Caco-2; active transport; P-glycoprotein; permeability

Citation: Kotze, S.; Ebert, A.; Goss, K.-U. Effects of Aqueous Boundary Layers and Paracellular Transport on the Efflux Ratio as a Measure of

5.2 The pH-dependence of efflux ratios determined with bidirectional transport assays across cellular monolayers

ELSEVIER

International Journal of Pharmaceutics: X

Volume 8, December 2024, 100269

The pH-dependence of efflux ratios determined with bidirectional transport assays across cellular monolayers

Soné Kotze [a], Kai-Uwe Goss [a b], Andrea Ebert [a]

Show more

https://doi.org/10.1016/j.ijpx.2024.100269

Abstract

MDCK/Caco-2 assays serve as essential in vitro tools for evaluating membrane permeability and active transport, especially mediated by P-glycoprotein (P-gp). Despite their utility, challenges remain in quantifying active transport and using the efflux ratio (ER) to determine intrinsic values for active efflux. Such an intrinsic value for P-gp facilitated efflux necessitates knowing whether this transporter transports the neutral or ionic species of a compound. Utilising MDCK-MDR1 assays, we investigate a method for determining transporter substrate fraction preference by studying ER pH-dependence for basic, acidic and non-dissociating compounds. These results are compared with model fits based on various assumptions of transporter species preference. As an unexpected consequence of these assays, we also give evidence for an additional influx transporter at the basolateral membrane, and further extend our model to incorporate this transport. The combined influences of paracellular transport, the previously unaccounted for basolateral influx transporter, as well as potential pH effects on the transporter impedes the extraction of intrinsic values for active transport from the ER. Furthermore, we determined that using inhibitor affects the measurement of paracellular transport. While clear indications of transporter species preference remain elusive, this study enhances understanding of the MDCK system.

References

[1] U. Fagerholm, "The role of permeability in drug ADME/PK, interactions and toxicity - presentation of a permeability-based classification system (PCS) for prediction of ADME/PK in humans", *Pharmaceutical Research*, vol. 25, pp. 625–638, 3 2008. DOI: 10.1007/s11095-007-9397-y.

[2] C. L. Stoner, M. D. Troutman, and C. E. Laverty, "Cancer drug design and disocvery", in Elsevier Inc., 2008, ch. Pharmacokinetics and ADME optimization in drug discovery, pp. 131–153.

[3] E. M. Aldred, "How do drugs get into cells?", in *Pharmacology*. Elsevier Inc., 2009, pp. 123–127. DOI: 10.1016/B978-0-443-06896-0.00016-5.

[4] N. J. Yang and M. J. Hinner, "Getting across the cell membrane: An overview for small molecules, peptides, and proteins", *Methods in Molecular Biology*, vol. 1266, pp. 29–53, 2015. DOI: 10.1007/978-1-4939-2272-7_3.

[5] I. I. A. Juvale, A. A. A. Hamid, K. B. A. Halim, and A. T. C. Has, "P-glycoprotein: New insights into structure, physiological function, regulation and alterations in disease", *Heliyon*, vol. 8, 6 2022. DOI: 10.1016/j.heliyon.2022.e09777.

[6] F. J. Sharom, "ABC multidrug transporters: Structure, function and role in chemoresistance", *Nature Reviews Cancer*, vol. 9, no. 1, pp. 105–127, 2008. DOI: 10.2217/14622416.9.1.105.

[7] R. B. Kim, "Drugs as P-glycoprotein substrates, inhibitors, and inducers", *Drug Metabolism Reviews*, vol. 34, no. 1-2, pp. 47–54, 2002. DOI: 10.1081/dmr-120001389.

[8] J. I. Fletcher, M. Haber, M. J. Henderson, and M. D. Norris, *ABC transporters in cancer: More than just drug efflux pumps*, Feb. 2010. DOI: 10.1038/nrc2789.

[9] P. Matsson, J. M. Pedersen, U. Norinder, C. A. Bergström, and P. Artursson, "Identification of novel specific and general inhibitors of the three major human ATP-binding cassette transporters P-gp, BCRP and MRP2 among registered drugs", *Pharmaceutical Research*, vol. 26, pp. 1816–1831, 8 Aug. 2009. DOI: 10.1007/s11095-009-9896-0.

[10] Q. Wang and T. M. Sauerwald, "Screening for p-glycoprotein (Pgp) substrates and inhibitors", *Methods in Pharmacology and Toxicology*, pp. 337–352, 2014. DOI: 10.1007/978-1-62703-742-6-20.

[11] H. Bohets, P. Annaert, G. Mannens, *et al.*, "Strategies for absorption screening in drug discovery and development", *Current Topics in Medicinal Chemistry*, vol. 1, no. 5, pp. 367–383, 2001. DOI: 10.2174/1568026013394886.

[12] D. A. Volpe, "Drug-permeability and transporter assays in Caco-2 and MDCK cell lines", *Future Medicinal Chemistry*, vol. 3, pp. 2063–2077, 16 2011. DOI: 10.4155/fmc.11.149.

[13] I. Pastan, M. M. Gottesman, K. Ueda, E. Lovelace, A. V. Rutherford, and M. C. Willingham, "A retrovirus carrying an MDR1 cDNA confers multidrug resistance and polarized expression of P-glycoprotein in MDCK cells", *Proceedings*

of the National Academy of Sciences of the United States of America, vol. 85, pp. 4486–4490, 1988.

[14] E. Gallagher, I. Minn, J. E. Chambers, and P. C. Searson, "In vitro characterization of pralidoxime transport and acetylcholinesterase reactivation across MDCK cells and stem cell-derived human brain microvascular endothelial cells (BC1-hBMECs)", *Fluids and Barriers of the CNS*, vol. 13, 1 2016. DOI: 10.1186/s12987-016-0035-0.

[15] D. Gartzke, J. Delzer, L. Laplanche, *et al.*, "Genomic knockout of endogenous canine P-glycoprotein in wild-type, human P-glycoprotein and human BCRP transfected MDCKII cell lines by zinc finger nucleases", *Pharmaceutical Research*, vol. 32, pp. 2060–2071, 6 Jun. 2015. DOI: 10.1007/s11095-014-1599-5.

[16] C. Wegler, M. Gazit, K. Issa, S. Subramaniam, P. Artursson, and M. Karlgren, "Expanding the efflux in vitro assay toolbox: A CRISPR-Cas9 edited MDCK cell line with human BCRP and completely lacking canine MDR1", *Journal of Pharmaceutical Sciences*, vol. 110, pp. 388–396, 1 Jan. 2021. DOI: 10.1016/j.xphs.2020.09.039.

[17] FDA, *In vitro drug interaction studies: Cytochrome p450 enzyme and transporter mediated drug interactions guidance for industry*, https://www.fda.gov/regulatory-information/search-fda-guidance-documents/in-vitro-drug-interaction-studies-cytochrome-p450-enzyme-and-transporter-mediated-drug-interactions, Accessed: 2023, U.S. Food and Drug Administration (FDA), 2020.

[18] FDA, *M12 drug interaction studies*, https://www.fda.gov/regulatory-information/search-fda-guidance-documents/m12-drug-interaction-studies, Accessed: 2023, U.S. Food and Drug Administration (FDA), 2022.

[19] EMA, *Guideline on the investigation of drug interactions*, https://www.ema.europa.eu/en/documents/scientific-guideline/guideline-investigation-drug-interactions-revision-1_en.pdf, Accessed: 2023, European Medicines Agency (EMA).

[20] P. A. Shore, B. B. Brodie, and C. A. M. Hogben, "The gastric secretion of drugs: A pH partition hypothesis", *Journal of Pharmacology and Experimental Therapeutics*, vol. 119, no. 3, pp. 361–369, 1957.

[21] A. Ebert, C. Hannesschlaeger, K. U. Goss, and P. Pohl, "Passive permeability of planar lipid bilayers to organic anions", *Biophysical Journal*, vol. 115, pp. 1931–1941, 10 Nov. 2018. DOI: 10.1016/j.bpj.2018.09.025.

[22] A. Avdeef, "Physicochemical profiling (solubility, permeability and charge state)", *Current Topics in Medicinal Chemistry*, vol. 1, pp. 277–351, 2001.

[23] K. Sugano, Y. Shirasaka, and S. Yamashita, "Estimation of michaelis-menten constant of efflux transporter considering asymmetric permeability", *International Journal of Pharmaceutics*, vol. 418, no. 2, pp. 161–167, 2011. DOI: 10.1016/j.ijpharm.2011.03.059.

[24] C. Dahley, K.-U. Goss, and A. Ebert, "Revisiting the pKa-flux method for determining intrinsic membrane permeability", *European Journal of Pharmaceutical Sciences*, vol. 106592, 2023. DOI: 10.1016/j.ejps.2023.106592.

[25] H. Gunaydin, M. M. Weiss, and Y. Sun, "De novo prediction of P-glycoprotein-mediated efflux liability for druglike compounds", *ACS Medicinal Chemistry Letters*, vol. 4, pp. 108–112, 1 Jan. 2013. DOI: 10.1021/ml300314h.

[26] R. Prajapati, U. Singh, A. Patil, *et al.*, "In silico model for p-glycoprotein substrate prediction: Insights from molecular dynamics and in vitro studies", *Journal of Computer-Aided Molecular Design*, vol. 27, pp. 347–363, 4 2013. DOI: 10.1007/s10822-013-9650-x.

[27] E. Dolghih, C. Bryant, A. R. Renslo, and M. P. Jacobson, "Predicting binding to P-glycoprotein by flexible receptor docking", *PLoS Computational Biology*, vol. 7, 6 2011. DOI: 10.1371/journal.pcbi.1002083.

[28] I. K. Pajeva, M. Hanl, and M. Wiese, "Protein contacts and ligand binding in the inward-facing model of human P-glycoprotein", *ChemMedChem*, vol. 8, pp. 748–762, 5 May 2013. DOI: 10.1002/cmdc.201200491.

[29] F. Klepsch, P. Vasanthanathan, and G. F. Ecker, "Ligand and structure-based classification models for prediction of P-glycoprotein inhibitors", *Journal of Chemical Information and Modeling*, vol. 54, pp. 218–229, 1 Jan. 2014. DOI: 10.1021/ci400289j.

[30] A. Kaczor, M. Nové, A. Kincses, *et al.*, "Search for ABCB1 modulators among 2-amine-5-arylideneimidazolones as a new perspective to overcome cancer multidrug resistance", *Molecules*, vol. 25, 9 May 2020. DOI: 10.3390/molecules25092258.

[31] S. A. S. Cleave, R. Panda, and P. K. Suresh, "In silico exploration of phenytoin binding site in two catalytic states of human p-glycoprotein models", *Indian Journal of Biochemistry and Biophysics*, vol. 50, pp. 7–13, 2013.

[32] D. Li, L. Chen, Y. Li, S. Tian, H. Sun, and T. Hou, "ADMET evaluation in drug discovery. 13.Development of in silico prediction models for p-glycoprotein substrates", *Molecular Pharmaceutics*, vol. 11, pp. 716–726, 3 Mar. 2014. DOI: 10.1021/mp400450m.

[33] V. K. Gombar, J. W. Polli, J. E. Humphreys, S. A. Wring, and C. S. Serabjit-Singh, "Predicting p-glycoprotein substrates by a quantitative structure-activity relationship model", *Journal of Pharmaceutical Sciences*, vol. 4, pp. 957–968, 93 Dec. 2003.

[34] J. E. Penzotti, M. L. Lamb, E. Evensen, and P. D. Grootenhuis, "A computational ensemble pharmacophore model for identifying substrates of P-glycoprotein", *Journal of Medicinal Chemistry*, vol. 45, pp. 1737–1740, 9 Apr. 2002. DOI: 10.1021/jm0255062.

[35] Y. Xue, C. W. Yap, L. Z. Sun, Z. W. Cao, J. F. Wang, and Y. Z. Chen, "Prediction of P-glycoprotein substrates by a support vector machine approach", *Journal of Chemical Information and Computer Sciences*, vol. 44, pp. 1497–1505, 4 Jul. 2004. DOI: 10.1021/ci049971e.

[36] Z. Wang, Y. Chen, H. Liang, A. Bender, R. C. Glen, and A. Yan, "P-glycoprotein substrate models using support vector machines based on a comprehensive data set", *Journal of Chemical Information and Modeling*, vol. 51, pp. 1447–1456, 6 Jun. 2011. DOI: 10.1021/ci2001583.

[37] M. A. Demel, O. Krämer, P. Ettmayer, E. E. Haaksma, and G. F. Ecker, "Predicting ligand interactions with ABC transporters in ADME", *Chemistry and Biodiversity*, vol. 6, pp. 1960–1969, 11 Nov. 2009. DOI: 10.1002/cbdv.200900138.

[38] P. D. C. Lima, A. Golbraikh, S. Oloff, Y. Xiao, and A. Tropsha, "Combinatorial QSAR modeling of P-glycoprotein substrates", *Journal of Chemical Information and Modeling*, vol. 46, pp. 1245–1254, 3 Sep. 2006. DOI: 10.1021/ci0504317.

[39] P. Crivori, B. Reinach, D. Pezzetta, and I. Poggesi, "Computational models for identifying potential P-glycoprotein substrates and inhibitors", *Molecular Pharmaceutics*, vol. 3, pp. 33–44, 1 Jan. 2006. DOI: 10.1021/mp050071a.

[40] M. A. Cabrera, I. González, C. Fernández, C. Navarro, and M. Bermejo, "A topological substructural approach for the prediction of P-glycoprotein substrates", *Journal of Pharmaceutical Sciences*, vol. 95, pp. 589–606, 3 Jun. 2006. DOI: 10.1002/jps.20449.

[41] J. Huang, G. Ma, I. Muhammad, and Y. Cheng, "Identifying P-glycoprotein substrates using a support vector machine optimized by a particle swarm", *Journal of Chemical Information and Modeling*, vol. 47, pp. 1638–1647, 4 2007. DOI: 10.1021/ci700083n.

[42] Y. H. Wang, Y. Li, S. L. Yang, and L. Yang, "Classification of substrates and inhibitors of P-glycoprotein using unsupervised machine learning approach", *Journal of Chemical Information and Modeling*, vol. 45, pp. 750–757, 3 2005. DOI: 10.1021/ci050041k.

[43] L. Chen, Y. Li, H. Yu, L. Zhang, and T. Hou, "Computational models for predicting substrates or inhibitors of P-glycoprotein", *Drug Discovery Today*, vol. 17, pp. 343–351, 7-8 Apr. 2012. DOI: 10.1016/j.drudis.2011.11.003.

[44] A. Seelig, "A general pattern for substrate recognition by P-glycoprotein", *European Journal of Biochemistry*, vol. 251, pp. 252–261, 1-2 Jan. 1998. DOI: 10.1046/j.1432-1327.1998.2510252.x.

[45] R. Didziapetris, P. Japertas, A. Avdeef, and A. Petrauskas, "Classification analysis of P-glycoprotein substrate specificity", *Journal of Drug Targeting*, vol. 11, pp. 391–406, 7 Aug. 2003. DOI: 10.1080/10611860310001648248.

[46] G. L. Amidon, H. Lennernas, V. P. Shah, and J. R. Crison, "A theoretical basis for a biopharmaceutic drug classification: The correlation of in vitro drug product dissolution and in vivo bioavailability.", *Pharmaceutical Research*, vol. 12, pp. 413–420, 3 1995.

[47] FDA, *M9 biopharmaceuticals classification*, https://www.fda.gov/regulatory-information/search-fda-guidance-documents/m9-biopharmaceutics-classification-system-based-bcs-guidance-industry, Accessed: 2023, U.S. Food and Drug Administration (FDA).

[48] C. Y. Wu and L. Z. Benet, "Predicting drug disposition via application of BCS: Transport/absorption/ elimination interplay and development of a biopharmaceutics drug disposition classification system", *Pharmaceutical Research*, vol. 22, pp. 11–23, 1 Jan. 2005. DOI: 10.1007/s11095-004-9004-4.

[49] H. Fischer, M. Kansy, A. Avdeef, and F. Senner, "Permeation of permanently positive charged molecules through artificial membranes-influence of physicochemical properties", *European Journal of Pharmaceutical Sciences*, vol. 31, pp. 32–42, 1 May 2007. DOI: 10.1016/j.ejps.2007.02.001.

[50] K. M. M. Doan, J. E. Humphreys, L. O. Webster, *et al.*, "Passive permeability and P-glycoprotein-mediated efflux differentiate central nervous system (CNS) and non-CNS marketed drugs", *Journal of Pharmacology and Experimental Therapeutics*, vol. 303, pp. 1029–1037, 3 Dec. 2002. DOI: 10.1124/jpet.102.039255.

[51] T. T. Wager, R. Y. Chandrasekaran, X. Hou, *et al.*, "Defining desirable central nervous system drug space through the alignment of molecular properties, in vitro ADME, and safety attributes", *ACS Chemical Neuroscience*, vol. 1, pp. 420–434, 6 Jun. 2010. DOI: 10.1021/cn100007x.

[52] F. Broccatelli, C. A. Larregieu, G. Cruciani, T. I. Oprea, and L. Z. Benet, "Improving the prediction of the brain disposition for orally administered drugs using BDDCS", *Advanced Drug Delivery Reviews*, vol. 64, no. 1, pp. 95–109, 2012. DOI: 10.1016/j.addr.2011.12.008.

[53] S. Kotze, A. Ebert, and K. U. Goss, "Effects of aqueous boundary layers and paracellular transport on the efflux ratio as a measure of active transport across cell layers", *Pharmaceutics*, vol. 16, 1 Jan. 2024. DOI: 10.3390/pharmaceutics16010132.

[54] K. Bittermann and K.-U. Goss, "Predicting apparent passive permeability of Caco-2 and MDCK cell-monolayers: A mechanistic model", *PLoS ONE*, vol. 12, no. 2017, e0190319, 2017. DOI: 10.1371/journal.pone.0190319.

[55] A. Avdeef, P. Artursson, S. Neuhoff, L. Lazorova, J. Gråsjö, and S. Tavelin, "Caco-2 permeability of weakly basic drugs predicted with the double-sink PAMPA pKa-flux method", *European Journal of Pharmaceutical Sciences*, vol. 24, no. 4, pp. 333–349, 2005. DOI: 10.1016/j.ejps.2004.11.011.

[56] A. Avdeef, "Leakiness and size exclusion of paracellular channels in cultured epithelial cell monolayers-interlaboratory comparison", *Pharmaceutical Research*, vol. 27, pp. 480–489, 3 Mar. 2010. DOI: 10.1007/s11095-009-0036-7.

[57] J. Karlsson and P. Artursson, "A method for the determination of cellular permeability coefficients and aqueous boundary layer thickness in monolayers of intestinal epithelial (caco-2) cells grown in permeable filter chambers", *International Journal of Pharmaceutics*, vol. 71, pp. 55–64, 1991.

[58] A. S. Verkman, "Solute and macromolecule diffusion in cellular aqueous compartments", *Trends in Biochemical Sciences*, vol. 27, pp. 27–33, 1 2002.

[59] S. L. Palay and L. J. Karlin, "An electron microscopic study of the intestinal villus: Ii. the pathway of fat absorption", *Journal of Biophysical and Biochemical Cytology*, vol. 5, no. 3, pp. 373–384, 1959. DOI: 10.1083/jcb.5.3.373.

[60] Z. Meng, S. L. Marchand, D. Agnani, M. Szapacs, H. Ellens, and J. Bentz, "Microvilli morphology can affect efflux active p-glycoprotein in confluent MDCKII -hMDR1-NKI and Caco-2 cell monolayers", *Drug Metabolism and Disposition*, vol. 45, pp. 145–151, 2 Feb. 2017. DOI: 10.1124/dmd.116.072157.

[61] C. Butor and J. Davoust, "Apical to basolateral surface area ratio and polarity of mDCK cells grown on different supports", *Experimental cell research*, vol. 203, pp. 115–127, 1992.

[62] S. Kotze, K. U. Goss, and A. Ebert, "The pH-dependence of efflux ratios determined with bidirectional transport assays across cellular monolayers", *International Journal of Pharmaceutics: X*, vol. 8, Dec. 2024. DOI: 10.1016/j.ijpx.2024.100269.

[63] N. Ulrich, S. Endo, T. N. Brown, *et al.*, *UFZ-LSER database v3.2.1*, http://www.ufz.de/lserd, 2017.

[64] I. Hubatsch, E. G. Ragnarsson, and P. Artursson, "Determination of drug permeability and prediction of drug absorption in Caco-2 monolayers", *Nature Protocols*, vol. 2, pp. 2111–2119, 9 Sep. 2007. DOI: 10.1038/nprot.2007.303.

[65] D. A. Perdikis, R. Davies, A. Zhurakov, B. Brenner, L. Etter, and M. D. Basson, "Differential effects of mucosal pH on human (Caco-2) intestinal epithelial cell motility, proliferation, and differentiation", *Digestive Diseases and Sciences*, vol. 43, pp. 1537–1546, 7 1998.

[66] E. Liang, P. Liu, and S. Dinh, "Use of a pH-sensitive fluorescent probe for measuring intracellular pH of Caco-2 cells", *International Journal of Pharmaceutics*, vol. 338, pp. 104–109, 1-2 Jun. 2007. DOI: 10.1016/j.ijpharm.2007.01.048.

[67] C. Dahley, T. Böckmann, A. Ebert, and K.-U. Goss, "Predicting the intrinsic membrane permeability of Caco-2/MDCK cells by the solubility-diffusion model", *European Journal of Pharmaceutical Sciences*, vol. 195, p. 106 720, 2024. DOI: https://doi.org/10.1016/j.ejps.2024.106720.

[68] M. D. Troutman and D. R. Thakker, "Novel experimental parameters to quantify the modulation of absorptive and secretory transport of compounds by p-glycoprotein in cell culture models of intestinal epithelium", *Pharmaceutical Research*, vol. 20, pp. 1210–1224, 8 2003.

[69] J. W. Polli, S. A. Wring, J. E. Humphreys, *et al.*, "Rational use of in vitro P-glycoprotein assays in drug discovery", *The Journal of Pharmacology and Experimental Therapeutics*, vol. 299, pp. 620–628, 2 2001.

[70] É. Hellinger, S. Veszelka, A. E. Tóth, *et al.*, "Comparison of brain capillary endothelial cell-based and epithelial (MDCK-MDR1, Caco-2, and VB-Caco-2) cell-based surrogate blood-brain barrier penetration models", *European Journal of Pharmaceutics and Biopharmaceutics*, vol. 82, pp. 340–351, 2 Oct. 2012. DOI: 10.1016/j.ejpb.2012.07.020.

[71] A. Avdeef, *Absorption and Drug Development: Solubility, Permeability, and Charge State*. John Wiley & Sons, Inc., 2012. DOI: 10.1002/9781118286067.

[72] Advanced Chemistry Development, *Percepta*, version 2020.1.2, Jun. 18, 2020. [Online]. Available: www.acdlabs.com.

[73] J. D. Irvine, L. Takahashi, K. Lockhart, *et al.*, "MDCK (madin-darby canine kidney) cells: A tool for membrane permeability screening", *Journal of Pharmaceutical Sciences*, vol. 88, pp. 28–33, 1 1999. DOI: 10.1021/js9803205.

[74] S. Neuhoff, "Refined in vitro models for prediction of intestinal drug transport. role of pH and extracellular additives in the Caco-2 cell model", Ph.D. dissertation, Uppsala University, Uppsala, 2005.

[75] A. T. Heikkinen, J. Mönkkönen, and T. Korjamo, "Kinetics of cellular retention during Caco-2 permeation experiments: Role of lysosomal sequestration and impact on permeability estimates", *Journal of Pharmacology and Experimental Therapeutics*, vol. 328, pp. 882–892, 2009. DOI: 10.1124/jpet.108.145797.

[76] K. Ito, H. Suzuki, T. Horie, and Y. Sugiyama, "Apical/basolateral surface expression of drug transporters and its role in vectorial drug transport", *Pharmaceutical Research*, vol. 22, pp. 1559–1577, 10 Oct. 2005. DOI: 10.1007/s11095-005-6810-2.

[77] V. Hutter, D. Y. Chau, C. Hilgendorf, *et al.*, "Digoxin net secretory transport in bronchial epithelial cell layers is not exclusively mediated by P-glycoprotein/MDR1", *European Journal of Pharmaceutics and Biopharmaceutics*, vol. 86, pp. 74–82, 1 Jan. 2014. DOI: 10.1016/j.ejpb.2013.06.010.

[78] A. Galetin, K. L. Brouwer, D. Tweedie, *et al.*, "Membrane transporters in drug development and as determinants of precision medicine", *Nature Reviews Drug Discovery*, 2024. DOI: 10.1038/s41573-023-00877-1.

[79] F. G. Russel, "Transporters: Importance in drug absorption, distribution, and removal", in *Enzyme- and Transporter-Based Drug-Drug Interactions: Progress and Future Challenges*. Springer New York, 2010, pp. 27–49. DOI: 10.1007/978-1-4419-0840-7-2.

[80] Z. M. Zaïr, J. J. Eloranta, B. Stieger, and G. A. Kullak-Ublick, "Pharmacogenetics of OATP (sLC21/SLCO), OAT and OCT (sLC22) and PEPT (SLC15) transporters in the intestine, liver and kidney", *Pharmacogenomics*, vol. 9, pp. 597–624, 5 May 2008. DOI: 10.2217/14622416.9.5.597.

[81] X. Li, P. Mu, J. Wen, and Y. Deng, "Carrier-mediated and energy-dependent uptake and efflux of deoxynivalenol in mammalian cells", *Scientific Reports*, vol. 7, 1 2017. DOI: 10.1038/s41598-017-06199-8.

[82] J. Li, Y. Wang, W. Zhang, Y. Huang, K. Hein, and I. J. Hidalgo, "The role of a basolateral transporter in rosuvastatin transport and its interplay with apical breast cancer resistance protein in polarized cell monolayer systems", *Drug Metabolism and Disposition*, vol. 40, pp. 2102–2108, 11 Nov. 2012. DOI: 10.1124/dmd.112.045666.

[83] D. Agnani, P. Acharya, E. Martinez, *et al.*, "Fitting the elementary rate constants of the P-gp transporter network in the hMDR1-MDCK confluent cell

monolayer using a particle swarm algorithm", *PLOS ONE*, vol. 6, no. 10, pp. 1–12, Oct. 2011. DOI: 10.1371/journal.pone.0025086.

[84] P. Acharya, M. P. O'Connor, J. W. Polli, A. Ayrton, H. Ellens, and J. Bentz, "Kinetic identification of membrane transporters that assist P-glycoprotein-mediated transport of digoxin and loperamide through a confluent monolayer of MDCKII-hMDR1 cells", *Drug Metabolism and Disposition*, vol. 36, pp. 452–460, 2 Feb. 2008. DOI: 10.1124/dmd.107.017301.

[85] J. Dunn and M. H. Grider, *Physiology, Adenosine Triphosphate*. StatPearls, Feb. 2023.

[86] R. M. Lynch and R. S. Balaban, "Energy metabolism of renal cell lines, A6 and MDCK: Regulation by Na-K-ATPase", *American Journal of Physiology - Cell Physiology*, vol. 252, 2 Feb. 2019.

[87] A. Flamholz, R. Phillips, and R. Milo, "The quantified cell", *Molecular Biology of the Cell*, vol. 25, pp. 3497–3500, 22 Nov. 2014. DOI: 10.1091/mbc.E14-09-1347.

[88] E. Bianconi, A. Piovesan, F. Facchin, *et al.*, "An estimation of the number of cells in the human body", *Annals of Human Biology*, vol. 40, pp. 463–471, 6 Nov. 2013. DOI: 10.3109/03014460.2013.807878.

[89] G. D. Eytan, R. Regev, and Y. G. Assaraf, "Functional reconstitution of P-glycoprotein reveals an apparent near stoichiometric drug transport to ATP hydrolysis*", *The Journal of Biological Chemistry*, vol. 271, pp. 3172–3178, 6 Feb. 1996.

[90] B. I. Escher, R. Abagyan, M. Embry, *et al.*, "Recommendations for improving methods and models for aquatic hazard assessment of ionizable organic chemicals", *Environmental Toxicology and Chemistry*, vol. 39, pp. 269–286, 2 Feb. 2020. DOI: 10.1002/etc.4602.

[91] A. Ebert, C. Dahley, and K. U. Goss, "Pitfalls in evaluating permeability experiments with Caco-2/MDCK cell monolayers", *European Journal of Pharmaceutical Sciences*, vol. 194, Mar. 2024. DOI: 10.1016/j.ejps.2024.106699.

[92] A. Walter and J. Gutknecht, "Membrane biology permeability of small nonelectrolytes through lipid bilayer membranes", *Journal of Membrane Biology*, vol. 90, pp. 207–217, 1986.

[93] A. Ebert and C. Dahley, "Can membrane permeability of zwitterionic compounds be predicted by the solubility-diffusion model?", *European Journal of Pharmaceutical Sciences*, vol. 199, Aug. 2024. DOI: 10.1016/j.ejps.2024.106819.

[94] F. Eckert and A. Klamt, "Fast solvent screening via quantum chemistry: COSMO-RS approach", *AIChE Journal*, vol. 48, pp. 369–385, 2 Feb. 2002. DOI: 10.1002/aic.690480220.

[95] E. Callegari, B. Malhotra, P. J. Bungay, *et al.*, "A comprehensive non-clinical evaluation of the CNS penetration potential of antimuscarinic agents for the treatment of overactive bladder", *British Journal of Clinical Pharmacology*, vol. 72, pp. 235–246, 2 Aug. 2011. DOI: 10.1111/j.1365-2125.2011.03961.x.

[96] B. Feng, J. B. Mills, R. E. Davidson, *et al.*, "In vitro P-glycoprotein assays to predict the in vivo interactions of P-glycoprotein with drugs in the central nervous system", *Drug Metabolism and Disposition*, vol. 36, pp. 268–275, 2 Feb. 2008. DOI: 10.1124/dmd.107.017434.

[97] Q. Wang, J. D. Rager, K. Weinstein, *et al.*, "Evaluation of the MDR-MDCK cell line as a permeability screen for the blood-brain barrier", *International Journal of Pharmaceutics*, vol. 288, pp. 349–359, 2 Jan. 2005. DOI: 10.1016/j.ijpharm.2004.10.007.

[98] S. Carrara, V. Reali, P. Misiano, G. Dondio, and C. Bigogno, "Evaluation of in vitro brain penetration: Optimized PAMPA and MDCKII-MDR1 assay comparison", *International Journal of Pharmaceutics*, vol. 345, pp. 125–133, 1-2 Dec. 2007. DOI: 10.1016/j.ijpharm.2007.05.057.

[99] T. Obradovic, G. G. Dobson, T. Shingaki, T. Kungu, and I. J. Hidalgo, "Assessment of the first and second generation antihistamines brain penetration and role of P-glycoprotein", *Pharmaceutical Research*, vol. 24, pp. 318–327, 2 Feb. 2007. DOI: 10.1007/s11095-006-9149-4.

[100] C. Chen, E. Hanson, J. W. Watson, and J. S. Lee, "P-glycoprotein limits the brain penetration of nonsedating but not sedating H1-antagonists", *Drug Metabolism and Disposition*, vol. 31, pp. 312–318, 3 2003.

[101] M. S. Park, H. Okochi, and L. Z. Benet, "Is ciprofloxacin a substrate of P-glycoprotein?", *Archives of Drug Information*, vol. 4, pp. 1–9, 1 Mar. 2011. DOI: 10.1111/j.1753-5174.2010.00032.x.

[102] M. Gertz, A. Harrison, J. B. Houston, and A. Galetin, "Prediction of human intestinal first-pass metabolism of 25 CYP3A substrates from in vitro clearance and permeability data", *Drug Metabolism and Disposition*, vol. 38, pp. 1147–1158, 7 2010. DOI: 10.1124/dmd.110.032649.

[103] C. Chang, P. M. Bahadduri, J. E. Polli, P. W. Swaan, and S. Ekins, "Rapid identification of P-glycoprotein substrates and inhibitors", *Drug Metabolism and Disposition*, vol. 34, pp. 1976–1984, 12 Dec. 2006. DOI: 10.1124/dmd.106.012351.

[104] U. G. Eriksson, H. Dorani, J. Karlsson, *et al.*, "Influence of erythromycin on the pharmacokinetics of ximelagatran may involve inhibition of P-glycoprotein-mediated excretion", *Drug Metabolism and Disposition*, vol. 34, pp. 775–782, 5 May 2006. DOI: 10.1124/dmd.105.008607.

[105] M. E. Taub, L. Podila, D. Ely, and I. Almeida, "Functional assessment of multiple p-glycoprotein (P-gp) probe substrates: Influence of cell line and modulator concentration on P-gp activity", *Drug Metabolism and Disposition*, vol. 33, pp. 1679–1687, 11 Nov. 2005. DOI: 10.1124/dmd.105.005421.

[106] L. Huang, Y. Wang, and S. Grimm, "ATP-dependent transport of rosuvastatin in membrane vesicles expressing breast cancer resistance protein", *Drug Metabolism and Disposition*, vol. 34, pp. 738–742, 5 May 2006. DOI: 10.1124/dmd.105.007534.

[107] J. D. Souza, L. Benet, Y. Huang, and S. Storpirtis, "Comparison of bidirectional lamivudine and zidovudine transport using MDCK, MDCK-MDR1, and Caco-2 cell monolayers", *Journal of Pharmaceutical Sciences*, vol. 98, pp. 4413–4419, 11 2009. DOI: 10.1002/jps.21744.

[108] S. Luo, D. Pal, S. J. Shah, D. Kwatra, K. D. Paturi, and A. K. Mitra, "Effect of hEPES buffer on the uptake and transport of p-glycoprotein substrates and large neutral amino acids", *Molecular Pharmaceutics*, vol. 7, pp. 412–420, 2 Apr. 2010. DOI: 10.1021/mp900193e.

[109] F. Tang, H. Ouyang, J. Z. Yang, and R. T. Borchardt, "Bidirectional transport of rhodamine 123 and hoechst 33342, fluorescence probes of the binding sites on P-glycoprotein, across MDCK-MDR1 cell monolayers", *Journal of Pharmaceutical Sciences*, vol. 93, pp. 1185–1194, 5 2004.

[110] W. Liu, H. Okochi, L. Z. Benet, and S. D. Zhai, "Sotalol permeability in cultured-cell, rat intestine, and PAMPA system.", *Pharmaceutical research*, vol. 29, pp. 1768–1774, 7 2012. DOI: 10.1007/s11095-012-0699-3.

[111] C. Chen, R. J. Mireles, S. D. Campbell, *et al.*, "Differential interaction of 3-hydroxy-3-methylglutaryl-CoA reductase inhibitors with ABCB1, ABCC2, and OATP1B1", *Drug Metabolism and Disposition*, vol. 33, pp. 537–546, 4 Apr. 2005. DOI: 10.1124/dmd.104.002477.

[112] L. Ye, X. Yang, Z. Yang, *et al.*, "The role of efflux transporters on the transport of highly toxic aconitine, mesaconitine, hypaconitine, and their hydrolysates, as determined in cultured Caco-2 and transfected mDCKII cells", *Toxicology Letters*, vol. 216, pp. 86–99, 2-3 Feb. 2013. DOI: 10.1016/j.toxlet.2012.11.011.

[113] U. Muenster, B. Grieshop, K. Ickenroth, and M. J. Gnoth, "Characterization of substrates and inhibitors for the in vitro assessment of BCRP mediated drug-drug interactions", *Pharmaceutical Research*, vol. 25, pp. 2320–2326, 10 Oct. 2008. DOI: 10.1007/s11095-008-9632-1.

[114] J. Zhang, L. Zhang, Y. Yan, *et al.*, "Are capecitabine and the active metabolite 5-FU CNS penetrable to treat breast cancer brain metastasis?", *Drug Metabolism and Disposition*, vol. 43, pp. 411–417, 3 Mar. 2015. DOI: 10.1124/dmd.114.061820.

[115] B. Feng, M. West, N. C. Patel, *et al.*, "Validation of human MDR1-MDCK and BCRP-MDCK cell lines to improve the prediction of brain penetration", *Journal of Pharmaceutical Sciences*, vol. 108, pp. 2476–2483, 7 Jul. 2019. DOI: 10.1016/j.xphs.2019.02.005.

[116] Y. Chen, S. Agarwal, N. M. Shaik, C. Chen, Z. Yang, and W. F. Elmquist, "P-glycoprotein and breast cancer resistance protein influence brain distribution of dasatinib", *Journal of Pharmacology and Experimental Therapeutics*, vol. 330, pp. 956–963, 3 2009. DOI: 10.1124/jpet.109.154781.

[117] Y. Xiao, R. Davidson, A. Smith, *et al.*, "A 96-well efflux assay to identify ABCG2 substrates using a stably transfected MDCK II cell line", *Molecular Pharmaceutics*, vol. 3, pp. 45–54, 1 Jan. 2006. DOI: 10.1021/mp050088t.

[118] A. Poirier, R. Portmann, A. C. Cascais, *et al.*, "The need for human breast cancer resistance protein substrate and inhibition evaluation in drug discovery and development: Why, when, and how?", *Drug Metabolism and Disposition*, vol. 42, pp. 1466–1477, 9 2014. DOI: 10.1124/dmd.114.058248.

[119] S. Marchetti, N. A. D. Vries, T. Buckle, *et al.*, "Effect of the ATP-binding cassette drug transporters ABCB1, ABCG2, and ABCC2 on erlotinib hydrochloride (Tarceva) disposition in in vitro and in vivo pharmacokinetic studies employing Bcrp1-/-/Mdr1a/1b-/- (triple-knockout) and wild-type mice", *Molecular Cancer Therapeutics*, vol. 7, pp. 2280–2287, 8 2008. DOI: 10.1158/1535-7163.MCT-07-2250.

[120] J. W. Polli, J. E. Humphreys, K. A. Harmon, *et al.*, "The role of efflux and uptake transporters in n-3-chloro-4-[(3- fluorobenzyl)oxy]phenyl-6-[5-([2-(methylsulfonyl)ethyl]aminomethyl)-2-furyl] -4-quinazolinamine (GW572016, lapatinib) disposition and drug interactions", *Drug Metabolism and Disposition*, vol. 36, pp. 695–701, 4 Apr. 2008. DOI: 10.1124/dmd.107.018374.

[121] A. Mahringer, J. Delzer, and G. Fricker, "A fluorescence-based in vitro assay for drug interactions with breast cancer resistance protein (BCRP, ABCG2)", *European Journal of Pharmaceutics and Biopharmaceutics*, vol. 72, pp. 605–613, 3 Aug. 2009. DOI: 10.1016/j.ejpb.2009.01.010.

[122] M. M. Parvez, A. Basit, P. B. Jariwala, *et al.*, "Quantitative investigation of irinotecan metabolism, transport, and gut microbiome activation", *Drug Metabolism and Disposition*, vol. 49, pp. 683–693, 8 Aug. 2021. DOI: 10.1124/dmd.121.000476.

[123] A. Kort, R. W. Sparidans, E. Wagenaar, J. H. Beijnen, and A. H. Schinkel, "Brain accumulation of the EML4-ALK inhibitor ceritinib is restricted by P-glycoprotein (P-GP/ABCB1) and breast cancer resistance protein (BCRP/ABCG2)", *Pharmacological Research*, vol. 102, pp. 200–207, Dec. 2015. DOI: 10.1016/j.phrs.2015.09.003.

[124] S. Agarwal, R. Sane, J. R. Ohlfest, and W. F. Elmquist, "The role of the breast cancer resistance protein (ABCG2) in the distribution of sorafenib to the brain", *Journal of Pharmacology and Experimental Therapeutics*, vol. 336, pp. 223–233, 1 Jan. 2011. DOI: 10.1124/jpet.110.175034.

[125] R. Mukkavilli, G. Jadhav, and S. Vangala, "Evaluation of drug transport in MDCKII-wild type, MDCKII-MDR1, MDCKII-BCRP and Caco-2 cell lines", *Current Pharmaceutical Biotechnology*, vol. 19, Mar. 2018. DOI: 10.2174/1389201019666180308091855.

[126] C. Zimmermann, K. V. D. Wetering, E. V. D. Steeg, E. Wagenaar, C. Vens, and A. H. Schinkel, "Species-dependent transport and modulation properties of human and mouse multidrug resistance protein 2 (MRP2/mrp2, ABCC2/abcc2)", *Drug Metabolism and Disposition*, vol. 36, pp. 631–640, 4 Apr. 2008. DOI: 10.1124/dmd.107.019620.

[127] M. T. Huisman, A. A. Chhatta, O. V. Tellingen, J. H. Beijnen, and A. H. Schinkel, "MRP2 (ABCC2) transports taxanes and confers paclitaxel resistance

and both processes are stimulated by probenecid", *International Journal of Cancer*, vol. 116, pp. 824–829, 5 Sep. 2005. DOI: 10.1002/ijc.21013.

[128] A. Guo, W. Marinaro, P. Hu, and P. J. Sinko, "Delineating the contribution of secretory transporters in the efflux of etoposide using Madin-Darby canine kidney (MDCK) cells overexpressing P-glycoprotein (Pgp), multidrug resistance-associated protein (MRP1), and canalicular multispecific organic anion transporter(cMOAT)", *Drug Metabolism and Disposition*, vol. 30, pp. 457–463, 4 2002.

[129] Y. Y. Lau, H. Okochi, Y. Huang, and L. Z. Benet, "Multiple transporters affect the disposition of atorvastatin and its two active hydroxy metabolites: Application of in vitro and ex situ systems", *Journal of Pharmacology and Experimental Therapeutics*, vol. 316, pp. 762–771, 2 Feb. 2006. DOI: 10.1124/jpet.105.093088.

[130] S. Nielsen, A. M. Westerhoff, L. G. Gé, K. L. Carlsen, M. D. L. Pedersen, and C. U. Nielsen, "MRP2-mediated transport of etoposide in MDCKII MRP2 cells is unaffected by commonly used non-ionic surfactants", *International Journal of Pharmaceutics*, vol. 565, pp. 306–315, Jun. 2019. DOI: 10.1016/j.ijpharm.2019.05.023.

[131] R. Jain, S. Agarwal, N. K. Mandava, Y. Sheng, and A. K. Mitra, "Interaction of dipeptide prodrugs of saquinavir with multidrug resistance protein-2 (MRP-2): Evasion of MRP-2 mediated efflux", *International Journal of Pharmaceutics*, vol. 362, pp. 44–51, 1-2 Oct. 2008. DOI: 10.1016/j.ijpharm.2008.06.013.

[132] F. Tang, K. Horie, and R. T. Borchardt, "Are MDCK cells transfected with the human MDR1 gene a good model of the human intestinal mucosa?", *Pharmaceutical Research*, vol. 19, no. 6, pp. 765–772, 2002. DOI: 10.1023/a:1016140429238.

[133] G. C. Williams, A. Liu, G. Knipp, and P. J. Sinko, "Direct evidence that saquinavir is transported by multidrug resistance-associated protein (MRP1) and canalicular multispecific organic anion transporter (MRP2)", *Antimicrobial Agents and Chemotherapy*, vol. 46, pp. 3456–3462, 11 Nov. 2002. DOI: 10.1128/AAC.46.11.3456-3462.2002.

[134] F. Wohnsland and B. Faller, "High-throughput permeability pH profile and high-throughput alkane/water log P with artificial membranes", *Journal of Medicinal Chemistry*, vol. 44, pp. 923–930, 6 Mar. 2001. DOI: 10.1021/jm001020e.

[135] O. V. Richter, H. Glavinas, P. Krajcsi, S. Liehner, B. Siewert, and K. Zech, "A novel screening strategy to identify aBCB1 substrates and inhibitors", *Naunyn-Schmiedeberg's Archives of Pharmacology*, vol. 379, pp. 11–26, 1 Jan. 2009. DOI: 10.1007/s00210-008-0345-0.

[136] E. M. Donato, C. L. Dias, R. C. Rossi, R. S. Valente, P. E. Fröehlich, and A. M. Bergold, "LC method for studies on the stability of lopinavir and ritonavir in soft gelatin capsules", *Chromatographia*, vol. 63, pp. 437–443, 9-10 May 2006. DOI: 10.1365/s10337-006-0785-y.

[137] A. Heikkinen, T. Korjamo, V. Lepikkö, and J. Mönkkönen, "Effects of experimental setup on the apparent concentration dependency of active efflux transport in in vitro cell permeation experiments", *Molecular Pharmaceutics*, vol. 7, no. 2, pp. 605–617, 2010. DOI: 10.1021/mp9003089.

[138] C. Li, T. Liu, L. Broske, *et al.*, "Permeability evaluation of peptidic hcv protease inhibitors in caco-2 cells-correlation with in vivo absorption predicted in humans", *Biochemical Pharmacology*, vol. 76, pp. 1757–1764, 12 Dec. 2008. DOI: 10.1016/j.bcp.2008.09.005.

[139] M. Tubic, D. Wagner, H. Spahn-Langguth, M. B. Bolger, and P. Langguth, "In silico modeling of non-linear drug absorption for the p-gp substrate talinolol and of consequences for the resulting pharmacodynamic effect", *Pharmaceutical Research*, vol. 23, pp. 1712–1720, 8 Aug. 2006. DOI: 10.1007/s11095-006-9020-7.

Appendix

A. List of Abbreviations

A	Filter area in cm^2
ABC	ATP-binding cassette transporters
ABCB1	ATP-binding cassette sub-family B member 1
ABL	Aqueous boundary layer
ABL,a	Apical aqueous boundary layer
ABL,a	Basolateral aqueous boundary layer
ADME	Absorption, distribution, metabolism and excretion
ATP	Adenosine triphosphate
BBB	Blood brain barrier
BCS	Biopharmaceutics classification system
BCRP	Breast cancer resistance protein
BDDCS	Biopharmaceutics Drug Disposition Classification System
ΔC	Concentration difference between acceptor and donor compartments
C_a	Concentration in the apical compartment in $\mu g/mL$
Caco-2	Basolateral Human colorectal adenocarcinoma cell line
CAPSO	3-(Cyclohexylamino)-1-propanesulfonic acid
C_b	Concentration in the basolateral compartment in $\mu g/mL$
CNS	Central nervous system
cyt	cytosol
D_{Cyt}	Diffusion coefficient in the cytosol
D_{hex}	Diffusion coefficient in hexadecane
D_{w}	Diffusion coefficient in water
DMEM	Dulbecco's modified Eagle medium
DMSO	Dimethyl sulfoxide
EMA	European Medicines Agency
ER	Efflux Ratio

EtOH	Ethanol
FBS	Fetal bovine serum
FDA	Food and Drug Administration
f_{i}	Ionic fraction
f_{n}	Fraction of neutral species
$f_{\mathrm{n,a}}$	Fraction of neutral species in the apical compartment
$f_{\mathrm{n,b}}$	Fraction of neutral species in the basolateral compartment
$f_{\mathrm{n,cyt}}$	Fraction of neutral species in the cytosol
HBSS	Hank's balanced salt solution
HEPES	4-(2-hydroxyethyl)-1-piperazineethanesulfonic acid
HPS	High porosity filter; stirred at 450 rpm assay conditions
HPU	High porosity filter; unstirred assays conditions
IVIVE	In vitro-in vivo extrapolation
J	Flux
$J_{\mathrm{pgp,\ active}}$	Maximal flux that can be facilitated by the pgp transporter
J_{active}	Maximal flux that can be facilitated by any efflux transporter
$K_{\mathrm{hex/w}}$	Hexadecane-water partition coefficient
$K_{\mathrm{lip/w}}$	Lipid-water partition coefficient
LC	Liquid chromatography
LC-MS	Liquid chromatography–mass spectrometry
LPS	Low porosity filter; stirred at 450 rpm assays conditions
LSER	Linear solvation energy relationships
LY	Lucifer Yellow
m,a	Apical membrane
m,b	Basolateral membrane
MDCK	Madin-Darby canine kidney cells
MDR	Multidrug resistance
MDR1	Multidrug-Resistance-Protein 1
MeOH	Methanol

MES	2-(N-morpholino)ethanesulfonic acid
MOPS	3-(N-morpholino)propanesulfonic acid
MRP2	Multi-drug resistance protein 2
OAT	Organic anion transporter
OCT	Organic cation transporter
P	Permeability
PAMPA	Parallel artificial membrane permeability assays
PBPK	Physiologically based pharmacokinetic
P_0	Intrinsic membrane permeability of the neutral species
$P_{0,\mathrm{MDCK}}$	Intrinsic membrane permeability in MDCK cell membranes
$P_{0,\mathrm{SDM}}$	Intrinsic membrane permeability predicted by the solubility diffusion model
para	Paracellular
$P_{\mathrm{ABL,a}}$	Permeability of the apical aqueous boundary layer
$P_{\mathrm{ABL,b}}$	Permeability of the basolateral aqueous boundary layer
P_{app}	Apparent permeability
$P_{app,A\rightarrow B}$	Apparent permeability in the apical to basolateral direction
$P_{app,B\rightarrow A}$	Apparent permeability in the basolateral to apical direction
P_{b}^{active}	Permeability facilitated by the basolateral uptake transporter
$P_{\mathrm{b,app}}^{active}$	Apparent permeability facilitated by the basolateral uptake transporter
P_{cyt}	Permeability of the cytosol
P_{filter}	Permeability of the filter
P-gp	P-Glycoprotein
P_{m}	Permeability of the cell membrane
$P_{\mathrm{m,a}}$	Permeability of the apical membrane
$P_{\mathrm{m,b}}$	Permeability of the basolateral membrane
$P_{\mathrm{pgp}}^{active}$	Permeability facilitated by P-glycoprotein
$P_{\mathrm{pgp,app}}^{active}$	Apparent permeability facilitated by P-glycoprotein
P_{para}	Paracellular permeability
P_{trans}	Transcellular permeability

PVDF	Polyvinylidene fluoride
QSAR	Quantitative Structure Activity Relationship
SDM	Solubility diffusion model
TAPS	tris(hydroxymethyl)methylamino]propanesulfonic acid
TEER	Transepithelial electrical resistance
trans	Transcellular
V_A	Volume of the acceptor compartment in cm^3
x_m	Thickness of membrane

B. Supplementary Materials

Table 6: Apparent permeabilities, recoveries and ER from MDCK-MDR1 bidirectional assays

Compound	Conc. $[\mu M]$	$P_{app,A\to B}$ $[10^{-6}cm/s]$	$logP_{app,A\to B}$	Recovery $A \to B$ [%]	$P_{app,B\to A}$ $[10^{-6}cm/s]$	$logP_{app,B\to A}$	Recovery $B \to A$ [%]	ER
Amprenavir	20	5.0 ± 0.6	-5.31	96	138 ± 9.9	-3.86	88	28
Brompheniramine	6	134 ± 7.6	-3.87	65	121 ± 51	-3.92	83	0.9
Chlorpheniramine	7	141 ± 7.3	-3.85	65	118 ± 50	-3.93	83	0.8
Chlorpromazine	13	131 ± 16	-3.88	32	78.3 ± 44	-4.11	60	0.6
Clemastine	3	76.8 ± 8.8	-4.11	67	73.9 ± 59	-4.13	73	1.0
Clomipramine†	16	76.3 ± 5.6	-4.12	79	5.6 ± 2.4	-4.23	84	0.7
Desipramine	8	1.6 ± 0.2	-5.81	98	2.9 ± 1.1	-5.54	98	1.9
Diphenhydramine	8	178 ± 7.8	-3.75	88	297 ± 65	-3.53	81	1.7
Doxylamine	7	135 ± 14	-3.87	102	142 ± 39	-3.85	95	1.1
Emetine	10	9.9 ± 1.2	-5.01	52	106 ±15	-3.93	82	11
Fluoxetine	6	31.8 ± 2.6	-4.50	74	41.5 ± 30	-4.38	72	1.3
Loperamide	10	94.1 ± 21	-4.03	89	134 ± 33	-3.87	76	1.4
Lopinavir	11	11.7 ± 1.1	-4.93	95	175 ± 52	-3.76	105	15
Loratadine	10	127 ± 9.9	-3.90	58	85.7 ± 59	-4.07	77	0.7
Phenelzine	110	2.5± 0.3	-5.60	113	61.8 ± 3.1	-4.21	100	25
Prazosin	5	43.6 ± 2.9	-4.36	81	138 ± 19	-3.86	83	3.2
Pyrilamine	7	182 ± 7.4	-3.74	100	187 ± 53	-3.73	101	1.0
Reserpine	7	24.2 ± 6.5	-4.62	97	61.8 ± 30	-4.21	90	2.6
Ritonavir	7	1.4 ± 0.2	-5.86	74	158 ± 77	-3.8	68	115
Sertraline†	16	108 ± 6.9	-3.97	90	55.4 ± 31	-4.26	95	0.5
Terfenadine	11	11.5 ± 3.4	-4.94	79	41.3 ± 21	-4.38	61	2.8
Verapamil	9	143 ± 9.1	-3.85	89	267 ± 57	-3.57	80	1.9

† One replicate only

Table 7: Apparent permeabilities, recoveries and ER from concentration-dependent MDCK-MDR1 bidirectional assays

Compound	Conc. $[\mu M]$	$P_{app,A\to B}$ $[10^{-6}cm/s]$	$logP_{app,A\to B}$	Recovery $A \to B$ [%]	$P_{app,B\to A}$ $[10^{-6}cm/s]$	$logP_{app,B\to A}$	Recovery $B \to A$ [%]	ER
Loperamide	0.1	12.6 ± 1.6	-4.9	78	189 ± 95	-3.72	79	15.0
	0.4	9.47 ± 1.7	-5.02	85	137 ± 66	-3.86	101	14.4
	4	16.2 ± 3.5	-4.79	70	137 ± 51	-3.86	69	8.4
	10	30.0 ± 5.3	-4.52	80	98.5 ± 20	-4.01	70	3.3
	21	61.4 ± 7.1	-4.21	85	68.4 ± 6.2	-4.17	81	1.1
Acebutolol	6	0.34 ± 0.1	-6.47	92	7.20 ± 2.4	-5.14	94	21.1
	12	0.32 ± 0.1	-6.50	94	6.52 ± 15	-5.19	94	20.5
	20	0.26 ± 0.1	-6.57	90	8.40 ± 2.9	-5.08	88	31.5
	60	0.31 ± 0.1	-6.51	91	7.78 ± 2.5	-5.11	93	25.3
	150	0.31 ± 0.1	-6.51	92	8.37 ± 1.2	-5.08	93	26.9
Quinidine	0.05	20.1 ± 2.1	-4.70	106	277 ± 64	-3.56	93	13.8
	0.5	14.7 ± 1.1	-4.83	108	182 ± 92	-3.55	110	19.2
	5	41.2 ± 4.0	-4.38	102	249 ± 56	-3.60	114	6.0
	20	100 ± 6.7	-4.00	117	148 ± 27	-3.83	114	1.5
	50	136 ± 0.3	-3.87	118	119 ± 15	-3.92	115	0.9
Prazosin	0.01	65.0 ± 4.6	-4.19	85	135 ± 24	-3.87	87	2.1
	0.1	51.4 ± 2.3	-4.29	83	154 ± 33	-3.81	94	3.0
	1	63.2 ± 3.7	-4.20	115	219 ± 65	-3.66	102	3.5
	8	54.8 ± 7.8	-4.26	71	98.0 ± 6.9	-4.01	88	1.8
	15	35.5 ± 3.2	-4.45	73	59.8 ± 14	-4.22	84	1.7
Eletriptan	0.1	9.72 ± 1.1	-5.01	86	187 ± 33	-3.73	73	19.3
	1	9.26 ± 1.4	-5.03	83	198 ± 32	-3.70	73	21.4
	10	13.6 ± 2.3	-4.87	99	170 ± 17	-3.77	85	12.5
	20	20.7 ± 4.1	-4.68	101	115 ± 5.5	-3.94	82	5.6
	40	28.6 ± 3.5	-4.54	91	70.7 ± 5.0	-4.15	79	2.5
Amprenavir	0.2	6.74 ± 0.9	-5.17	91	160 ± 27	-3.80	99	23.8
	2	6.15 ± 0.7	-5.21	74	166 ± 21	-3.78	78	27.0
	10	6.07 ± 0.8	-5.22	75	166 ± 20	-3.78	78	27.4
	15	4.90 ± 0.4	-5.31	102	109 ± 10	-3.96	110	22.3
	20	5.27 ± 0.8	-5.28	107	111 ± 12	-3.96	96	21.0

Table 8: Experimental conditions, recovery, apparent permeabilities and calculated P_0 and $logK_{hex/w}$ values from PAMPA experiments.

Compound	Conc. $[\mu g/mL]$	Time $[h]$	pH	Replicate	Recovery [%]	Corrected $\log P_{\text{app}}$	$\log P_{0,}$	$\log K_{hex/w}$
Amprenavir	30	24	6	1	115	-6.17	-6.16	-1.68
				2	106	-6.13	-6.12	-1.65
				3	115	-6.17	-6.16	-1.68
Darifenacin	100	24	6	1	109	-5.68	-2.97	1.48
				2	100	-5.69	-2.98	1.47
				3	98	-5.69	-2.97	1.47
Desloratadine †	200	4	5.5	1	114	-7.20	-2.77	1.61
				2	118	-7.22	-2.78	1.60
				3	114	-7.25	-2.82	1.57
	200	4	6.5	1	107	-5.83	-2.51	1.88
				2	106	-5.86	-2.53	1.85
				3	105	-5.85	-2.52	1.86
Eletriptan	200	24	7.5	1	118	-5.99	-4.27	0.15
				2	116	-5.98	-4.26	0.16
				3	115	-5.99	-4.27	0.15
Emetine †	1000	2	6.5	1	122	-6.39	-3.12	1.34
				2	129	-6.41	-3.14	1.32
				3	127	-6.40	-3.14	1.33
	1000	2	7	1	115	-5.63	-3.24	1.23
				2	122	-5.61	-3.22	1.25
				3	111	-5.58	-3.18	1.29
Gefitinib	200	24	4.5	1	112	-7.66	-4.91	-4.91
				2	110	-7.66	-4.90	-4.90
				3	102	-7.66	-4.90	-4.90
Mequitazine	40	24	6	1	116	-4.80	-1.97	2.41
				2	118	-4.92	-2.13	2.25
				3	116	-4.93	-2.14	2.25
Nelfinavir	70	24	7	1	92	-6.03	-3.71	0.79
				2	96	-5.99	-3.67	0.83
				3	94	-6.05	-3.73	0.77
Phenelzine †	200	4	6	1	107	-6.40	-4.67	-0.45
				2	110	-6.52	-4.79	-0.57
				3	109	-6.50	-4.77	-0.55
	200	4	8	1	94	-5.51	-5.33	-1.11
				2	77	-5.56	-5.37	-1.15
				3	81	-5.56	-5.37	-1.15
Prazosin	80	24	7.5	1	95	-7.99	-4.22	-3.42
				2	84	-8.30	-4.22	-3.73
				3	87	-8.19	-4.22	-3.62

Table 8 continued from previous page

Compound	Conc. $[\mu g/mL]$	Time $[h]$	pH	Replicate	Recovery [%]	Corrected $\log P_{\text{app}}$	$\log P_{0,}$	$\log K_{hex/w}$
Terfenadine	100	4	4	1	105	-5.56	0.36	4.82
				2	105	-5.55	0.37	4.83
				3	104	-5.51	0.42	4.88
Erlotinib	100	24	4	1	122	-5.75	-5.11	-0.69
				2	113	-5.72	-5.09	-0.66
				3	125	-5.72	-5.09	-0.66
Verapamil	500	4	5	1	91	-5.40	-1.69	2.76
				2	92	-5.41	-1.70	2.75
				3	92	-5.41	-1.70	2.76

† Performed without EtOH extraction. Instead, assay performed at two pH values for verification.

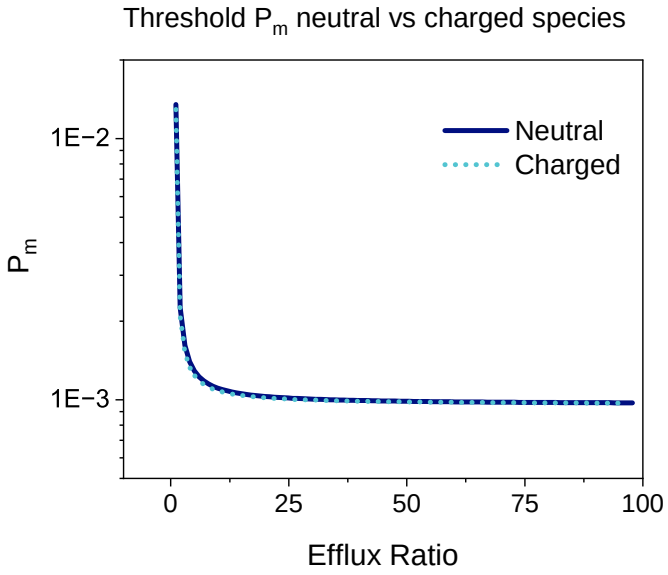

Figure 19: Sensitivity analysis of threshold P_m value based on compound species.

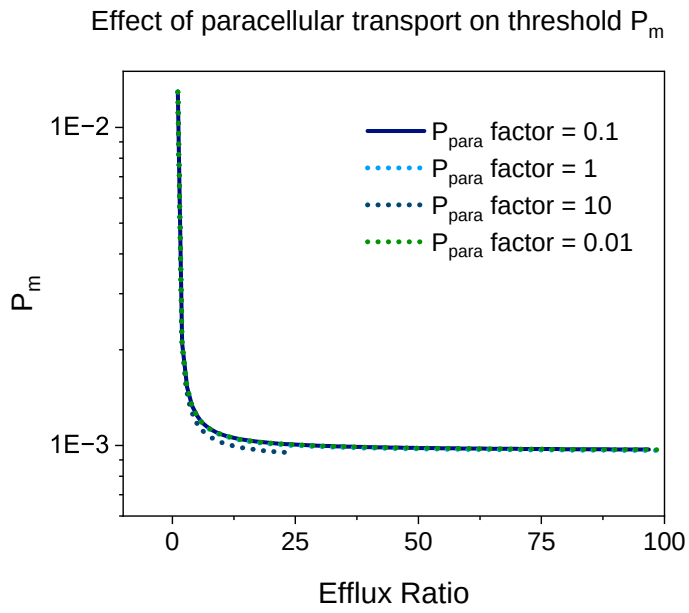

Figure 20: Sensitivity analysis of threshold P_m value based on magnitude of paracellular transport.

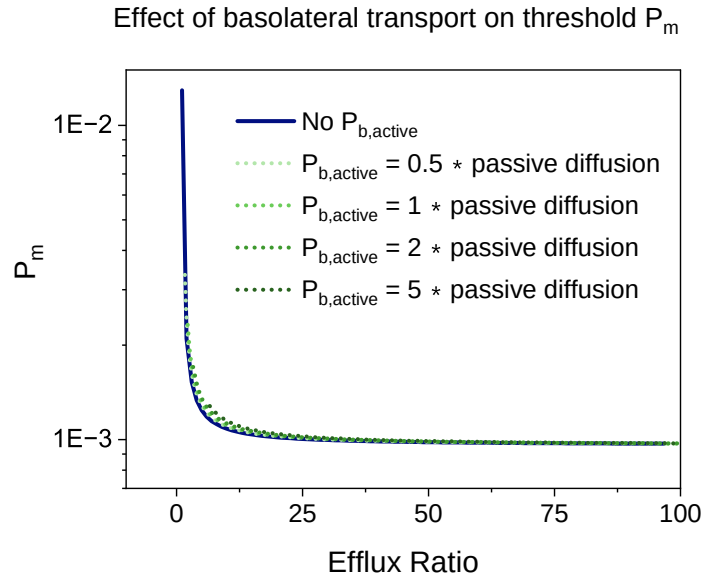

Figure 21: Sensitivity analysis of threshold P_m value based on magnitude of basolateral uptake transporter activity.

Acknowledgements

First and foremost I would like to thank my supervisor, Prof. Dr. Kai-Uwe Goss, for giving me this opportunity. I am deeply appreciative of the concentrated attention and guidance I was given under his supervision. His excellent scientific thinking, as well as his open-door policy and willingness to offer guidance at any moment was essential for this project. I would also like to thank Dr. Andrea Ebert as my unofficial second supervisor for her patient guidance, mentorship and support. I am deeply grateful that she is so approachable even though I often describe her to others as one of the smartest people (and best bakers) I have ever met.

I would also like to sincerely thank the people I shared a lab with. Especially Dr. Carolin Dahley for her help and patient instruction in almost every lab technique I used. Almost everything she did for her PhD made my own path easier, and she was an excellent role-model to me. Sandra Jäsch was also indispensable to my project. Her humbling technical expertise and the fact that she can solve every problem always kept our lab running smoothly (and she always made sure that I have enough home-grown vegetables on my desk). Lastly, I would like to thank Silke Aulhorn for helping me with my cell culture and Peter the pH meter, and for kindly letting me use her labs for my experiments.

I also owe my deepest gratitude to my friends, whose company helped preserve my sanity as I (maybe somewhat naively) tried to take on moving to another continent alone and starting a PhD simultaneously. Anina, thank you for your unwavering friendship despite the distance and for always forgiving the gaps in communication. To my partner, Carl, I am deeply grateful for your company, your patience and the numerous adventures we undertook together that maintained balance in my life. I owe you my deepest appreciation, thanks and love for enriching my life in Leipzig.

Laaste maar beslis die belangrikste, wil ek graag my liewe familie bedank. Aan my broer, André (een van die ander slimste mense in my lewe): dit was 'n onverwagse maar lekker voorreg dat ons kon kuier in Münster, Leipzig, Dresden, Tsjeggo-Slowakye en Spanje (amper) oor die jare hierso. Mamma, Pappa... dit is onmootlik om my volle dankbaarheid aan julle uit te druk. "Dankie" is net nie genoeg om te sê hoe baie ek julle jare en jare se ondersteuning waardeer nie. Maar vir nou moet dit maar genoeg wees: Dankie dat julle my aangemoedig het om dinge oorsee te gaan probeer. Dankie dat julle elke Sondagaand daar was op die anderkant van die telefoonlyn, aan die anderkant van die wêreld. Sonder die tallose geleenthede wat julle vir my gegun het, julle liefde, en julle ondersteuning sou ek dit nooit eers probeer het nie, en verseker nie tot 'n einde gebring het nie.

Curriculum Vitae

Name: Soné Kotze
Date of birth: 14.05.1996
Place of birth: Windhoek

2022-2025	Helmholtz-Zentrum für Umweltforschung Leipzig Doctoral researcher in the department of Computational Biology and Chemistry "The characterisation of active transport accross cell membranes"
2020-2021	Stellenbosch University, South Africa Master of Science (M.Sc) in Biochemistry (cum laude) in the Systems Biology department "The role of a positive feedforward loop in the regulation of yeast glycolytic intermediate dynamics."
2019	Stellenbosch University, South Africa Bachelor of Science Honours (B.Sc hons) in Biochemistry (cum laude) in the Systems Biology department "The allosteric regulation of yeast pyruvate kinase by fructose-1,6-bisphosphate and its effect on glycolytic intermediate dynamics."
2016-2018	Stellenbosch University, South Africa Bachelor of Science (B.Sc) in Molecular Biology and Biotechnology
2010-2014	Windhoek Gymnasium Private School, Namibia Namibian Senior Secondary Certificate

_____ Leipzig, 02.12.2024

Soné Kotze

Publications and Conferences

2023 22nd Barrier- and Transporter-Days, Bad Herrenalb
The effect of aqueous boundary layers on the efflux ratio
Poster

2024 Kotze, S.; Ebert, A.; Goss, K.-U.
Effects of Aqueous Boundary Layers and Paracellular Transport on the Efflux Ratio as a Measure of Active Transport Across Cell Layers.
Pharmaceutics, 16, 1, 132.

2024 23rd Barrier- and Transporter-Days, Bad Herrenalb
The pH-dependence efflux ratios determined with bidirectional transport assays across cellular monolayers
Poster

2024 Kotze, S.; Goss, K.-U.; Ebert, A.
The pH-dependence of efflux ratios determined with bidirectional transport assays across cellular monolayers.
International Journal of Pharmaceutics: X, 8.

Eidesstattliche Erklärung

Ich erkläre an Eides statt, dass ich die Arbeit selbstständig und ohne fremde Hilfe verfasst, keine anderen als die von mir angegebenen Quellen und Hilfsmittel benutzt und die den benutzten Werken wörtlich oder inhaltlich entnommenen Stellen als solche kenntlich gemacht habe. Außerdem erkläre ich, dass ich noch keine vergeblichen Promotionsversuche unternommen habe und die vorliegende Dissertationsschrift weder in der gegenwärtigen noch in einer anderen Fassung bei einer anderen Fakultät vorgelegen hat.

Leipzig, 02.12.2024

Soné Kotze